UNIVERSITÉ DE SHERBROOKE
Faculté de génie
Département de génie civil

ASSESSMENT OF GFRP-REINFORCED CONCRETE COLUMNS SUBJECTED TO QUASI-STATIC CYCLIC LOAD

ÉTUDE DU COMPORTEMENT DE COLONNES EN BÉTON ARMÉ D'ARMATURE EN PRFV SOUMISES À DES CHARGES CYCLIQUES QUASI-STATIQUES

Thèse de doctorat
Spécialité: génie civil

GIRISH NARAYAN PRAJAPATI

A dissertation submitted in partial fulfillment
of the requirements for the degree of
Doctor of Philosophy
(Civil Engineering)

Sherbrooke (Québec), Canada
June 2021

MEMBRES DU JURY

Prof. Brahim BENMOKRANE

Directeur

Prof. Adel K. ELSAFTY

Évaluateur

Prof. P. V. VIJAY

Évaluateur

Prof. Sébastien LANGLOIS

Rapporteur et évaluateur

ABSTRACT

Corrosion of the steel reinforcement in the conventional concrete structure is a serious and expensive problem which adversely affect the service life of the structure. The use of fiber-reinforced polymer (FRP) as internal reinforcing bar offers structurally safe alternative in concrete members such as beams, and slabs; due to its corrosion resistance, durability, and high strength-to-weight ratio when to compared to traditional steel bars. However, there is a lack of information concerning the performance of the reinforced-concrete columns confined with FRP bars under simulated seismic load. Study of reinforced concrete columns is useful for the construction of building, highway, and railway bridge columns. Currently, several highway and railway bridge columns and buildings need rehabilitation work due to deterioration of internal steel reinforcement (mainly transverse reinforcement) due to corrosion which affects the economy of the country. Thus, the experimental work is needed to verify the confinement effect of FRP bars on concrete columns subjected to quasi-static cyclic load to be use in new construction.

The present study investigates the experimental performance of reinforced-concrete columns confined with glass fiber-reinforced polymers (GFRP) spiral and cross tie. Eight full-scale columns were constructed with entirely GFRP reinforcement. Four other columns were constructed with hybrid reinforcement consisting of longitudinal steel rebars and confined with GFRP spirals and cross ties. The columns had a cross section of 400 × 400 mm with an overall height of 1850 mm. The columns were tested to failure under combined constant axial compression and quasi-static reversed cyclic loading. Parameters under study were longitudinal bar type (GFRP and steel), longitudinal reinforcement ratio (1.48% and 2.14%), transverse reinforcement size (#3, #4, and #5) and spacing of transverse reinforcement (100, 120 and 150 mm). Overall performance of each specimen was examined in terms of cracking patterns, hysteresis response, strain developed in reinforcing bars, energy dissipation capacity, drift capacity, and strength capacity.

Based on the test results, well-confined concrete columns showed a stable performance attending acceptable drift capacity which meets the recommendation of most design codes. The longitudinal reinforcement type significantly affected the column performance in terms of important seismic parameters. The hybrid-reinforced columns consisting of longitudinal steel and transverse GFRP reinforcement (spiral and cross tie) exhibited higher ductility and dissipated more energy than the GFRP-reinforced concrete columns. Failure progression of GFRP-reinforced column was more gradual with no strength degradation contrary to columns reinforced with longitudinal steel bars. The column behavior was patently influenced by longitudinal and transverse reinforcement ratio. The strain developed in transverse GFRP spirals and cross ties showed its effectiveness in confining the column core irrespective of the longitudinal bar type. Proposed displacement deformability index based on experiment showed reasonably good prediction for GFRP-reinforced concrete columns. The test results achieved comparable strength compared to North American design codes for columns reinforced with hybrid longitudinal steel and transverse GFRP reinforcement while, the low elastic modulus of the GFRP longitudinal bar had a significant impact on the theoretical capacity of the concrete columns.

Keywords: Glass fiber-reinforced polymer (GFRP); concrete columns; failure; longitudinal and transverse reinforcement ratio; quasi-static cyclic loading; hysteresis response; drift; energy dissipation; deformability index; ductility; strain; design codes.

RÉSUMÉ

La corrosion de l'armature d'acier dans les structures en béton est un problème sérieux et coûteux et qui réduit la durée de vie de l'ouvrage. L'utilisation des barres d'armature composites en polymère renforcé de fibres (PRF) offre une très bonne alternative pour les éléments en béton tels que les poutres et les dalles notamment en raison de leur résistance à la corrosion, de durabilité et de son rapport résistance / poids élevé par rapport aux barres d'acier traditionnelles. Cependant, il y a un manque d'information technique sur le comportement des colonnes en béton armé avec des barres en PRF sous charges sismiques. L'étude des colonnes en béton armé est utile pour la construction de nombreux ouvrages dont les bâtiments et les ponts. Actuellement, plusieurs colonnes d'ouvrages nécessitent des travaux de réhabilitation en raison de la détérioration des armatures d'acier (principalement des armatures transversales) due à la corrosion. Ainsi, des travaux expérimentaux sont nécessaires pour vérifier l'utilisation de barres en PRF comme armature longitudinale et transversale dans des colonnes en béton armé soumises à des charges latérales cycliques.

La présente étude examine les performances expérimentales de colonnes en béton armé avec armature transversale en composite de polymère renforcé de fibres de verre (PRFV) de forme spirale en spirale et en épingle. Huit colonnes à pleine échelle ont été construites avec un renforcement entièrement en PRFV (armature longitudinale et transversale). Quatre autres colonnes ont été construites avec une armature hybride constituée d'armature d'acier longitudinale et d'armature transversale constituée de spirales et d'épingles en PRFV. Les colonnes ont une section transversale de 400 mm x 400 mm avec une hauteur totale de 1850 mm. Les colonnes ont été testées jusqu'à la rupture sous une charge axiale constante combinée à un chargement cyclique latéral. Les paramètres d'étude considérés sont : le type de barre longitudinale (PRFV et acier), le taux de renforcement longitudinal (1,48% et 2,14%), la grosseur des armatures transversales (#3-10 mm, #4-13 mm et #5-15 mm) et l'espacement des armatures transversales (100, 120

et 150 mm). Les performances globales de chaque colonne ont été examinées en termes de réseaux de fissuration, de la courbe d'hystérésis, de déformation dans les barres d'armature, de capacité de dissipation d'énergie, de taux de déplacement latéral et de résistance.

Sur la base des résultats des essais, les colonnes en béton bien confinées avec de l'armature transversale en PRFV ont montré une performance stable correspondant à une capacité de déplacement latéral acceptable qui répond aux recommandations de la plupart des codes de conception. Le type de renforcement longitudinal (acier ou PRFV) a eu un impact significatif sur les performances des colonnes en termes de paramètres sismiques. La colonne renforcée avec de l'armature hybride constituée d'acier (armature longitudinale) et de PRFV (armature transversale) présentait une ductilité plus élevée et dissipait plus d'énergie que la colonne en béton armé entièrement en PRFV. La progression de la rupture dans les colonnes en béton armé d'armature en PRFV (armature longitudinale et transversale) était plus progressive et sans dégradation de la résistance contrairement aux colonnes en béton armé avec des barres d'acier longitudinales. Aussi, le comportement des colonnes a été clairement influencé par le taux d'armature longitudinale et transversale. La déformation développée dans les spirales transversales et les épingles en PRFV a montré l'efficacité de la spirale et des épingles en PRFV quel que soit le type de barre longitudinale de la colonne (acier ou PRFV). L'indice de déformabilité proposé en se basant sur les résultats expérimentaux obtenus a montré une bonne prédiction pour les colonnes en béton armé de PRFV. Les résistances des colonnes testées concordent très bien avec les prédictions des normes de conception nord-américains aussi bien pour les colonnes avec armature hybride ou entièrement en PRFV. Le module d'élasticité réduit de la barre longitudinale de GFRP a eu un impact significatif sur la capacité des colonnes de béton armé de PRFV.

Mots clés: Polymère renforcé de fibres de verre (GFRP); colonnes en béton; rupture; taux d'armature longitudinale et transversale; chargement cyclique quasi-statique; courbe d'hystérésis; taux de déplacement latéral; dissipation d'énergie; indice de déformabilité; ductilité; déformation; codes de conception.

Acknowledgement

I wish to express my deep sense of gratitude and indebtedness to my elite supervisor Prof. ***Brahim Benmokrane***, Professor, Department of Civil Engineering, Université de Sherbrooke, for being helpful and a great source of inspiration. I am thankful to him for his persistent interest, constant encouragement, vigilant supervision, and critical evaluation. His helping nature, invaluable suggestions and scholastic guidance are culminated in the form of the present work.

I would like to express my deepest and sincere gratitude to Dr. ***Ahmed Farghaly***, Research Associate, Department of Civil Engineering, Université de Sherbrooke, for his constant encouragement and guidance throughout the research work. I am thankful to him for his valuable assistance with planning, experimental work, testing, and analysis, and for his dedicated hours of discussions and enlightenments.

Sincere thanks to my colleagues and technical staffs Mr. ***Steven MacEachern*** and Mr. ***Jerome Lacroix***, Department of Civil Engineering, Université de Sherbrooke, for their help during the casting and testing of specimens.

I am thankful to Mr. ***Islam Shabana***, research scholar, Department of Civil Engineering, Université de Sherbrooke for his help during the casting of specimens and being supportive.

I find myself fortunate to express my gratitude to my parents, who have forever been a source of inspiration and strength to me. I am also thankful to my friends scattered around the world for their continuous support.

Girish Narayan Prajapati

Table of Contents

List of Tables

List of Figures

Chapter 1
INTRODUCTION

1.1 GENERAL

In recent years, there is an increase in the application of fiber-reinforced-polymer (FRP) reinforcing material in concrete structures. In contrast with steel bars, FRP bars possess high strength-to-weight ratio, high resistance and low relaxation characteristics which offers structurally safe alternative concrete members such as beams and slabs. However, the stress-strain relationship of FRP bars is linear elastic until failure which arises concern on the use of FRP bars in concrete structures prone to seismic event and wind loads. The characteristics like lateral drift, ductility and energy dissipation are critical for the concrete-structural members subjected to seismic loads and demands investigation when reinforced with FRP bars (Mohamed et al. 2014).

For an earthquake resistant structure, the excessive strength is neither essential nor desirable. The inelastic structural response which provides ductility is the important aspect of maintaining the strength of the structure subjected to reversals of inelastic deformations under seismic loads. The locations where inelastic deformations may occur and as a response dissipate the absorbed energy is termed as plastic hinge. In addition, the required shear strength for the concrete structures must exceed the required flexural strength to prevent failure due to inelastic shear deformations which means enough confinement or transverse reinforcement in the region of plastic hinge.

The earthquake resistant structure follows strong column-weak beam design philosophy which looks for seismic energy dissipation initially in the well-confined beam plastic hinge whereas, a column plastic hinge is yet to form at the base of the column. Figure 1.1(a) shows the well-confined beam yielded prior to column and the hinge distributed evenly in every storey of the building which refers to global failure mechanism with large

displacement at collapse. In the Figure 1.1(b), in case of the weak column-strong beam, column at the ground level start yielding causing local failure mechanism of the building with minimal displacement at collapse.

The column is the critical member in the structure; consequently, it is important to ensure ductile behavior of the column by having adequate confinement in the region of the plastic hinge. The design codes (CSA A23.3-19 and ACI 318-19) specify special confinement ratio for the moment resisting structure in the region of plastic hinge. However, there is lack of information concerning the performance of FRP bar reinforced concrete columns subjected to lateral reversals loads. Thus, the present study focuses on the behavior of confinement of FRP-reinforced concrete columns subjected to quasi-static cyclic load.

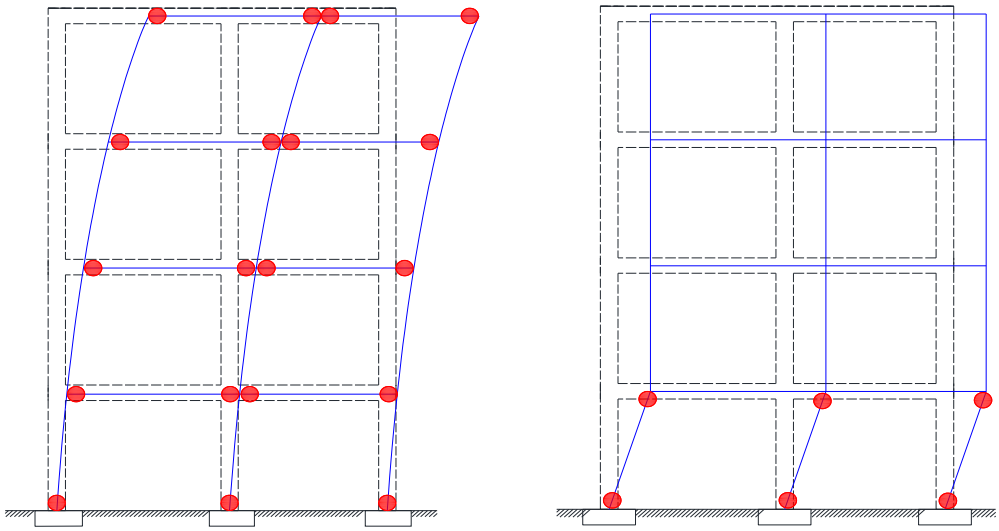

Figure 1.1- (a) Global failure mechanism (b) Local failure mechanism

1.2 PROBLEM DEFINITION

The use of conventional steel bars in reinforced concrete structures in seismic prone zones are due to its favourable properties like tensile strength, stiffness, ductility, and elastic-plastic behavior. However, the corrosion of the reinforcing steel is the major cause of

deterioration in concrete. The expansion of steel due to resulting rust creates tensile stresses in concrete, which lead to cracking, delamination, and spalling. There is loss of serviceability, reduction in load carrying capacity of the structure and eventually partial or full collapse when a natural calamity occurs. The alkaline environment of concrete (pH of 12 to 13) provides a protective or passive layer against the corrosion of steel. However, once the passive layer is destroyed, corrosion can occur. There are two main reasons for the destruction of passive layer: when the alkalinity of the concrete is reduced due to carbonation and when the chloride concentration in concrete is increased. The primary cause of premature corrosion of steel reinforcement is the exposure of reinforced concrete to chloride ions. If oxygen and moisture are available to sustain the reaction, the interference of chloride ions present in de-icing salts and seawater into reinforced concrete can cause steel corrosion. The chlorides in water reach the steel through cracks. The risk increases as the chloride content of concrete increases. If the chloride content exceeds a threshold value, corrosion will occur in availability of water and oxygen. Federal Highway Administration (FHWA) found a threshold limit of 0.20 percent total chloride (acid-soluble) by weight of cement can induce corrosion of reinforcing steel. Another factor which causes the corrosion of steel is carbonation. Carbonation occurs when the carbon dioxide from the air penetrates the concrete and reacts with hydroxides (calcium hydroxide) to form carbonates which eventually reduces the pH of the pore solution to as low as 8.5, at this level the protective film on the steel is not stable. Carbonation is a slow process; in high-quality concrete it will proceed at a rate up to 1 mm per year. The rate of carbonation in concrete increases with a high water-to-cement ratio, low cement content, short curing period, low strength, and highly porous paste. The relative humidity of the concrete between 50 and 75 increases the rate of carbonation; below 25 is considered insignificant. Different protection techniques are used to mitigate the corrosion problems like increasing concrete cover, use of corrosion inhibiting admixtures, coating of reinforcement using epoxy resin, by improving the permeability of concrete, use of sealers and membranes on the concrete surface. However, none of these solutions is found to be effective in eliminating the problem completely. Thus, steel reinforced concrete structures

may require repairing, strengthening and rehabilitation against corrosion which will increase the cost and may cause safety issue ("Corrosion of Embedded Materials,"). The cost to repair and rehabilitate bridge columns in North America has been estimated at hundred of million of dollars (Renew Canada 2014). This generates interest in using alternative materials like glass fiber-reinforced polymer (GFRP) as reinforcement in new reinforced concrete structure due to following characteristics:

(a) GFRP bars have resistance against moisture, alkali effects and chemical attack which mostly depend on the selection of appropriate resin, manufacturing process and application of protective coatings. Thus, the GFRP bars have resistance against deterioration due to chloride ions and carbonation.

(b) The GFRP bars exhibit linear elastic behavior until failure with attained large strains. The high elasticity of GFRP bars can control the damages with less residual deformation post-earthquake comparing to steel bars (Mohamed et al. 2014).

(c) GFRP bars are non-conductive and magnetic-free, which is favorable in structures where electric and magnetic interference is undesirable.

There is insufficient experimental evidence on the behaviour of concrete columns confined with GFRP reinforcement subjected to seismic loading. Thus, they are not well documented in design codes (CSA and ACI). The current FRP design codes and guidelines such as ACI 440.1R, 2015; CSA S6, 2014; CSA S806, 2012; AASHTO, 2018 does not have considerable seismic provisions for the design of the reinforced concrete columns confined with GFRP reinforcement subjected to seismic loads.

1.3 OBJECTIVES AND SCOPE

The main aim was to assess the confinement effectiveness of GFRP spiral and cross ties. The scope of this study involved casting and testing twelve full-scale concrete columns reinforced with longitudinal steel and GFRP bars and confined with GFRP spiral and cross

ties. The column between the footing and mid-height of the first storey (point of contra-flexure) as shown in Figure 1.2 was selected as the test specimen as it is more critical to earthquake loads. The test specimens measured 1850 mm long with effective height of 1650 mm and 400 × 400 mm cross-sectional dimension The columns were subjected to displacement based reversed lateral cyclic load. The performance of GFRP bars, steel bars, GFRP spiral and cross ties were observed through strain measurements in most-damaged region. Further, the impact of studied parameters on failure progression were patently highlighted.

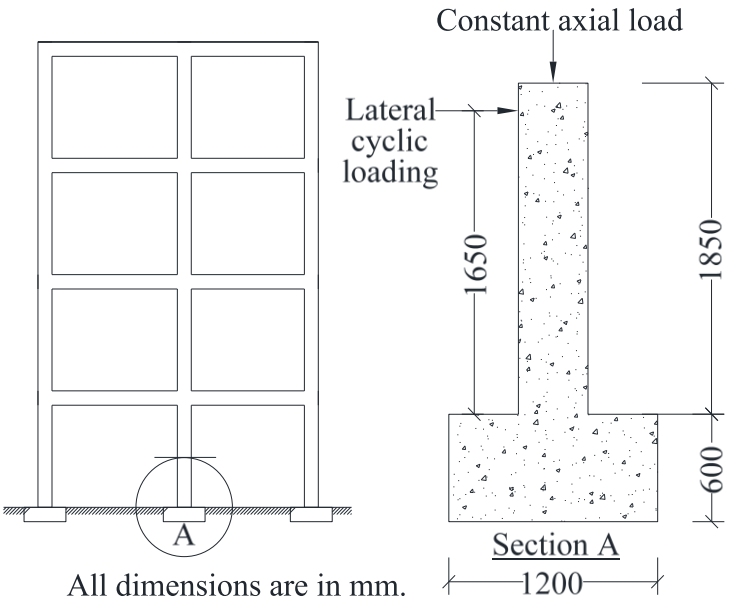

Figure 1.2- Depiction of test specimen in the multi-story building

The following points summarize the specific objectives of the study:

(i) To study the behavior of the concrete columns reinforced with GFRP bars subjected to reverse cyclic loading in terms of its composite behavior, failure modes, deformability, and overall stiffness to examine the seismic performance.

(ii) To access the experimental performance of the hybrid-reinforced concrete columns reinforced with longitudinal steel and confined with transverse GFRP reinforcement subjected to quasi-static reversed cyclic load.

(iii) To investigate the confinement behavior of full-scale concrete columns confined with GFRP spiral and cross ties.

(iv) To study the effect of different parameters on the behavior of GFRP-reinforced concrete columns and accordingly on the design equations. The different parameters under consideration are longitudinal reinforcement type, longitudinal reinforcement ratio, transverse reinforcement size, and spacing of transverse reinforcement.

(v) To address the preliminary concepts and recommendations for design guidelines of the concrete columns reinforced with GFRP bars and subjected to lateral loads in the Canadian and American design codes.

1.4 THESIS ORGANIZATION

This thesis is organized into seven chapters including the introduction.

Chapter 1 includes brief introduction, problem statement, scope, and objectives of the study.

Chapter 2 provides a brief review of the work done on reinforced concrete columns subjected to cyclic loading. Also, it includes FRP bars as reinforcing material, its properties and behavior.

Chapter 3 describes different design code provisions for the design of the reinforced concrete columns with special provision for seismic load. Experimental program is discussed in this chapter with test matrix, experimental setup, and testing procedure.

Chapter 4 presents a detailed analysis of experiment test results of GFRP-reinforced concrete columns in terms of failure modes, hysteresis response and energy dissipation capacity. The deformability index of GFRP-reinforced concrete columns and effect of reinforcement parameters were also discussed.

Chapter 5 assesses the performance of concrete column reinforced with longitudinal steel and transverse GFRP reinforcement. The column behavior is discussed in terms of crack progress, displacement ductility, strain developed in longitudinal steel and transverse GFRP bars. Moreover, it compares the results with available North American design codes.

Chapter 6 compares the behavior of hybrid-reinforced concrete column with GFRP-reinforced concrete columns regarding their failure mode, hysteresis response and strain progression in longitudinal bar. Evaluation of ductility parameters, stiffness degradation, and lateral load capacity prediction were also presented.

Chapter 7 presents conclusion and recommendation for future work.

Chapter 2
LITERATURE REVIEW

2.1 GENERAL

Considerable amount of research has been done on the FRP-reinforced concrete columns subjected to axial compression. However, the research on seismic behavior of FRP-reinforced concrete columns is minimal. Further, the studies on hybrid-reinforced columns reinforced with longitudinal steel and transverse FRP bars is in early stage. This chapter summarizes relevant research on steel-reinforced concrete columns and recently conducted experimental research on FRP- and hybrid-reinforced columns.

2.2 FIBER REINFORCED POLYMER

Fiber-reinforced-polymer (FRP) is a high-strength composite material made up of high strength fibers (carbon, glass, aramid, etc.) and a polymer matrix (epoxy, polyester, vinyl ester, etc.). The GFRP bars were first investigated in the 1950s for structural use. However, the FRP was considered for the structural engineering applications in the 1970s. In present days, the FRP products are manufactured in many different forms such as bars, fabrics, 2D grids, 3D grids or standard structural shapes. FRP can be used both externally and internally to improve the existing structure or to build the new structure, respectively. The FRP fabrics are generally used externally to retrofit or rehabilitate the existing structure in coastal areas and seismic zones. FRP as internal reinforcement such as bars is used to build new structures. The primary concern in this research is the use of FRP composite bars in structures prone to earthquake loads. Thus, to stay within the scope of the present research, the following section will focus on the FRP composite bars as internal reinforcement.

2.2.1 FRP Constituents

FRP composite materials consisting of reinforcing fibers which are stronger than the polymer matrix. The fiber-volume fraction should be more than 55 percent for the proper functioning of the reinforcement. The mechanical properties of the FRP product depend on the fiber quality, shape, orientation, volumetric ratio, and bond to the matrix. The mechanical properties of the FRP product mostly depend on the manufacturing process, because simply mixing fibers and matrix does not assure a quality product. Additives and fillers are added appropriately for the fiber and resin for curing or other reasons.

2.2.2 Fibers

The fibers should have high strength, stiffness, durability, toughness, and preferably low cost for the manufacturing of composite materials. The length, cross-sectional shape and chemical composition affect the performance of the fibers. The most used fibers for FRPs are carbon, glass, aramid, and basalt.

Glass fibers are widely used among all other fibers because of minimal cost, high elasticity, chemical resistance, and insulating properties. The disadvantages are moderately low elastic modulus, high density, and low fatigue resistance. Four types of glass fibers are available: E-glass (high electrical resistance), S-glass (high strength), C-glass (high chemical resistance) and AR-glass (high alkali resistance). In the present study, GFRP bars are used for experiments due to its high deformability compared to other available FRP type reinforcement.

2.2.3 Resins

The physical and thermal properties of the resins significantly influence the mechanical properties as well as the manufacturing process of the composites. The matrix should develop higher ultimate strain than the fibers; to be able to utilize full strength of the fiber (Phillips 1989). The matrix not only protects the fibers from the mechanical abrasion, but mainly transfers stresses between the fibers. The other important roles of the matrix are

transfer of inter-laminar and in-plane shear in the composite and provides lateral support to fibers against buckling when subjected to compressive loads. Thermosetting and thermoplastic are two different types of polymetric matrices used for FRP composites. Thermosetting polymers are used more often than thermoplastic.

2.2.4 FRP stress-strain relationship

The FRP bars are unidirectional because of the arrangement of the fibers in one direction. The FRP composites have a linear stress-strain relationship due to which the bars exhibit linear elastic behaviour until the failure. FRP bars have higher tensile strength than the conventional steel. The stress-strain relationship of FRP bars in comparison to typical idealized steel bars are shown in Figure 2.1.

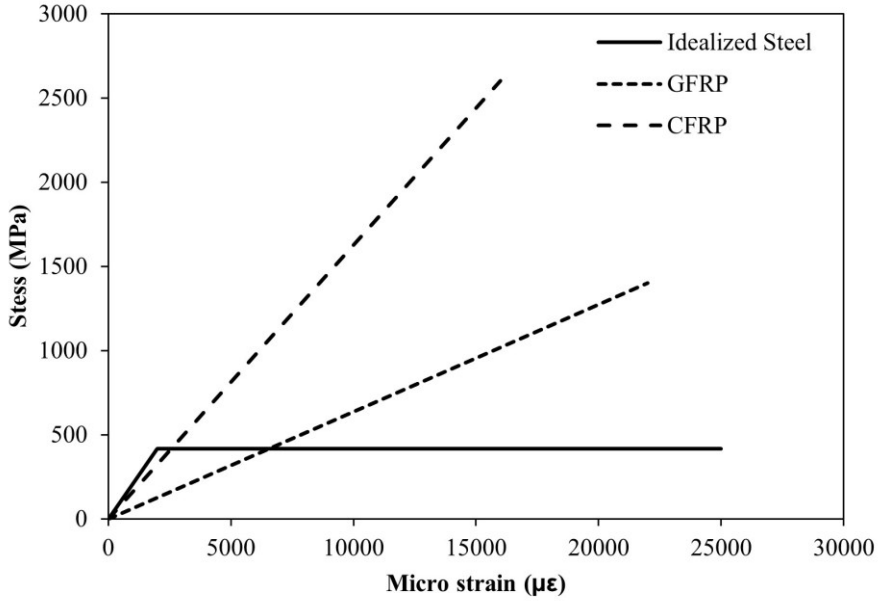

Figure 2.1- Stress-strain relationship of FRP reinforcement

2.2.5 Physical properties

2.2.5.1 *Density*

FRP bars have a density one-sixth to one-fourth of that of steel. Due to lower density, there is a reduction in the transportation costs and ease handling of the bars during the construction. The densities of the different FRP are listed in Table 2.1.

Table 2.1- Typical densities of different FRP bars (ACI Committee 440 2015)

Steel	GFRP	CFRP	AFRP
7..9 g/cm^3	1.25 to 2.10 g/cm^3	1.50 to 1.60 g/cm^3	1.25 to 1.40 g/cm^3

2.2.5.2 *Coefficient of thermal expansion*

The coefficients of thermal expansion (CTE) of FRP bars vary in the longitudinal and transverse directions depending on the types of fiber, resin, and volume fraction of fiber. The value of longitudinal CTE is controlled by fiber thermal expansion coefficient whereas the value of transverse CTE is controlled by resin thermal expansion coefficient (Bank 1993). Therefore, the value of longitudinal CTE is smaller than transverse CTE as fiber thermal expansion coefficient are smaller than resin thermal expansion coefficient. The coefficients of thermal expansion of FRP bars are listed in Table 2.2.

Table 2.2- Coefficient of thermal expansion of FRP bars (ACI Committee 440 2015)

Direction	Steel	GFRP	CFRP	AFRP
Longitudinal (αL *x 10^{-6}/^{o}C*)	11.7	6 to 10	-9 to 0	-6 to -2
Transverse (αL *x 10^{-6}/^{o}C*)	11.7	21 to 23	74 to 104	60 to 80

2.2.6 Mechanical properties

2.2.6.1 *Tensile behaviour*

Table 2.3 summarized the tensile properties of FRP bars. The ratio of the volume of fiber to the overall volume of the FRP (fiber-volume fraction) notably influence the tensile

properties of the FRP bars. Strength and stiffness variations will occur in bars with different fiber-volume fractions, even in bars with the same diameter, appearance, and constituents. The mechanical characteristics of the bar is affected by the rate of curing, manufacturing process and manufacturing quality control (Wu 1990).

Table 2.3- Tensile properties of reinforcing bars (ACI Committee 440 2015)

Properties	Steel	GFRP	CFRP	AFRP
Nominal yield stress (MPa)	276 to 517	N/A	N/A	N/A
Tensile strength (MPa)	483 to 690	483 to 1600	600 to 3690	1720 to 2540
Elastic Modulus (GPa)	200	35 to 51	120 to 580	41 to 125
Yield strain (%)	0.14 to 0.25	N/A	N/A	N/A
Rupture strain (%)	6.0 to 12.0	1.2 to 3.1	0.5 to 1.7	1.9 to 4.4

2.2.6.2 *Compressive behaviour*

The design of FRP bars to resist compressive stresses is not recommended. Tests on FRP bars with a length-diameter ratio from 1:1 to 2:1 have shown that the compressive strength is lower than the tensile strength (Wu 1990). The mode of failure for FRP bars subjected to longitudinal compression can include transverse tensile failure, fiber micro buckling, or shear failure depends on the type of fiber, the fiber-volume fraction, and the type of resin. Compressive strength of 55, 78 and 20 percent of the tensile strength have been reported for GFRP, CFRP, and AFRP respectively (Mallick 1988; Wu 1990). Generally, the bars with higher tensile strength have higher compressive strengths except in case of AFRP. The compressive modulus of elasticity of FRP reinforcing bars are smaller than its tensile modulus of elasticity. Test on samples containing 55 to 60 percent volume fraction of continuous E-glass fibers in a matrix of vinyl ester or isophthalic polyester resin indicate a compressive modulus of elasticity of 35 to 48 GPa (Wu 1990). The compressive modulus of elasticity is approximately 80 percent for GFRP, 85 percent for CFRP, and 100 percent for AFRP of the elastic modulus of elasticity for the same product (Ehsani 1993; Mallick 1988). The lower values of modulus of elasticity in compression due to the premature

failure resulting from end brooming and internal fiber micro buckling under compressive loading.

2.2.6.3 *Shear behaviour*

Most FRP bar composites are comparatively weak in interlaminar shear where layers of unreinforced resin lie between layers of fibers. Because the interlaminar shear strength is governed by the relatively weak polymer matrix. Depending on the degree of offset, orientation of the fibers in an off-axis direction across the layers of fiber will increase the shear resistance. This can be accomplished by braiding or winding fibers transverse to the main fibers. The required shear properties of the FRP bar can be obtained from the bar manufacturer (ACI Committee 440 2015).

2.2.6.4 *Bond behaviour*

Bond performance of an FRP bar is dependent on the design, manufacturing process, mechanical properties of the bar itself, and the environmental conditions (Al-Dulaijan et al., 1996; Bakis et al., 1998; Bank et al., 1998; Freimanis et al., 1998; Nanni et al., 1997). When anchoring a steel reinforcing bar in concrete, the bond force can be transferred by adhesion resistance of the interface; frictional resistance of the interface against slip; and mechanical interlock due to irregularity of the interface. But in case of FRP bars, the bond force is transferred through the resin to the reinforcement fibers, and a bond-shear failure in the resin is also possible. When a bonded deformed bar is subjected to increasing tension, the adhesion between the bar and the surrounding concrete breaks down, and the deformations on the surface of the bar cause inclined contact forces between the bar and the surrounding concrete. The stress at the surface of the bar resulting from the force component in the direction of the bar can be considered the bond stress between the bar and the concrete. The bond properties of FRP bars can be investigated by pullout tests, splice tests and cantilever beam to determine an empirical equation for embedment length (Benmokrane, 1997; Ehsani et al., 1996; Faza & GangaRao, 1991; Mosley, 2002; Shield et al., 1999; Tighiouart et al., 1999; Wambeke & Shield, 2006).

2.3 REVIEW OF PREVIOUS WORKS

2.3.1 Behaviour of FRP-RC columns under compression

Wu (1990) conducted a series of study on the thermomechanical properties of Fiber Reinforced Polymer (FRP) bars. In the compression test, the compressive strength of the FRP bars were found to be lower than their tensile strength. The compressive strengths of GFRP, CFRP and AFRP were 55 %, 78 % and 22 % of the corresponding tensile strength, respectively. Considering the bars in columns are confined with lateral ties, they are likely to contribute in the axial capacity of the columns. Alsayed et al. 1999 casted and tested fifteen (15) rectangular concrete columns reinforced with equal volume GFRP bars and ties as in steel RC column to investigate its behaviour. The columns with 450 × 250 × 1200 mm dimension were subjected to concentric monotonic axial loading. For the prediction of average axial capacity of the columns, modified ACI 318-95 (ACI Committee 318 1995) equation were used as:

For steel section,

$$P = 0.85 f_c^{'} \left(A_g - A_{st} \right) + f_y A_{st} \qquad \text{for } \varepsilon_s \geq \varepsilon_y \qquad 2.1$$

$$P = 0.85 f_c^{'} \left(A_g - A_{st} \right) + \varepsilon_s E_s A_{st} \qquad \text{for } \varepsilon_s < \varepsilon_y \qquad 2.2$$

For GFRP section,

$$P = 0.85 f_c^{'} \left(A_g - A_{st} \right) + 0.6 f_{uf} A_{st} \qquad \text{for } \varepsilon_f \geq 0 \qquad 2.3$$

where, P is average axial capacity of the column, $f_c^{'}$ is concrete compressive strength, A_g is gross area of concrete, A_{st} is area of the longitudinal reinforcements, ε_s is applied strain of the longitudinal steel bar, ε_y is yield strain of the longitudinal steel bar, E_s is elastic modulus of steel, f_{uf} is ultimate tensile capacity of the GFRP bars, ε_f is applied strain on the GFRP bars.

The author reported the failure of specimens with longitudinal steel bars was due to buckling of the reinforcing bars at the mid-height of the columns, whereas the failure of specimens with longitudinal GFRP bars resulted from crushing of concrete and breakage of the bars at the mid-height. Reduction in the axial capacity of concrete columns reinforced with GFRP bars by 13 % in comparison to steel bars were reported and reduction by 10 % with GFRP ties. Due to low stiffness of GFRP bars, the columns with GFRP lateral ties showed similar behaviour with the columns with no reinforcement, until 80 % of ultimate capacity. But under higher loads, the GFRP ties were found to be effective in providing lateral confinement which increased the ultimate capacity of the column. The comparison of the test results with the predicted equations for the axial capacity were overestimated by 10% for columns reinforced with steel bars and by 12% for columns reinforced with GFRP bars.

Behaviour of full-scale GFRP-RC columns under pure axial load using 610 × 610 mm square cross-sectional columns were tested (De Luca et al., 2010). Total of five specimens were tested in which one was reinforced with steel bars as a control specimen. GFRP bars from two different manufacturers were used to ensure the similar performance of GFRP bars irrespective of the manufacturer found to be ineffective in the performance of the column if the bars are of comparable quality. The specimens reinforced with GFRP bars showed identical behaviour to that reinforced with steel bars. The peak compressive concrete strength was close to $0.85f_c^{'}$ (value defined in ACI 318-08) in all test specimens. The contribution of the GFRP bars was less than 5 % of the peak load, which found to be lower than that of approximately 12 % of the steel bars which contributed to the conclusion that the contribution of GFRP bars may be ignored when evaluating the nominal capacity of an axially loaded RC column. The design of the transverse reinforcement for GFRP-RC columns cannot follow the same criteria as for the steel transverse reinforcement based on ACI 318-08. Because it resulted in brittle failure of the GFRP reinforced specimens but with closely spaced ties the GFRP-RC columns had less brittle failure. Author suggested further investigation with more efficient and closed grip GFRP tie spacing.

Tobbi et al. (2012) conducted an experimentally study on the behaviour of full-scale GFRP square RC columns of 350 × 350 × 1400 mm dimensions under concentric loading to investigate the contribution of transverse reinforcement in the confinement of the concrete core. Eight specimens with different tie configuration as shown in Figure 2.2 were tested with reinforcement ratio equals to $0.019A_g$. Displacement control was applied at a rate of 2.5 kN/s. During the experiment, it was observed that early spalling of concrete cover occurred with reduction in axial capacity before any significant contribution for the lateral confinement. Later, the strength gains and toughness due to confinement of the core took place. When closely spaced ties about 80 mm was used instead of 120 mm, the axial capacity was increased by 20 % due to confinement and it enhances the buckling resistance of the longitudinal bars. Other conclusions drawn from the study were the strength reduction factor of 0.85 can be adopted for GFRP-RC columns which is same for steel sections. For estimating the compressive strength of column, the author suggested setting the compressive strength of GFRP bars to 35 % of GFRP maximum tensile strength yields a reasonable estimate but it needs further investigation. The contribution from GFRP bars was 10 % of the column capacity which is close to steel's contribution (12 %).

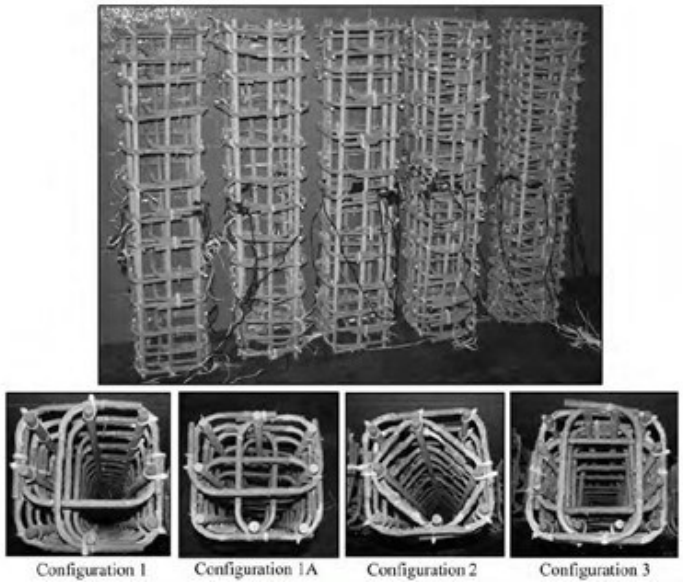

Figure 2.2- Layout of GFRP RC columns (Tobbi et al. 2012)

Afifi et al. (2014) studied the performance of concrete columns reinforced with FRP bars and confined with FRP hoops and spirals subjected to axial load. Sand-coated GFRP and CFRP reinforcement was used. Fourteen full-scale columns were casted comprises of six GFRP-RC columns, six CFRP-RC columns, one with steel reinforcement and last one without reinforcement. It was observed that using GFRP, CFRP and steel reinforcement increase the peak load up to 1.20, 1.40 and 1.27 times in comparison to plain concrete specimen. In comparison to steel and CFRP RC columns, GFRP-RC columns showed a lower rate of strength decay. Ductile failure mode with spalling of concrete cover, followed by buckling of the longitudinal bars and rupture of spirals or hoops was observed in GFRP and steel-RC columns. But the failure of the CFRP-RC columns was more brittle, identical to plain concrete specimen. It was concluded that GFRP and CFRP-RC columns showed a similar behaviour with control steel reinforced specimen. Further, the CSA S806 (2012) limitations for confinement showed a good agreement with the experimental results.

In summary, the GFRP-RC columns under pure axial load had showed similar behaviour to that of steel counterpart in terms of damage progression and peak capacity. In axial load carrying capacity of columns, more than 85 % of the resistance come from the concrete while less than 15 % contributed by steel reinforcement as mentioned in the literature. This leads to the conclusion that the main contribution of the internal reinforcement in columns is mainly to strengthen the concrete core to provide ductility (to prevent sudden failure).

Paramanantham (1993) investigated the behaviour of concrete columns reinforced with FRP rebars under concentric and eccentric loading. GFRP bar was used as longitudinal and transverse reinforcement. Fifteen FRP-RC blocks and sixteen FRP-RC columns were casted and tested under concentric and eccentric loading, respectively. The concentric test was conducted to investigate the effect of tie spacing and bar local buckling on axial capacity of the test specimens. For these three different ties spacing was selected as 100, 150, and 200 mm. The author does not notice any significant difference in the concentric capacity due to tie spacing, but small improvement in the strength due to better buckling resistance of FRP reinforcement in case of 100 mm tie spacing was noticed. FRP bars contributed to the load carrying capacity corresponding to 0.003 strains which represents

about 20-30 % of the ultimate strength of the FRP reinforcement. The other sixteen columns tested under combined axial load and moment failed in compression crushing mode. The column behaviour was distinguished with the ratios of moment-deflection curve slopes into three parts; the first two parts were linear whereas the third was nonlinear. When the ratio of first slope to second slope varies between 1.25 and 1.85, the failure mode was defined as compression failure. For ratio between 2.22 and 2.37, the failure was defined as compression with tensile cracking. When the ratio between 5.5 and 6.0, the failure was defined as compression-flexure failure. Tie spacing of 100 mm was found to be efficient. The author compared the experimental results with a moment-axial force interaction diagram derived analytically based on the plane section analysis. This comparison showed higher experimental strength values except for four columns. The compression-controlled portion of interaction diagrams was similar for both FRP and steel-RC columns, but the tension governing portions were different. For the columns subjected to concentric loading, the developed equation for axial capacity of the column:

$$P = 0.85 f_c^{'} \left(A_g - A_f \right) + 0.003 E_f A_f \qquad 2.4$$

For eccentric loading case:

$$P_n = C_c + C_f - T_f \qquad 2.5$$

where,

$$C_c = 0.85 f_c^{'} \beta_1 ab \qquad 2.6$$

$$C_f = 0.50 A_f \varepsilon_c^{'} E_{fc} \qquad 2.7$$

$$T_f = 0.50 A_f \varepsilon_t A_{fc} \qquad 2.8$$

$f_c^{'}$ is concrete compressive strength, C_c is compressive force carried by concrete, C_f is force carried by the bars in compression, T_f is force carried by the bars in tension, A_g is gross cross-sectional area of column, A_f is area of FRP reinforcement, E_f is tensile

modulus of elasticity of FRP bars, β_1 is ratio of depth of rectangular compression block to depth to the neutral axis, a is depth of equivalent rectangular stress block, b is width of compression face of the member, $\varepsilon_c^{'}$ is compressive strain of FRP bars, E_{fc} is compressive modulus of elasticity of FRP bars and ε_t is tensile strain of FRP bars.

To understand the behaviour of concrete members reinforced with FRP bars and the failure mechanism exhibited by these columns; Choo et al. (2006) studied the strength of rectangular concrete columns reinforced with FRP bars. Based on an analytical study of strength axial load-moment interaction curve, the author identified two failure mechanisms of rectangular FRP-RC columns. The interaction curves were developed following an identical approach as for steel-RC column, in which the outermost concrete fiber in compression reaches its ultimate compression strain. The parameters included in the study were compressive-to-tensile elastic modulus ratio, concrete compressive strength, and the ratio of the distance between the outermost layer of reinforcement to the height of the column cross-section in the direction of bending. The two failure mechanisms studied were premature compression failure and brittle tension failure. The premature compression failure of concrete columns reinforced with FRP could happen when the FRP bars in compression rapture occurs prior to crushing of the concrete. The possibility of this failure is very low as the ultimate compressive strain of FRP is more than ultimate compressive strain of concrete. The brittle tension failure occurs when the ultimate strain of the outermost tension FRP bars and the ultimate compression strain of concrete were reached prior to reaching pure flexure strength. Tension rupture of FRP bars in concrete column is more adverse as it is sudden and unstable. Thus, the concrete crushing failure is more desirable for FRP-RC columns. The conclusion drawn from the study were when the requirement of minimum FRP reinforcement ratio is satisfied; the brittle tension failure can be avoided, and failure may occur due to crushing of the concrete. To avoid premature compression failure, the author recommended that FRP bars should have ultimate compression strains greater than that of concrete compression strain ($\varepsilon_{cu} = 0.003$).

2.3.2 Behavior of hybrid-RC columns under compression

Pantelides et al. (2013) experimentally evaluated the axial load behaviour of concrete columns to determine whether replacing steel with GFRP spirals would reduce the corrosion of vertical steel bars in hybrid-reinforced columns. A total number of 10 spirally reinforced concrete short columns with 254 mm diameter and 711 mm height were casted. Six columns were confined with GFRP spiral and four with steel spiral. Four columns were hybrid-reinforced columns (steel as longitudinal reinforcement and GFRP spiral as transverse reinforcement) as shown in Figure 2.3. Corrosion cured hybrid-reinforced columns 11HYBCOR and 12HYBCOR showed no change in overall capacity compared to control hybrid-reinforced columns 9HYBCTL and 10HYBCTL as shown in Figure 2.4. From the experiments, the author concluded that hybrid-reinforced column and entirely GFRP-RC column achieved 87 % and 84 % of the axial capacity in comparison to the entirely steel-RC columns. Further, the author suggested to achieve a similar performance, hybrid-reinforced columns must be reinforced with a GFRP spiral with higher transverse reinforcement ratio. For GFRP-RC columns, the transverse as well as longitudinal reinforcement ratio should be higher.

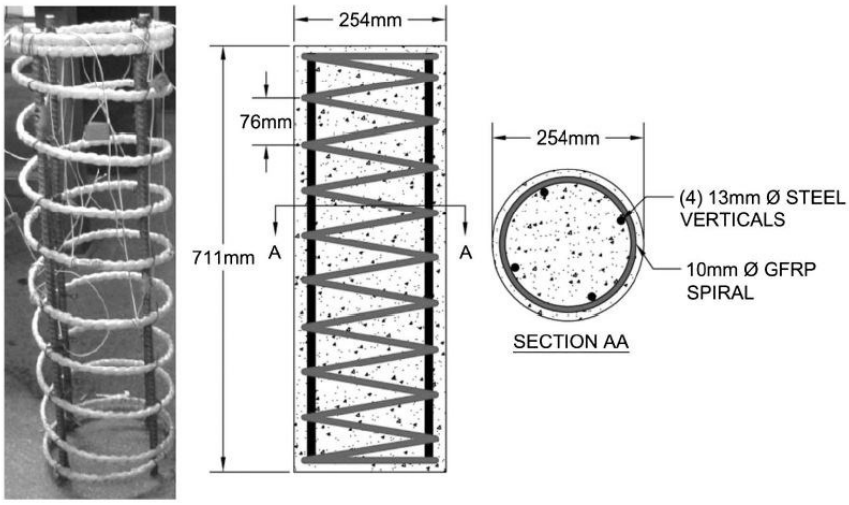

Figure 2.3- Specimen details of hybrid-reinforced column (Pantelides et al. 2013)

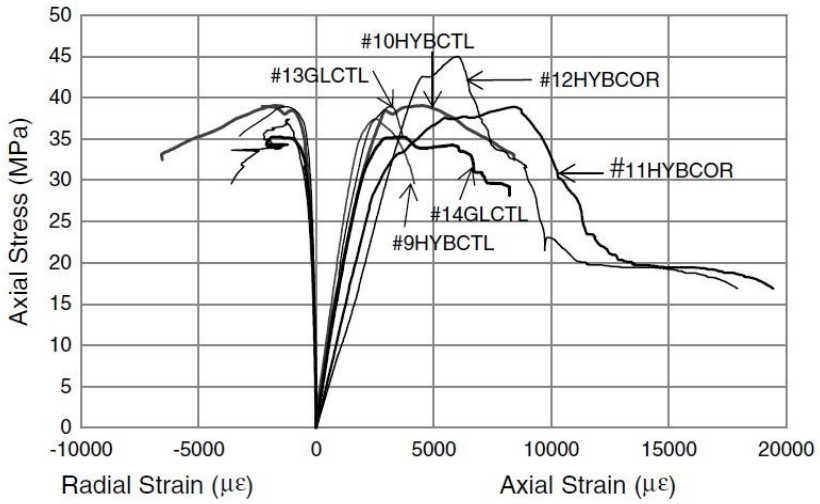

Figure 2.4- Stress-strain curves of columns with a GFRP spiral (Pantelides et al. 2013)

Experimental behavior of concentrically loaded FRP reinforced concrete columns with different reinforcement types were studied by Tobbi et al. (2014). Eleven columns were reinforced with longitudinal steel bars and FRP transverse reinforcement with 350 × 350 × 1400 mm dimension were casted and tested under axial compression. Observed failure mode of hybrid-reinforced columns was due to excessive longitudinal steel bar buckling which induced opening of FRP reinforcement as shown in Figure 2.5. Author reported that hybrid-reinforced columns showed good gains in compressive strength and ultimate axial strain with transverse FRP reinforcement restraining the expansion of the concrete core.

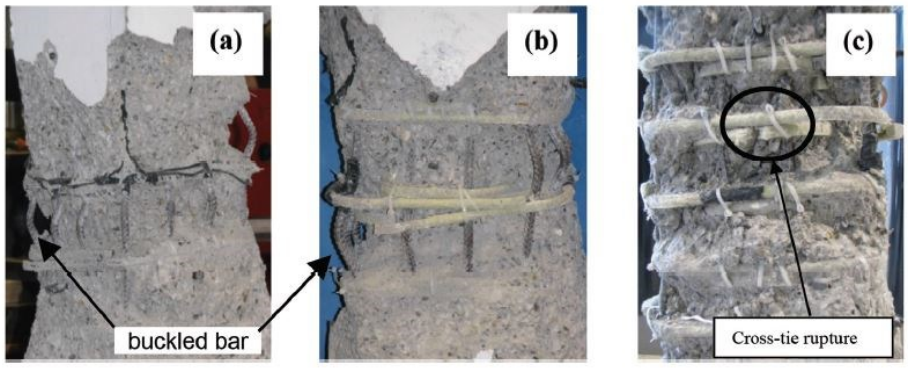

Figure 2.5- Failure hybrid-reinforced column under axial compression (Tobbi et al. 2014a)

2.3.3 Behaviour of Steel-RC columns under cyclic loading

A considerable amount of experimental and analytical research has been performed on the steel-reinforced concrete columns. Sheikh and Yeh (1990) experimentally examined the behaviour of steel reinforced concrete columns section confined by rectilinear ties under constant axial load and flexure to large inelastic deformations. The parameters studied were the distribution of longitudinal and lateral steel including unsupported longitudinal bars, and level of axial load. The test result indicates higher strength and ductility in large number of laterally supported longitudinal bars. The unsupported longitudinal bars perform better at small deformations, but buckle at large deformations, which results in brittle behaviour due to loss of confinement, especially under higher axial load. The level of axial load and lateral steel have significant effect on the behaviour of the columns, higher axial load decreases the strength and ductility whereas, increase in lateral steel improves the flexural behaviour of the column section.

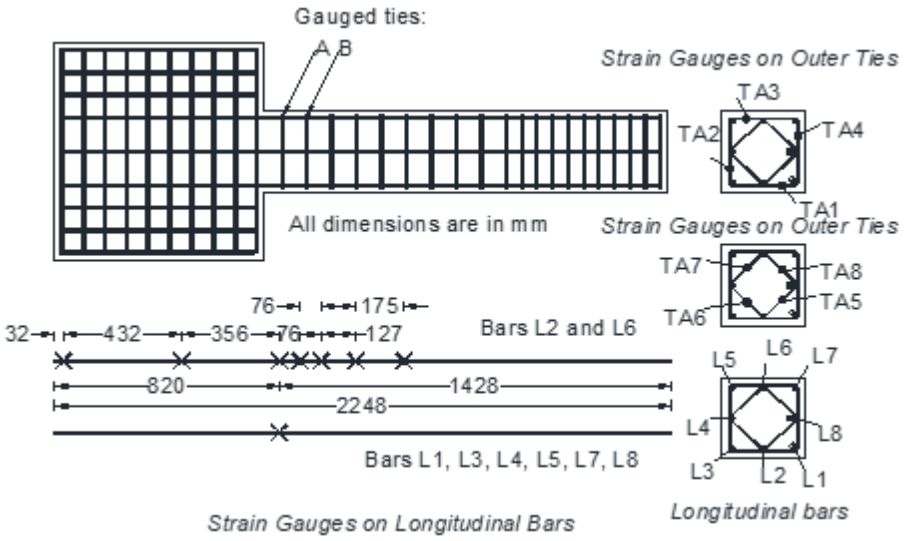

Figure 2.6- Specimen details with location of strain gauges (Bayrak and Sheikh 1998)

The behaviour of the Ultra-High strength concrete (UHSC) and high strength concrete (HSC) columns under reversed cyclic displacement were studied experimentally (Bayrak and Sheikh 1998). The specimen details with position of strain gauges shown in Figure 2.6.

The evaluation was based on effects of concrete strength, reinforcement configuration, amount of lateral reinforcement and level of axial load. The authors reported that if enough lateral steel were provided than the UHSC columns could behave in a ductile manner under high axial loads. In comparison to HSC and normal strength concrete (NSC) columns, the confinement provided by rectilinear ties had high impact on the ductile behaviour of UHSC columns. During the design of confinement reinforcement, the reinforcement configuration and axial load level must be considered.

Grira (1998) tested to develop new techniques for columns confinement. Thirty-one full scale reinforced concrete (RC) columns were constructed following the confinement requirements of ACI 318-95 (ACI Committee 318 1995). The variables of the study were concrete strength, longitudinal bar configuration, transverse reinforcement ratio, spacing of girds and axial load level. The author concluded that if the welding process does not affect the strength and ductility of reinforcement, then welded reinforcement grids can be utilize as transverse confinement reinforcement. The columns confined with FRP grids showed ductile response. The failure in most of the columns were caused by crushing of concrete, but in few columns' failure of FRP grids at the joints initiate the failure of column.

Saatcioglu and Baingo (1999) experimentally investigated the behaviour of full-scale HSC columns with circular cross-section tested under simulated seismic loading. The studied variables were concrete strength and cover; axial load level, spacing and type of transverse reinforcement. Author reported that the flexural failure was limited to one-third of column near footing. The post-yield displacement loading increased the cracking inducing spalling of concrete cover and gradual decay of strength. Observed failure progression in column RC-5 is shown in Figure 2.7. The proper confinement of the HSC columns, which are used for normal strength concrete can improve the deformability of the columns significantly. Further, it was reported that the spiral transverse reinforcement found to be more effective than the circular hoops in improving the stability of longitudinal bars during inelastic deformations.

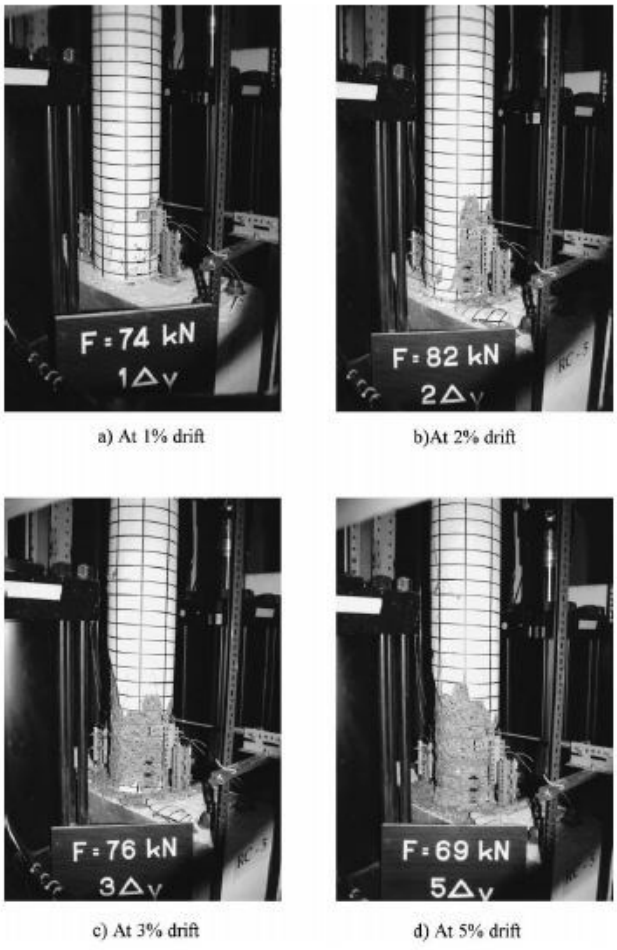

Figure 2.7- Failure progression (Saatcioglu and Baingo 1999)

Hwang and Yun (2004) experimentally investigated the performance of eight one-third scale HSC columns under constant axial compression (30%) and cyclic load-inducing bending moment to check the effects of tie configuration, transverse reinforcement volumetric ratio and tie yield strength. It was observed that the buckling of the longitudinal bars occurred after yielding of transverse steel ties. It was reported that use of high-strength transverse reinforcement in HSC columns results in larger spacing satisfying the seismic provisions of ACI 318-02 but leads to early buckling of longitudinal reinforcement. The HSC columns with only peripheral hoops exhibit more ductile behaviour than other tie configurations.

Bae and Bayrak (2008) conducted experimental and analytical study to predict the plastic hinge length of reinforced concrete columns including the effect of axial load level and shear span-to-depth ratio. From experimental results it was reported that specimens tested under high axial loads tend to develop longer plastic hinges, illustrating the influence of axial load level on plastic hinge length.

Ho (2011) proposed a theoretical equation based on flexural ductility analysis to correlate confinement steel volumetric ratio within critical region to core section area ratio, yield strength of longitudinal and transverse steel, longitudinal reinforcement ratio, concrete strength, and axial load level. Then, eight squared section high strength reinforced concrete (HSRC) columns were tested under constant compressive axial load and reversed cyclic inelastic displacements to verify the validity of the proposed equation. Based on the experimental results, it was suggested that the proposed design is suitable for HSRC columns of tall buildings in low to moderate seismic risk zones.

To reduce the higher construction costs, Yin et al. (2011) designed square-shaped reinforced concrete columns with different confinement configuration details and tested under axial compressive load only; combined axial load and lateral cyclic excursions. The confinement configuration details include conventional, welded wire grids, multi-spirals and combination of spirals and ties. The multi-spiral tie configuration was found to be effective confinement with comparative higher strength and ductility and reduced cost.

Caballero-Morrison et al., (2012) performed experimental tests on fourteen steel-fiber-reinforced NSC slender columns under combined constant axial and lateral cyclic loads (test specimen shown in Fig. 2.8). The studied variables were the slenderness, axial load level, transverse reinforcement ratio and steel-fiber volumetric ratio. The test specimens were designed to represent two semi-columns of adjacent storeys connected by stub which simulate the stiffening effect of a column-foundation joint or, an intermediate slab. From the experimental results, it was concluded that the deformation capacity depends on the test variables. The steel fibers into the concrete mixture helps in the improvement of

deformation capacity. A minimum transverse reinforcement criterion is required to enhance the effectiveness of the steel fibers.

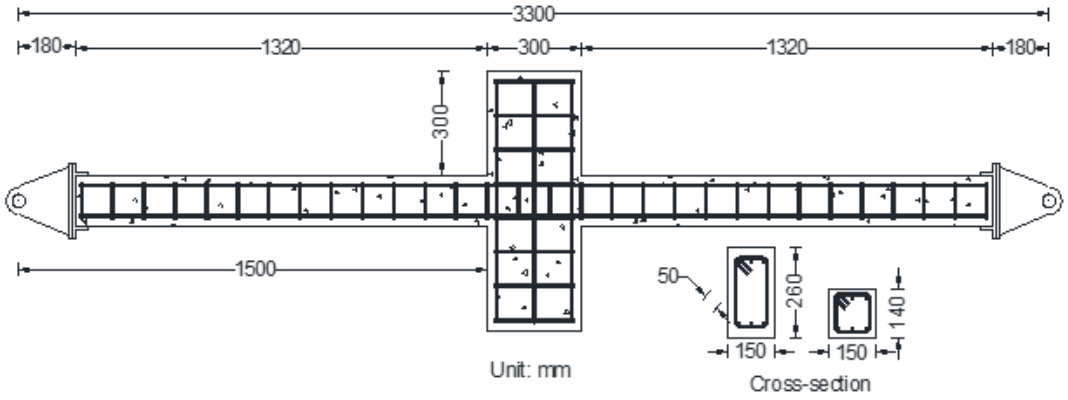

Figure 2.8- Specimens details of slender column (Caballero-Morrison et al. 2012)

2.3.4 Behaviour of FRP-RC columns under cyclic loading

Sharbatdar (2003) tested FRP bars and grids reinforced concrete columns and beams under monotonic and reversed cyclic loading. Column dimensions with FRP grids is shown in Figure 2.9. The main objective of the research was to develop detailing requirements for FRP reinforced concrete columns and beams. Ten full-scale CFRP reinforced concrete columns were tested under constant axial compression and reversal lateral deformations considering the variables such as spacing of transverse reinforcement, longitudinal bar arrangements, axial load level and shear span. The author concluded that increasing the confinement reinforcement ratio in column section following CSA S806 (2002) increased the deformability with enough lateral drift. Columns with twelve longitudinal bars arrangement showed better strength and deformability in flexural dominant long columns. CFRP reinforced columns under high axial loads exhibit higher lateral force but showed reduction in the inelastic deformability in comparison to columns under low axial loads.

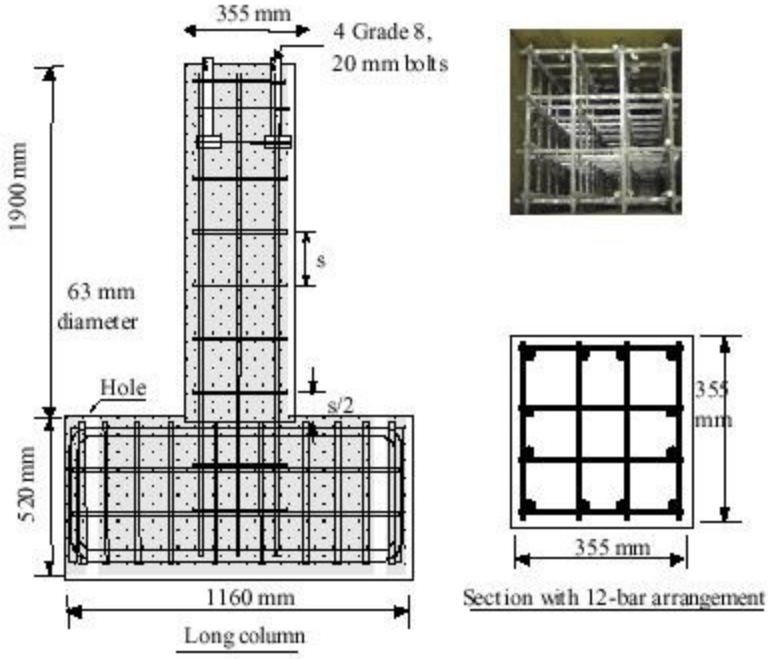

Figure 2.9- Specimen details (Sharbatdar 2003)

Choo et al. (2006) developed the axial load-moment curvature relationships to predict the behaviour of FRP-RC columns using ultimate strength approach as well as examined the slenderness effects of FRP reinforced concrete columns using numerical integration technique. Based on the analytical studies, it was concluded that the FRP-RC column cross-section strength interaction diagram showed a failure point before reaching the pure bending condition which classified as brittle-tension failure. Further, it was suggested that ignoring the contribution of the FRP reinforcement in compression zone may be conservative if the compressive failure does not occur in FRP bars which can be ensure by checking the ultimate compressive strain in FRP reinforcing bars.

Tavassoli et al. (2015) experimentally tested nine full-scale glass fiber-reinforced polymer (GFRP) reinforced circular columns (specimens details shown in Fig. 2.10) under simulated seismic loads with different variables such as GFRP bar type, column type, concrete strength, axial load level, and amounts of FRP and steel confinement. From the experimental results, GFRP bars reinforced concrete circular columns showed a stable

performance than steel bars as well as accomplished higher lateral drift ratio than the design requirement by CSA S806 (2012). Furthermore, it was concluded that the amount and detailing of FRP transverse reinforcement influenced the ductility of the GFRP RC columns when subjected to higher axial loads. Under higher axial loads, columns showed lower levels of ductility in comparison to low axial loads. With increased deformation, the GFRP spirals were found to be effective in increasing the confinement level.

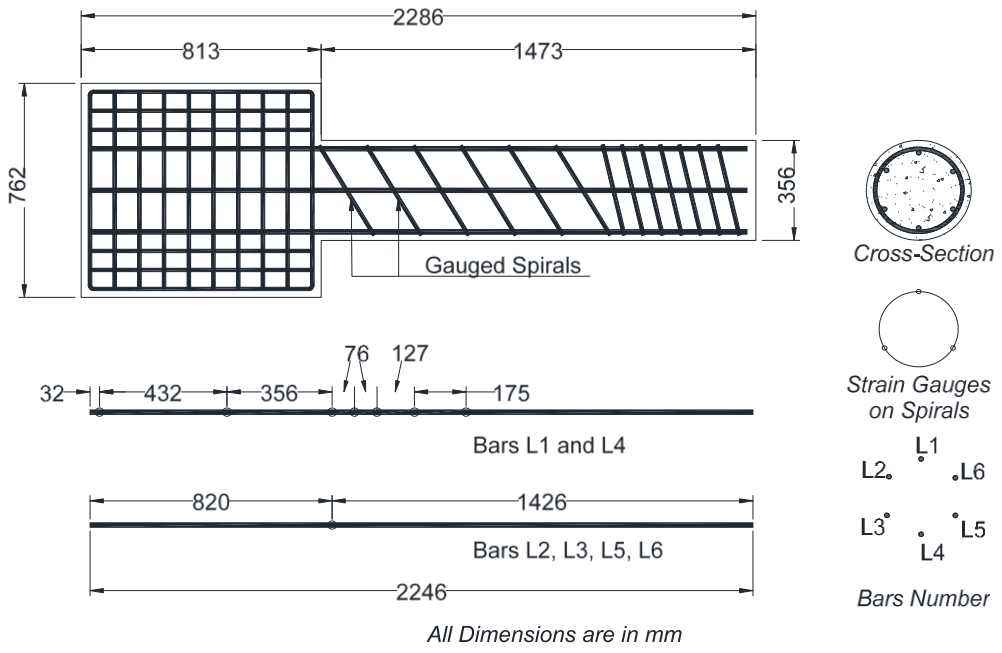

Figure 2.10- Specimens details with strain gauges location (Tavassoli et al. 2015)

Ali and El-salakawy (2015) investigated the seismic behaviour of concrete columns internally reinforced with GFRP bars and stirrups. One control with steel reinforcement and seven GFRP reinforcement full-scale columns with variables reinforcement type, longitudinal reinforcement ratio, stirrup spacing, and axial load level were tested under combined constant axial compression and quasi-static cyclic load. The plastic hinge region decreases with increase in the spacing of the transverse GFRP reinforcement was reported as shown in Figure 2.11. The authors concluded that contrast to steel RC column, GFRP

RC columns absorbed one-half of the cumulative energy during the reversed cyclic loading. Low level of deformability was reported with increase in the lateral capacity for GFRP columns with higher reinforcement ratio. Increasing the axial load, adversely affect the performance of the columns at the failure. The GFRP transverse reinforcement found to be more effective in confinement of the concrete core up to failure.

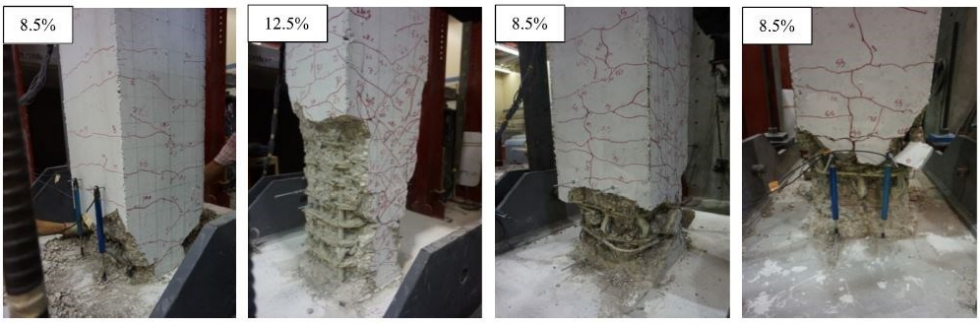

Figure 2.11- Reinforcement details (Ali and El-salakawy 2015)

To check the performance of GFRP bars reinforced concrete columns under constant axial compression and quasi-static cyclic load. Elshamandy et al. (2018) tested nine full-scale concrete columns reinforced with GFRP bars and two columns reinforced with steel reinforcement for comparison. The studied variables were different detailing configurations (shown in Fig. 2.12), longitudinal reinforcement ratios, volumetric transverse reinforcement ratio and axial load level. From the experimental observations, a stable behaviour of the GFRP-reinforced columns was reported. Increasing the axial load ratio reduces the ductility of the GFRP-reinforced columns. Further, the GFRP rectilinear spirals and cross ties performs better then steel transverse reinforcement and improves the confinement of concrete core which delays the crushing of concrete. Also, it was reported that the size of the longitudinal reinforcement influences the transverse reinforcement requirement.

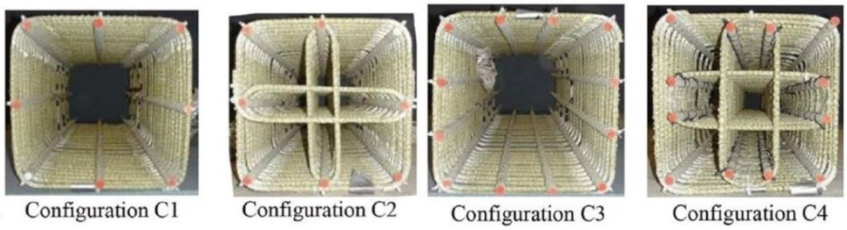

Figure 2.12- Different configurations details (Elshamandy et al. 2018)

2.3.5 Behaviour of hybrid-RC columns under cyclic loading

Figure 2.13- Plastic hinge region of circular columns (Tavassoli and Sheikh 2017)

The feasibility of using GFRP spiral as transverse reinforcement and steel as longitudinal reinforcement in reinforced concrete columns subjected to simulated earthquake forces was addressed by Tavassoli and Sheikh (2017). Experimental study consists of casting and testing of seven circular concrete columns of 1470 mm long and 356 mm. Parameters under investigation were axial load ratio and transverse GFRP reinforcement ratio. The buckling of longitudinal steel bar after GFRP spiral ruptured were reported in columns with closely spaced transverse reinforcement. Column failure was due to a combination of buckling of longitudinal bars with crushing of concrete core which led to drop in axial load were

observed and reported as shown in Figure 2.13. The author concluded that the overall behavior of studied hybrid-reinforced column was similar to those confined with steel. Further, the decrease in GFRP spiral pitch improved the performance of columns resulting in a more ductile behavior.

2.4 SUMMARY

From the review of tested steel RC columns subjected to simulated seismic loading, it is evident that proper confinement of the plastic hinge region is the necessary criteria for the ductile behaviour during an earthquake event. Recent tests on concrete columns reinforced with GFRP bars and ties showed that spacing of transverse reinforcement has impact on the behavior of the column. The proper confinement of concrete core is essential to enhance its strength and deformability. GFRP-reinforced column under axial compression should be reinforced with higher longitudinal and transverse ratio to achieve similar level of behavior compared to steel-reinforced column was reported in literature. Thus, there is a need to verify performance of such GFRP-reinforced concrete columns under simulated seismic loading. Hybrid-reinforced Column reinforced with longitudinal steel and confined with transverse GFRP reinforcement exhibited better performance. However, the reported research in literature is limited to circular cross section. Thus, it is required to verify the seismic performance of such columns with rectangular cross section.

Chapter 3
EXPERIMENTAL PROGRAM

3.1 GENERAL

The objective of the present experimental program is to examine the confinement effect of GFRP spirals and cross ties in reinforced concrete columns. To fulfill the objective; twelve columns were casted and tested under combined constant axial compression and quasi-static reversed cyclic loading. This chapter deals with different design criteria available in codes for design of columns, details of test specimen, preparation of specimen, instrumentation, test set-up and loading procedure.

3.2 DESIGN PHILOSOPHY

For an earthquake resistant structure, the inelastic response which provides ductility is significant for maintaining the strength of the structure. The locations where inelastic deformations may occur and as a response dissipate the absorbed energy is termed as plastic hinge. The structure should have enough confinement or transverse reinforcement in plastic hinge zone to avoid failure due to inelastic shear deformations. The earthquake resistant structure follows strong column-weak beam design philosophy which looks for seismic energy dissipation first in the well-confined beam plastic hinges whereas, a column plastic hinge is yet to form at the base of the column as shown in Figure 1.1.

The test specimens were designed according to the available design codes (CSA and ACI) and previous research on FRP-reinforced concrete columns (Choo et al., 2006; Tavassoli et al., 2015; Ali & El-salakawy, 2015; Elshamandy et al., 2018) to reach an adequate number of test specimens for the research study with variable parameters. The GFRP-RC columns were designed following the CSA S806-12 design code; the assumptions and

recommendations of ACI 318-14; ACI 440.1R-15 and moreover the recommendations from the previous research. The design code provisions for both steel and FRP-RC columns are discussed in the following sections.

3.3 DESIGN CODE PROVISIONS

3.3.1 Design for flexure and axial load

According to design code provisions CSA S806 2012- clause 8.4.1, ACI 440.1R 2015- clause 7.1, CSA A23.3 2014, clause 10.1 and ACI Committee 318 2014, clause 22.2, the design of flexure for steel and FRP reinforced concrete can be based on same assumptions with taking into account the difference in material behaviour. The assumptions for designing the section are as follows:

- Plane section remains plane after bending (i.e., the strain in concrete and steel or FRP bars at any level is proportional to the distance from the neutral axis).
- The maximum strain at the concrete compression fiber is 0.0035.
- The tensile strength of concrete is ignored for tensile strength calculations.
- Perfect bond exists between the concrete and the reinforcement.
- The compressive strength of the FRP is neglected.
- The FRP has linear elastic stress-strain relationship up to failure.

3.3.1.1 *Canadian code for steel (CSA A23.3, 2014)*

In addition to above assumptions, the design for flexure of steel section requires the following limitations:

- When the tension reinforcement reaches its yield strain, the concrete in compression should reach its maximum strain of 0.0035 (balanced strain conditions) (clause 10.1.4).

- The longitudinal reinforcement should not be less than 1 % of the gross area, A_g of the section and should not be more than 8 % of the gross area, A_g , of the section including regions containing lap splices. But the maximum value can be limited to 4 % to overcome practical difficulties in placing and compacting the concrete. (clause 10.9.1 and 10.9.2).

- The minimum number of longitudinal reinforcing bars in compression should be four for rectangular or circular ties and six for spirals with spiral reinforcement ratio should not be less than: (clause 10.9.3 and 10.9.4)

$$\rho_s = 0.5\left(\frac{A_g}{A_c} - 1\right)^{1.4} \frac{f_c^{'}}{f_y} \qquad 3.1$$

where,

f_y = specified yield strength of spiral reinforcement (< 500 MPa).

A_c = area of the core of spirally reinforced compression member measured to outside diameter of spiral.

- The maximum factored axial load resistance $P_{r,\max}$, of compression members should be calculated as follows:

a) For spirally reinforced columns:

$$P_{r,\max} = 0.90 P_{ro} \qquad 3.2$$

b) For tied columns:

$$P_{r,\max} = 0.80 P_{ro} \qquad 3.3$$

where,

$$P_{ro} = \alpha_1 \phi_c f_c^{'}\left(A_g - A_{st}\right) + \phi_s f_y A_{st} \qquad 3.4$$

A_{st} = total area of the longitudinal reinforcement.

ϕ_s = resistance factor for steel.

f_y = yield strength of steel.

The moment can be calculated by using plane section analysis to draw the axial force-moment interaction curve.

3.3.1.2 *American code for steel (ACI Committee 318 2014)*

The ACI committee 318 (2014), according to clause 22.2.2.1 assume upper strain limit in concrete to be 0.003 instead of 0.0035. Most of the conditions and limitations are identical with the Canadian code (CSA A23.3-14). The maximum axial strength, $P_{n,\max}$ should be greater than the nominal axial strength, P_n in the compression member which can be calculated using Table 22.4.2.1 (clauses 10.5.2.1 and 22.4.2.1). The equations are as follows:

a) For spirally reinforced columns:

$$P_{n,\max} = 0.85P_o \tag{3.5}$$

b) For tied columns:

$$P_{n,\max} = 0.80P_o \tag{3.6}$$

where,

$$P_o = 0.85f_c^{'}\left(A_g - A_{st}\right) + f_y A_{st} \tag{3.7}$$

3.3.1.3 *Canadian code for FRP (CSA S806 2012)*

Following the provision of clause 8.2.1, CSA S806 2012, the design of the section shall be such that the failure of all FRP reinforced concrete section is initiated by crushing of the concrete in the compression zone. Because of concrete crushing, the flexure member exhibits some plastic behaviour before failure in FRP reinforced members. Thus, the over-reinforced section should be followed to prevent sudden failure (brittle failure) due to FRP bar rupture. For over-reinforced section, the assumed strain in the concrete at extreme compression fiber is 0.0035.

Relationship between the compressive stress and concrete strain may be based on stress-strain curves. It can be satisfied by an equivalent rectangular concrete stress distribution defined by a concrete stress of $\alpha_1\phi_c f_c^{'}$ which is assumed to be uniformly distributed over an equivalent compression zones between the edges of the cross-section and a straight line parallel to the neutral axis at a distance $a = \beta_1 c$ from the extreme fiber of compression strain as shown in Figure 3.1. The factors α_1 and β_1 shall be taken as follows (clause 8.4.1.5):

$$\alpha_1 = 0.85 - 0.0015 f_c^{'} \geq 0.67 \quad 3.8$$

$$\beta_1 = 0.97 - 0.0025 f_c^{'} \geq 0.67 \quad 3.9$$

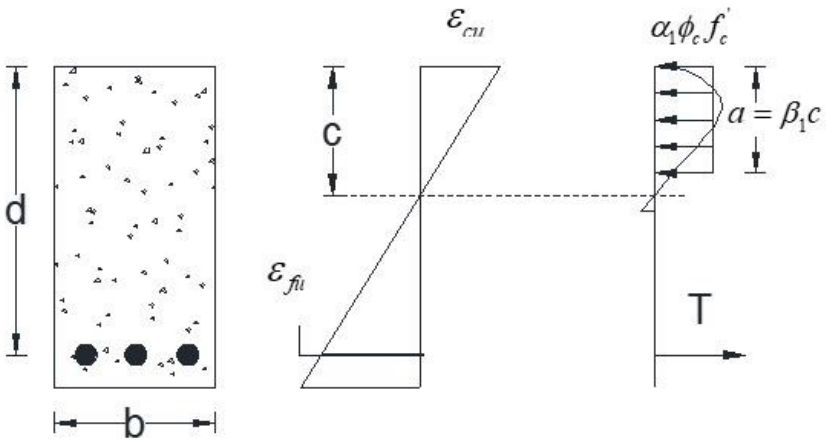

Figure 3.1- Strain and stress distribution at ultimate (balanced condition)

where,

c is distance from extreme compression fiber to neutral axis, it should be measured in a direction perpendicular to neutral axis and ϕ_c is resistance factor for concrete.

To ensure compression concrete failure, the actual longitudinal reinforcement ratio should be greater than the balanced reinforcement ratio i.e.

$$\rho_{frp} < \rho_{frpb} \tag{3.10}$$

where,

$$\rho_{frp} = {A_{frp}}/{bd} \tag{3.11}$$

$$\rho_{frpb} = \alpha_1 \beta_1 \frac{\phi_c}{\phi_f} \frac{f_c^{'}}{f_{frpu}} \left(\frac{\varepsilon_{cu}}{\varepsilon_{cu} + \varepsilon_{fu}} \right) \tag{3.12}$$

ϕ_f is resistance factor for FRP, 1.0, f_{frpu} is ultimate tensile strength of FRP, ε_{cu} is ultimate strain in concrete, 0.0035 and ε_{fu} is strain in FRP in tension at extreme fiber.

For the over-reinforced section, the stress in FRP bars at crushing concrete failure, f_{frp} can be computed as

$$f_{frp} = 0.5 E_{frp} \varepsilon_{cu} \left[\left(1 + \frac{4\alpha_1 \beta_1 f_c^{'}}{\rho_{frp} E_{frp} \varepsilon_{cu}} \right)^{1/2} - 1 \right] \tag{3.13}$$

where, E_{frp} is tensile modulus of elasticity for FRP bars.

The moment of resistance can be computed using the following equation:

$$M_r = A_{frp} f_{frp} \phi_f \left(d - \frac{\beta_1 c}{2} \right) \tag{3.14}$$

According to clause 8.4.3.6, the maximum factored axial load resistance, $P_{r,\max}$, of compression members shall be:

a) For spirally reinforced columns:

$$P_{r,\max} = 0.85 P_{ro} \tag{3.15}$$

b) For tied columns:

$$P_{r,\max} = 0.80P_{ro} \tag{3.15}$$

3.3.1.4 *American code for FRP (ACI Committee 440 2015)*

According to clause 7.2, for balanced FRP reinforcement ratio can be calculated as

$$\rho_{frpb} = 0.85\beta_1 \frac{f_c^{'}}{f_{frpu}} \frac{E_{frp}\varepsilon_{cu}}{E_{frp}\varepsilon_{cu} + \varepsilon_{fu}} \tag{3.16}$$

For $\rho_{frp} > \rho_{frpb}$, the stress in FRP bars, f_{frp} and the flexure moment, M_r at the crushing concrete failure can be computed as

$$f_{frp} = E_{frp}\varepsilon_{cu} \frac{\beta_1 d - \alpha}{\alpha} \tag{3.17}$$

$$M_r = A_{frp} f_{frp} \left(d - \frac{\alpha}{2} \right) \tag{3.18}$$

where,

$$\alpha = \frac{A_{frp} f_{frp}}{0.85 f_c^{'} b} \tag{3.19}$$

3.3.2 Design for shear and confinement

3.3.2.1 *Canadian code for steel (CSA A23.3, 2014)*

According to clause 11.3.3, the factored shear resistance can be computed as

$$V_r = V_c + V_s \tag{3.20}$$

where,

$$V_r \text{ should be less than } V_{r\max} = 0.25\phi_c f_c^{'} b_w d_v \tag{3.21}$$

$$V_c = \phi_c \lambda \beta \sqrt{f_c^{'}} b_w d_v \tag{3.22}$$

$$V_s = \frac{\phi_s A_v f_y d_v \cot\theta}{s} \tag{3.23}$$

b_w is minimum effective web width, d_v is effective shear depth, greater of $0.9d$ or $0.72h$, λ is factor to account for low-density concrete, 1.0 and β is factor to account for shear

resistance of cracked concrete. See clauses 11.3.6.2 and 11.3.6.3 for simplified method. For general method, see clause 11.3.6.4, A_v is area of shear reinforcement within a distance s, θ is angle of inclination of diagonal compressive stresses to the longitudinal axis of the member, s is center to center spacing of transverse reinforcement and h is overall thickness or height of the member.

According to clause 11.3.8.1, maximum spacing of transverse reinforcement should be less than $0.7d_v$ or 600 mm but if factored shear force $V_f > 0.125\lambda\phi_c f_c' b_w d_v$, the maximum spacings should be reduced by one-half.

Minimum shear reinforcement (clauses 11.2.8.1 and 11.2.8.2), should be

$$A_v \geq 0.06\sqrt{f_c'}\frac{b_w s}{f_y} \qquad 3.24$$

3.3.2.1.1 Special provisions for seismic design

The area of longitudinal reinforcement should not be less than 1.0% and more than 6.0% of the gross area, A_g of the section (clause 21.3.2.5.1).

The confinement reinforcement should satisfy the following:

a) The volumetric ratio of circular hoop reinforcement, ρ_s, should not be less than (clause 21.2.8.2)

$$\rho_s = C_c k_p \frac{f_c'}{f_{yh}} \qquad 3.25$$

where, C_c = 0.3 for systems with ductility force modification factor R_d = 2.0 or 2.5 and 0.4 for systems with $R_d > 2.5$.

k_p is axial load ratio = $P_f / A_g \alpha_1 f_c'$.

f_{yh} is yield strength of hoop reinforcement < 500 MPa.

b) The total effective area of rectangular hoop reinforcement, A_{sh} , should be larger of the following (cl. 21.2.8.2):

$$A_{sh} = C_h k_n k_p \frac{A_g f_c^{'}}{A_{ch} f_{yh}} s h_c \quad 3.26$$

$$A_{sh} = 0.09 \frac{f_c^{'}}{f_{yh}} s h_c \quad 3.27$$

where,

$C_h = 0.15$ for $R_d = 2.0$ or $2.5 / 0.2$ for $R_d > 2.5$.

k_n = factor to account for effectiveness of transverse reinforcement = $n_l / (n_l - 2)$, n_l , total number of longitudinal bars in the column that are laterally supported by the corner of the hoops or hooks or seismic cross ties.

A_{ch} = cross-section area of the core.

h_c =dimension of concrete core of rectangular section measured perpendicular to the direction of the hoop bars to outside of peripheral hoop.

c) The maximum confinement reinforcement should not exceed the least of the following (clause 21.3.2.6.3):

- ¼ of the minimum member dimension.
- Six times the diameter of the smallest longitudinal bar.
- $s_x = 100 + \left(\frac{350 - h_x}{3} \right)$

where, h_x = maximum horizontal center to center spacing between longitudinal bars on all faces of the column that are laterally supported by seismic hoops or cross-ties legs (clause 21.4.4.3).

d) The confinement reinforcement should be provided over a length, l_0, from the face of each joint and on sides of any section where flexural yielding can occur. The length l_0 can be determined as (clause 21.3.2.6.5):

- Where $P_f \leq 0.5\phi_c A_g f_c^{'}$, l_0 should not be less than 1.5 times the largest cross-sectional dimension.
- Where $P_f > 0.5\phi_c A_g f_c^{'}$, l_0 should not be less than twice the largest cross-sectional dimension or 1/6th of clear span of the member.

The shear reinforcement should be designed to requirements of clause 11, with following:

- $\beta \leq 0.10$ and $\theta \geq 45^o$ should be used for point (d) above.
- The transverse reinforcement should be hoops or spirals.

3.3.2.2 *American code for steel (ACI Committee 318 2014)*

According to clause 22.5.1.1, the shear strength V_r at a section can be computed using equation $V_r = V_c + V_s$

3.20.

For (clauses 22.5.6.1 and 22.5.10.5.3)

$$V_c = 2\left(1 + \frac{N_c}{2000 A_g}\right)\lambda\sqrt{f_c^{'}}\, b_w d \qquad 3.28$$

$$V_s = \frac{A_v f_y d}{s} \qquad 3.29$$

According to clause 10.6.2.2, the minimum shear reinforcement $A_{v,\min}$ should be greater of $0.75\sqrt{f_c^{'}}\frac{b_w s}{f_{yt}}$ or $50\frac{b_w s}{f_{yt}}$.

The maximum spacing for ties should not exceed the least of $16d_b$ of longitudinal bar, $48d_b$ of tie bar, and smallest dimension of the member (clause 25.7.2.1).

For spirals, the volumetric spiral reinforcement ratio, $\rho_s \geq 0.45\left(\frac{A_g}{A_{sh}}-1\right)\frac{f_c'}{f_{yt}}$.

3.3.2.2.1 Special provisions for seismic design

According to clauses 18.4.3.3 and 18.7.5.1, at both ends of the column, hoops should be provided at spacing s over a length l_0, such that the spacing should not exceed the smallest of eight times the diameter of the smallest longitudinal bar, 24 times the diameter of the hoop bar, one-half of the smallest cross-sectional dimension of the column, 300 mm and the length l_0 should not be less than 1/6th of clear span of column, maximum cross-sectional dimension of column and 450 mm. The first hoop should be located not more than $s/2$ from the joint face.

The area of longitudinal reinforcement should not be less than 1 % and more than 6 % of the gross area, A_g of the section (clause 18.7.4.1).

The maximum confinement reinforcement should not exceed the least of the following:

- ¼ of the minimum member dimension.
- Six times the diameter of the smallest longitudinal bar.
- $s_x = 100 + \left(\frac{350 - h_x}{3}\right)$

The transverse reinforcement for columns of special moment frames should be according to Table 18.7.5.4 of ACI 318-14.

3.3.2.3 ***Canadian code for FRP (CSA S806 2012)***

According to clause 8.4.4.4, the factored shear resistance can be computed by:

$$V_r = V_c + V_{sf} \tag{3.30}$$

Provided that V_r should not exceed $V_{r,\max} = 0.22\phi_c f_c' b_w d_v$

where, shear strength of concrete (clauses 8.4.4.5 and 8.4.4.11),

$$V_c = \left[0.05\lambda\phi_c k_m k_r \left(f_c' \right)^{1/3} b_w d_v \right] k_s k_a \left(1 - \frac{N_f}{14A_g} \right) \tag{3.31}$$

Such that the quantity in the square bracket should not be greater than $0.22\phi_c \sqrt{f_c'} b_w d_v$ or less than $0.11\phi_c \sqrt{f_c'} b_w d_v$. The product of last two term $k_a \left(1 - \frac{N_f}{14A_g} \right)$ should not be taken greater than 3. The factored axial load normal to the cross-section occurring with factored shear force (V_f), N_f, should be taken negative for compression.

k_m = coefficient taken to account for the effect of moment at section on shear strength = $\sqrt{\frac{V_f d}{M_f}} \le 1.0$.

k_r = coefficient taken to account for the effect of reinforcement rigidity on its shear strength = $1 + \left(E_{frp} \rho_{fw} \right)^{1/3}$.

k_s = coefficient taken to account for the effect of member size on its shear strength = $\frac{750}{450 + d} \le 1.0$.

k_a = coefficient taken to account for the effect of arch action on member shear strength = $2.5 \le \frac{2.5}{\frac{M_f}{V_f d}} \ge 1.0$.

ρ_{fw} = longitudinal FRP reinforcement ratio.

$$V_{sf} = \frac{0.4\phi_f A_{fv} f_{fv} d_v}{s} \cot\theta \qquad 3.32$$

f_{fv} should not be greater than $0.005E_{frp}$.

A_{fv} is minimum area of transverse FRP shear reinforcement.

According to clause 8.4.5.2, the minimum shar reinforcement should be

$$A_{fv} = 0.07\sqrt{f_c'}\,\frac{b_w s}{0.4 f_{fv}} \qquad 3.33$$

where, f_{fv} should not be greater than 2000 MPa or $0.005E_{frp}$.

The minimum spacing of shear reinforcement, s, should not exceed $0.6d_v \cot\theta$ or 400 mm.

3.3.2.3.1 Special provisions for seismic design

According to clause 12.7.5.2, the transverse FRP reinforcement for a moment resisting frame member with both longitudinal and transverse FRP reinforcement should be provided in form of circular spirals, circular hoops, rectilinear hoops, overlapping hoops, grids, and cross ties. The required area of the transverse FRP reinforcement, A_{sh} should be computed using clauses 12.7.3.3 and 12.7.3.4.

$$A_{sh} = 14 s h_c \frac{f_c'}{f_{fh}} \left(\frac{A_g}{A_c} - 1\right) \frac{P}{P_o} \frac{\delta}{\sqrt{k_c}} \qquad 3.34$$

Where, $\frac{P}{P_o} \geq 0.2$

$\left(\frac{A_g}{A_c} - 1\right) \geq 0.3$

δ is design lateral drift ratio should not be less than 0.04 for columns with $R_d = 4.0$ and 0.025 for columns with $R_d = 2.5$.

f_{fh} is design stress in FRP transverse confinement reinforcement, lesser of $0.006E_{frp}$ or $\phi_f f_{frpu}$.

k_c = 1.0 for circular spirals and circular hoops or $0.15\sqrt{\frac{h_c}{s}\frac{h_c}{s_l}}$ for rectilinear reinforcement.

A_c is cross-sectional area of the core, h_c is cross-sectional dimension of the column core, and s_l is spacing of tie legs in the cross-sectional plane of the column.

The maximum space between the transverse reinforcement should not exceed the least of the following:

- 1/4th of the minimum member dimension.
- 150 mm.
- 6 times diameter of the smallest longitudinal bar.

The transverse reinforcement should be provided over the length, l_0, from each face. l_0 should not be less than the maximum of the following (clause 12.7.5.3):

- Depth of the member at the face of the joint or at the section where maximum moment can occur.
- 1/6th of the clear span of the member.
- 450 mm.

In rest of the column, the center-to-center spacing of transverse reinforcement should not be less than 150 mm.

3.3.2.4 *American code for FRP (ACI Committee 440 2015)*

According to clause 8.2, the nominal shear strength of a reinforced concrete cross-section, V_r is same as equation $V_r = V_c + V_{sf}$

3.30.

where,

$$V_c = 0.4\sqrt{f_c'}\, b_w (kd) \quad (3.35)$$

$$V_{sf} = \frac{A_{fv} f_{fv} d}{s} \quad (3.36)$$

$k = \sqrt{2\rho_f n_f + (\rho_f n_f)^2} - \rho_f n_f$ (clause 7.3.2.2b)

ρ_f = FRP longitudinal reinforcement ratio.

f_{fv} should be equal to $0.004E_{frp}$ but less than or equal to ultimate tensile strength of main bar f_{frpu}

According to clause 8.2.2, the minimum area of shear reinforcement should be

$$A_{fv,\min} = 0.35\frac{b_w s}{f_{fv}} \quad (3.37)$$

The maximum spacing of the vertical stirrups should be smaller of $d/2$ or 600 mm it ensures each shear crack is checked by at least one stirrup.

There is no special provision for the seismic design in this code.

3.4 DETAILS OF TEST SPECIMEN

The experimental program includes casting and testing of twelve (12) full-scale rectangular columns of 400 × 400 mm cross-sectional dimension with effective height of 1650 mm and overall height of 1850 mm. Eight columns were entirely reinforced with GFRP

reinforcement and rest four columns were hybrid-reinforced columns reinforced with longitudinal steel bars and transverse GFRP spiral and cross ties. All the columns were supported by footing (stub) of 600 mm height and 1200 × 1200 mm cross-sectional dimension. The stub was heavily reinforced with M20 steel bars. The dimensional details of the test specimen are shown in Figure 3.2. The length of the longitudinal bars embedded inside the stub was 550 mm which satisfies the requirement of the development length in CSA S806 (2012). A clear cover of 25 mm was maintained in all columns. Test specimen details are shown in Figure 3.3.

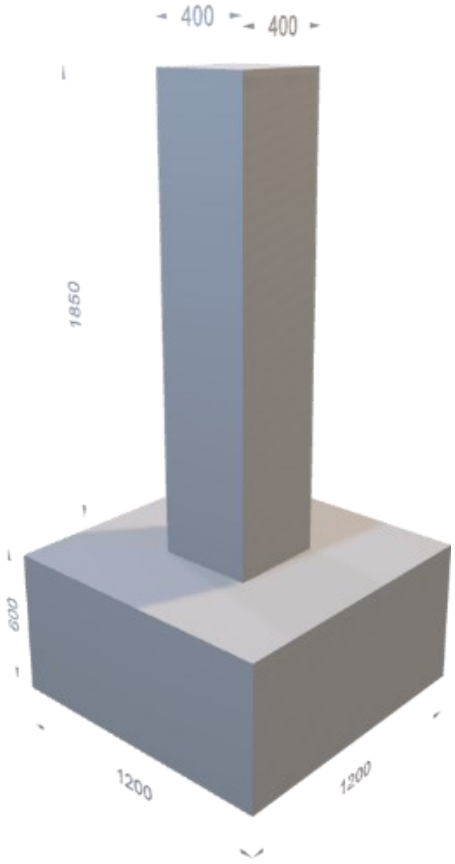

Figure 3.2- Dimensional details of test specimen (Unit: mm).

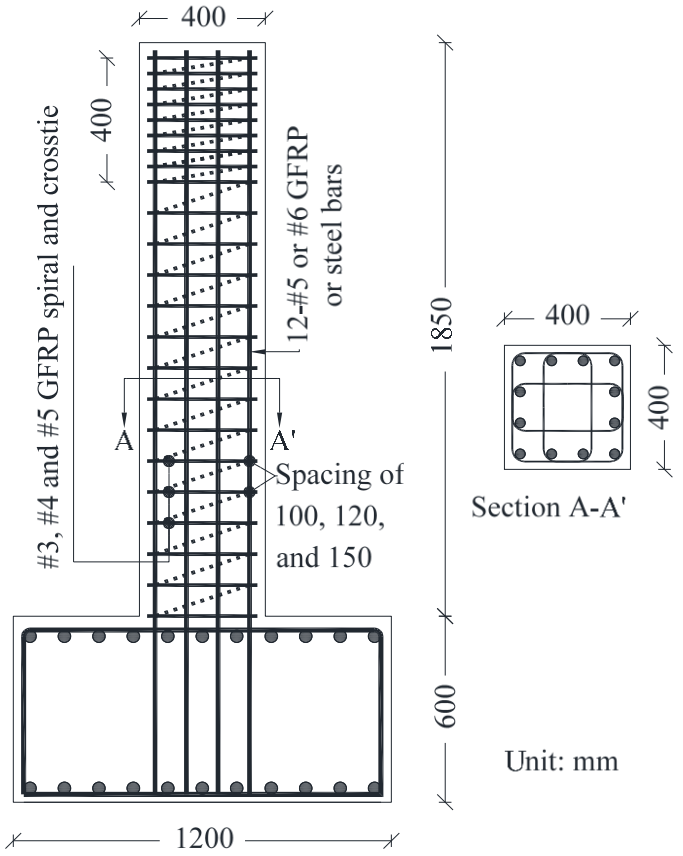

Figure 3.3- Test specimen details

The parameters under study were longitudinal reinforcement type, longitudinal reinforcement ratio, size and spacing of transverse reinforcement. From the review of past studies and equation 3.34, it is evident that confinement have a major role in the enhancement of deformability of the columns. The confinement of GFRP-RC column was represented by size of transverse reinforcement and its spacing near the plastic hinge region. Two different longitudinal reinforcement ratios (1.48% and 2.14%) satisfying the code recommendation were used with variable transverse reinforcement ratio for the verification of effect of the longitudinal reinforcement on the transverse FRP reinforcement. When increasing the axial load ratio (ALR), there was no significant improvement in the deformability and strength capacity of column as observed in the previous studies (Elshamandy et al. 2018; Tavassoli et al. 2015). Therefore, the axial loads

ratio of 20% of the column axial capacity; which is the minimum requirement as per design code CSA S806 (2012) was maintained for all test columns.

The specimens' identified as W#X-#Y-Z, where W represents type of column longitudinal reinforcement 'G' for GFRP and 'S' for steel bars. #X represents the size of the longitudinal bar (#5 and #6), as designated by the manufacturer. The third part (#Y) represents the size of GFRP transverse reinforcement (#3, #4 and #5). And the last part (Z) represents the spacing of the transverse GFRP reinforcement (100, 120 and 150). The spacing of transverse GFRP reinforcement satisfy the requirements of CSA S806 (2012) and AASHTO (2018) for bridge column. The details of the test specimens are provided in Table 3.1 and shown in Figure 3.3.

Table 3.1- Details of test specimens

Column	$f_c^{'}$ MPa	d_b mm	$\S$ mm	ρ_l %	ρ_{sv} %
G#5-#3-100	32.6	15.87	100	1.48	0.71
G#5-#4-100	31.6	15.87	100	1.48	1.27
G#5-#4-120	34.2	15.87	120	1.48	1.06
G#5-#4-150	33.5	15.87	150	1.48	0.85
G#6-#4-100	34.4	19.07	100	2.14	1.27
G#6-#5-100	34.4	19.07	100	2.14	1.98
G#6-#4-120	34.7	19.07	120	2.14	1.06
G#6-#4-150	34.1	19.07	150	2.14	0.85
S#5-#4-100	34.3	15.87	100	1.48	1.27
S#5-#4-120	34.6	15.87	120	1.48	1.06
S#5-#4-150	34.6	15.87	150	1.48	0.85
S#6-#4-100	35.6	19.05	100	2.14	1.27

where, $f_c^{'}$ is concrete compressive strength, d_b is the diameter of individual bar, $\S$ is spacing of transverse reinforcement, ρ_l is the longitudinal reinforcement ratio and ρ_{sv} is the transverse reinforcement ratio.

3.5 MATERIAL PROPERTIES

3.5.1 Concrete

The ready-mix normal weight concrete with a target compressive strength of 30 MPa and 50 MPa after 28 days were used for the casting of columns and stubs, respectively. The actual compressive strength of concrete for each specimen was determined by testing three-standard cylinder measuring 100 × 200 mm on the day of testing. The average concrete compressive strength of the concrete is listed in Table 3.1.

3.5.2 Reinforcement

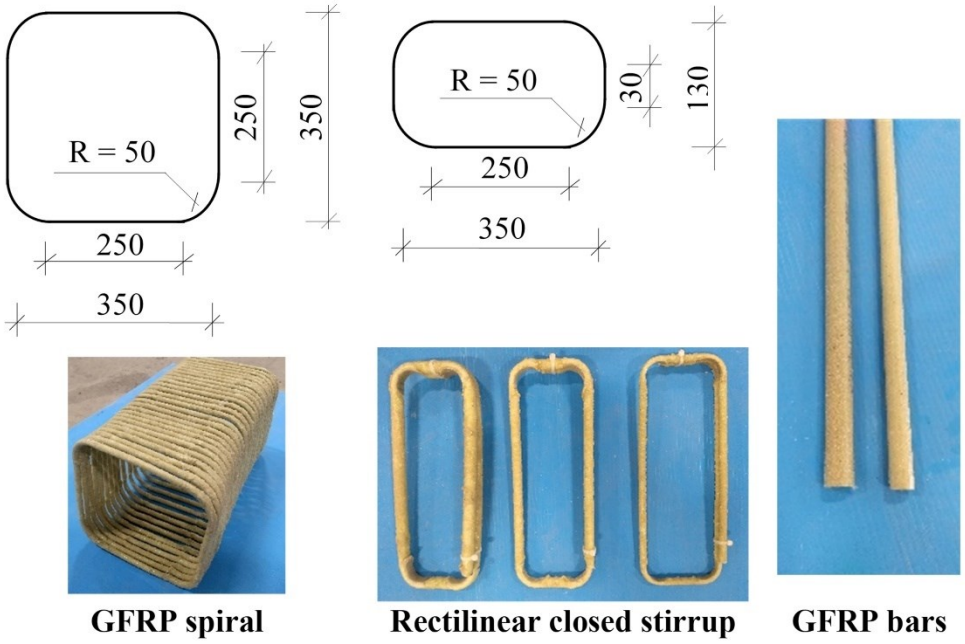

Figure 3.4- Details of the GFRP bars, spirals, and cross ties (unit: mm)

Grade 60-#5 and #6 longitudinal steel reinforcement were used in the columns. Table 3.2 provides the properties of the steel bar as given by the manufacturer. GFRP materials are supplied by Pultrall Inc. (Thetford Mines, Quebec). Sand-coated, Grade III, high modulus GFRP bars were used as longitudinal and transverse reinforcement conforming to CSA

S807 (2010). The type of resin and fiber used in the manufacturing were vinyl ester and E-glass, respectively. GFRP rectilinear spiral and cross tie were used in the study as shown in Figure 3.4. The tensile properties of the straight bars were determined by testing five samples according to ASTM-D7205 (2011); and the bent bars were tested according to ASTM D7914 (2014). The material properties of the GFRP reinforcing bars are presented in Table 3.2.

Table 3.2- Reinforcement material properties

Bar type		d_b (mm)	A_b (mm^2)	E_s (GPa)	f_y (MPa)	ε_y (%)
Straight	Steel #5	15.87	198	200	414	0.2
	Steel #6	19.05	284	200	414	0.2
Bar type		d_b (mm)	A_b (mm^2)	E_f (GPa)	f_{fu} (MPa)	ε_{fu} (%)
Straight	GFRP #5	15.87	198 (229) *	67	1433	2.13
	GFRP #6	19.07	285 (323) *	65	1399	2.16
Spiral and cross tie	GFRP #3	9.50	71 (95) *	56	1232	2.19
				-	691†	-
	GFRP #4	12.70	127 (151) *	63	1570	2.48
				-	800†	-
	GFRP #5	15.87	198 (234) *	60	1488	2.48
				-	749†	-

* Values in parentheses are the cross-sectional area calculated based on Annex A in CSA S806 (2012).
† Strength of bent portion of GFRP spirals and cross ties
where, d_b is the diameter of individual bar, A_b is the nominal cross-sectional area; E_s is the elastic modulus of steel; f_y is the steel yield strength; ε_y is the steel yielding strain; E_f is the modulus of elasticity of FRP; f_{fu} is the guaranteed tensile strength of FRP; and ε_{fu} is the ultimate strain of FRP

3.6 PREPARATION AND CASTING OF TEST SPECIMEN

Twelve column specimens were casted at the centre de mise à l'échelle (CME), Université de Sherbrooke. The formwork for the column and stub was constructed with the plywood and woods. The lateral movements of the formwork were restrained using the steel angles fixed with threaded rods. To fix the stub to the strong floor of the four polyvinyl chloride (PVC) pipes were placed at 1 m from each other to create holes to pass the DYWIDAG bars (high strength steel bars). Before the casting of stubs and columns, the inner surface of the formwork was coated by a layer of form-oil. The stub of all the columns were casted first then after two days, the columns were casted. The column was casted using pump and high slump value of 140 mm.

The various steps in the process of specimen preparation are as follows.

- Prepared stub formwork as shown in Figure 3.5.
- Placed PVC pipes and steel caging of stub as shown in Figure 3.6.
- Instrumentation of column cage with strain gauges Figure 3.7.
- Prepared column cage entirely reinforced with GFRP reinforcement and instrumentation with strain gauges as shown in Figure 3.8.
- Prepared column cage reinforced with longitudinal steel and transverse GFRP reinforcement and instrumentation with strain gauges as shown in Figure 3.9.
- Aligned column into the stub as shown in Figure 3.10.
- Aligning column formwork as shown in Figure 3.11.
- Casting of the stubs as shown in Figure 3.12.
- Column's casting using pump as shown in Figure 3.13.
- Prepared column for testing as shown in Figure 3.14.

Figure 3.5- Stub formwork

Figure 3.6- Placed PVC pipes and stub steel caging

(a) GFRP-reinforced column (b) Hybrid-reinforced column

Figure 3.7- Strain gauge installation

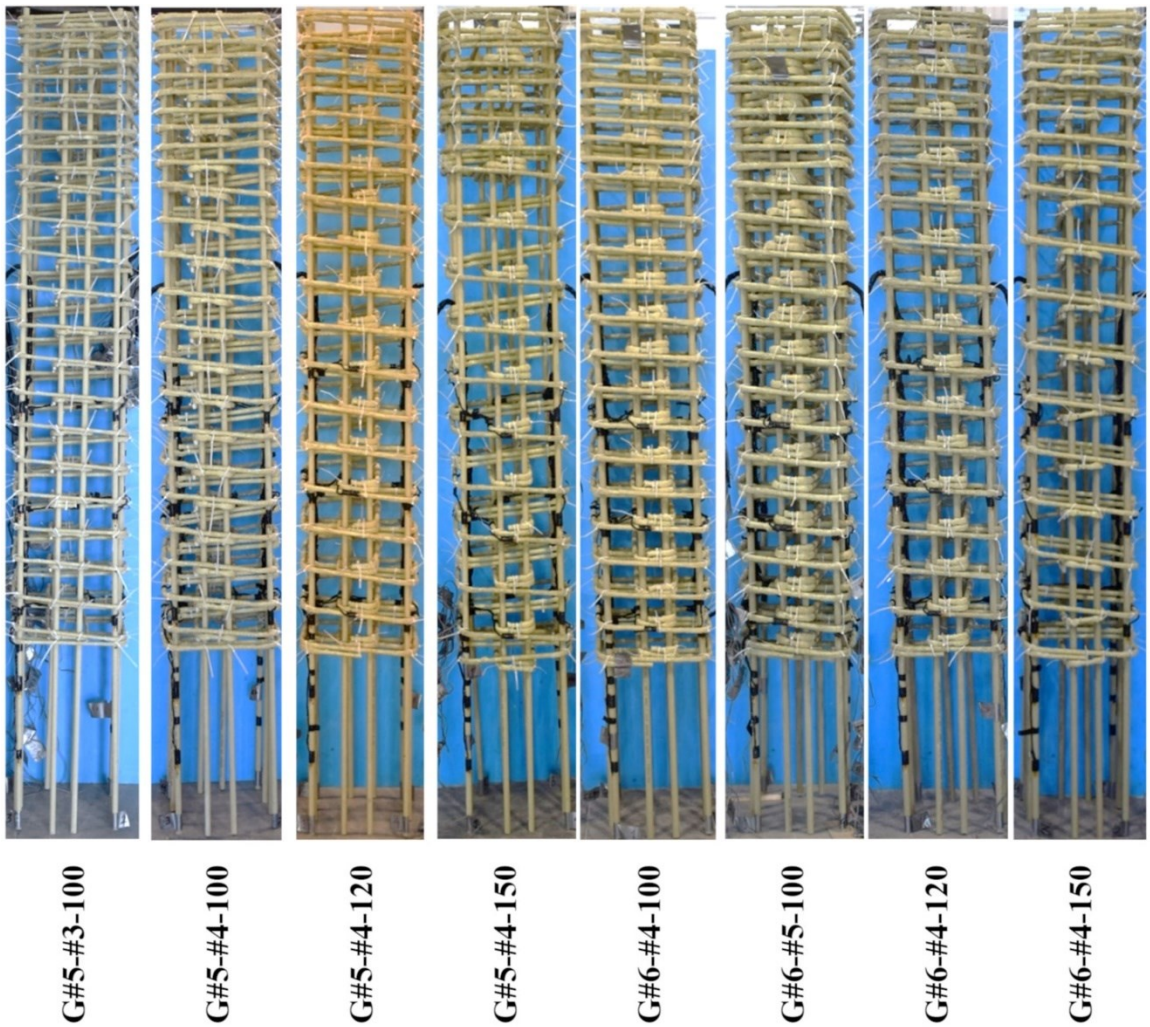

Figure 3.8- GFRP-reinforced column cage

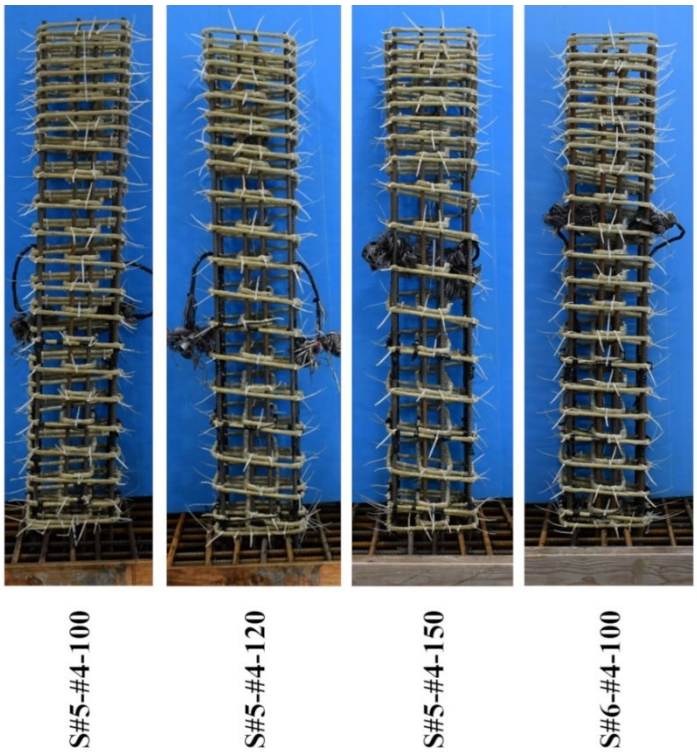

Figure 3.9- Hybrid-reinforced column cage

Figure 3.10- Placing column inside the stub steel cage

Figure 3.11- Covering the column cage with formwork.

Figure 3.12- Casting of stub

Figure 3.13- Casting of column

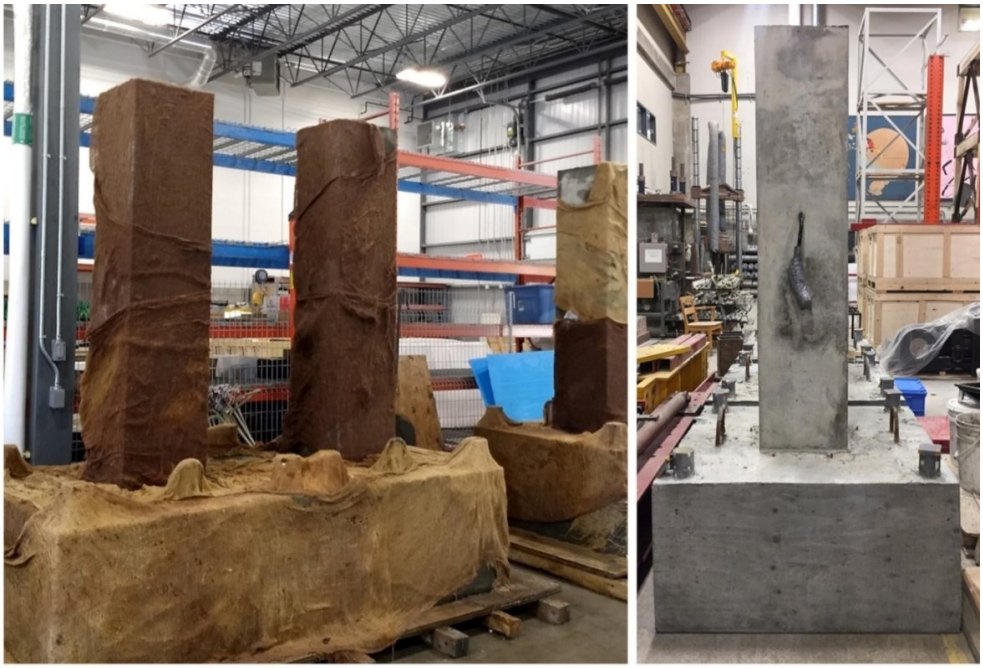

Figure 3.14- (a) Curing (b) casted column ready for testing

3.7 INSTRUMENTATION

All the test specimens were instrumented comprehensively to monitor strains, displacements, and rotations. To cover the essential plastic hinge, at different levels the

strain gauges and LVDTs were placed. The four corner bars, spiral and cross ties were instrumented with strain gauges at three levels 50, 350 and 650 mm from column-stub interface. Two strain gauges at two different location in diagonally opposite longitudinal bars were installed below the column-footing interface, to measure the strain variation inside the footing. They were installed at 250 and 450 mm from the column-footing base. Four LVDTs were installed horizontally at different position of the column height to measure the lateral displacement of the column. They were installed at the distance of 100, 400, 700 and 1650 mm from column-stub interface. To measure the curvature, six LVDTs were placed in both side of the test column at three different levels 100, 400 and 700 mm above column-stub interface. To check the sliding between the column and footing during the test, one LVDT was placed. Also, one more LVDT was installed after the first crack. The illustrative location of the strain gauges and LVDTs are shown in Figure 3.15.

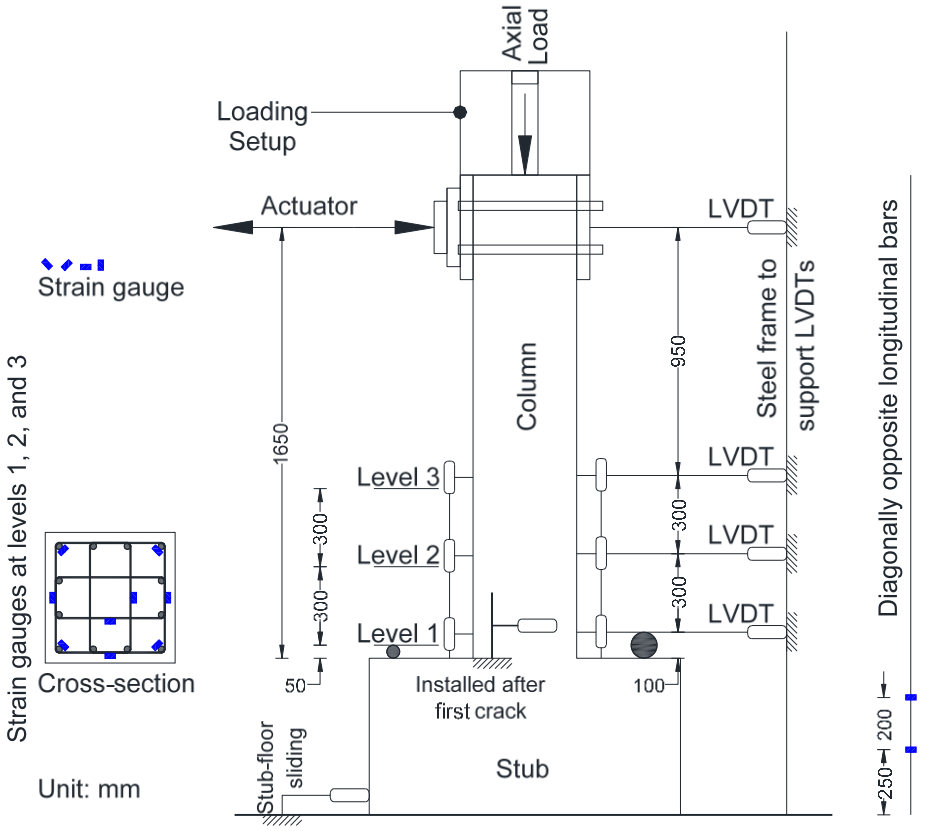

Figure 3.15- Strain gauges and LVDTs location

3.8 TEST SETUP

The test setup is shown in Figure 3.16. The columns were tested in a vertical upright position. A constant axial load of 20% of axial capacity of the test column was applied at the top. The test set-up was built at the structural laboratory of Université de Sherbrooke. The following steps were followed to build the set-up:

a) The test column was fixed to the laboratory strong floor using two steel beams and four 66 mm diameter DYWIDAG bars (high strength steel bars) to prevent the uplifting and sliding of the specimen during the test.

b) The lateral actuator was connected to the column tip through two plates and six high strength threaded rods of 40 mm diameter.

c) MTS hydraulic actuator of 500 kN capacity was attached to the laboratory strong reaction wall.

d) The axial load was applied through two hydraulic jacks of 100 tonnes of capacity and using steel rigid beam which is on the top of the column. The axial load transferred through using two high strength 66 mm diameter DYWIDAG steel bars placed on both side of the column. After reaching the axial load of 20% of column capacity, the axial load was maintained constant during the test.

Figure 3.16- Experimental setup

3.9 LOADING PROCEDURE

The axial load was applied and maintained constant after reaching 20% of the axial capacity of the test specimen. The testing was conducted under displacement control quasi-static reversed cyclic loading, to moderate applied displacements in each step. As the drift capacity of the test cannot be predicted accurately if the applied drift steps are too large or the drift steps are too small, the loading repetitions results in low maximum lateral strength and unnaturally more drift capacity. Too small drifts will also result in low energy dissipation due to small rate of change of energy stores, compared to the change in the natural seismic event. Hence, the small drift increment may avoid undesirable brittle failure of the test specimen that may occur during the major seismic event. According to clause 5.2, ACI 374.2R (2013), two parameters are essential in defining the loading history for the unidirectional load reversals: a) the increment of deformation control parameter to define each deformation level and b) the number of cycles at each deformation level. The drift ratio should be such that significant changes in the test specimen behaviour should be captured. The code suggested a minimum of two cycles at each deformation level is enough to cause damage related with the number of cycles at a given drift level. The selection of number of cycles at each level depends on the judgement of the researcher and the degradation characteristics of the test specimen. If the degradation is rapid, two cycles at each drift level may be appropriate to study wider range of specimen performance before the loss of most strength. The testing should be continued until the severe strength degradation is observed. Since, the test specimen in the study was new material GFRP bars, two cycles at each deformation level were selected. Further, the code (ACI 374.2R 2013) suggested tests performed to investigate hysteretic features of the specimen or to develop hysteretic models, may need one or more smaller deformation reversals within each drift level.

Displacement controlled cyclic loading was applied which was followed in previous research (Mohamed et al., 2014; Elshamandy et al., 2018). A typical displacement-based loading history is shown in Figure 3.17.

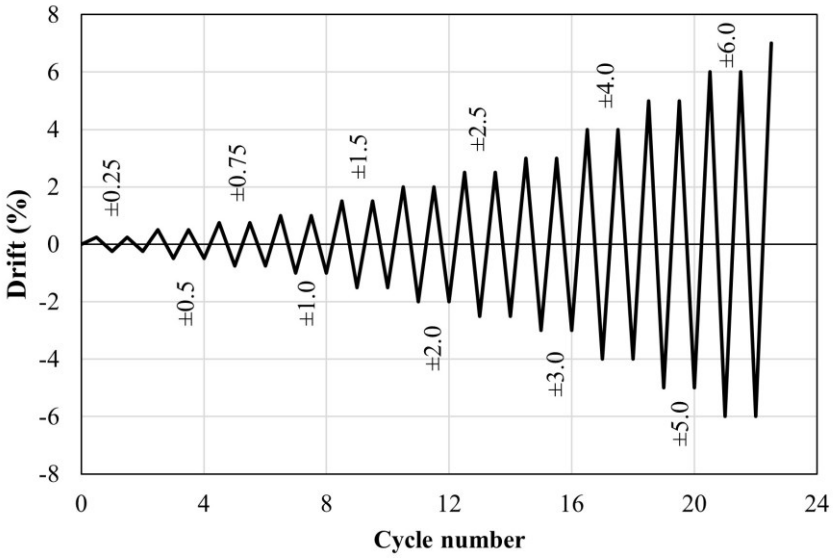

Figure 3.17- Load history for the quasi-static load reversal test

Chapter 4

BEHAVIOR OF GFRP-REINFORCED CONCRETE COLUMNS SUBJECTED TO SIMULATED SEISMIC LOAD

Comportement de colonnes en béton armé d'armature en PRFV soumises à une charge sismique simulée.

Foreword

Authors and affiliation:

- **Girish Narayan Prajapati**, Ph.D. Candidate, Department of Civil Engineering, Université de Sherbrooke, Sherbrooke, QC, Canada, J1K 2R1.
- **Ahmed Sabry Farghaly,** Research Associate, Department of Civil Engineering, Université de Sherbrooke, Sherbrooke, QC, Canada, J1K 2R1.
- **Brahim Benmokrane**, **FACI**, Professor of Civil Engineering and Tier-1 Canada Research Chair in Advanced Composite Materials for Civil Structures and NSERC Research Chair in Innovative FRP Reinforcement for Concrete Structures, Department of Civil Engineering, Université de Sherbrooke, Sherbrooke, QC, Canada, J1K 2R1.

Journal: ACI Structural Journal

Status: Accepted, June 2021

Abstract

This paper presents the results of an experimental study on concrete columns reinforced with glass fiber-reinforced polymer (GFRP) reinforcement under reversed cyclic lateral load. The investigation included testing of eight full-scale square concrete columns reinforced with GFRP bars, spirals, and cross ties and of a cross section of 400 × 400 mm (15.8 × 15.8 in) with a total height of 1850 mm (72.8 in). The parameters studied were the longitudinal reinforcement and transverse reinforcement ratios. The columns were reinforced with 12 longitudinal bars 15.9 mm (0.6 in.) in diameter and 19.1 mm (0.7 in.) in diameter. Spirals and cross ties measuring 9.5 mm (0.4 in.), 12.7 mm (0.5 in.), and 15.9 mm (0.6 in.) in diameter were used as transverse reinforcement. The specimens were subjected to cyclic lateral loading and constant axial loading of 20% the capacity of the column. The test results indicate that the longitudinal and transverse reinforcement ratios produced no significant changes in dissipated energy. The spacing of the lateral reinforcement influenced column strength and drift capacity at the lower longitudinal reinforcement ratio but did not significantly affect the columns at the higher longitudinal reinforcement ratio. GFRP spirals and cross ties affected the lateral strength and deformability of the column after spalling of the concrete cover. The displacement deformability index computed at a concrete compressive strain of 3000 με showed reasonably good prediction.

4.1 INTRODUCTION

The corrosion of the reinforcing steel is the major cause of deterioration in concrete structures. Rust causes the steel to expand, generating tensile stresses in the concrete that lead to cracking, delamination, and spalling. The outcomes can be loss of serviceability, reduction in load-carrying capacity of the structure, and eventual partial or full collapse when a natural calamity occurs. Recent studies found that such issues can be overcome by using fiber-reinforced polymers (FRPs) as reinforcing material. Unlike steel bars, FRP bars have high strength-to-weight ratios, high resistance, and high tensile strength, offering

structurally safe field alternatives for concrete members such as beams and slabs (El-Salakawy et al. 2005; Kassem et al. 2011). The stress–strain relationship of FRP bars, however, is linear elastic until failure, which raises concern about the use of FRP bars in concrete structures prone to seismic events. In contrast, recent experimental studies have showed the viability of FRP reinforcement in shear walls and reinforced concrete columns subjected to seismic loading (Ali and El-Salakawy 2015; Elshamandy et al. 2018; Hassanein et al. 2019; Mohamed et al. 2014a; Tavassoli et al. 2015).

Columns are the critical members in structures that can be exposed to severe environmental conditions. Past studies using FRP reinforcement under axial compressive loading (Afifi et al. 2014; Alsayed et al. 1999; Choo et al. 2006; De Luca et al. 2010; Pantelides et al. 2013; Tobbi et al. 2012, 2014b; Zadeh and Nanni 2012) and under combined axial and flexural loads (Elchalakani et al. 2020; Hadhood et al. 2017) have demonstrated the feasibility of FRPs as internal reinforcing bars. Earlier research on FRP columns under reversed cyclic loading reinforced with FRP bars and grids revealed increased deformability with adequate lateral drift (Sharbatdar 2003). As FRP manufacturing technology has advanced, FRP can now be produced as spirals and stirrups of various shapes and dimensions, although further investigation of their uses is needed. Recent research has validated the use of glass fiber-reinforced polymer (GFRP) bars in reinforced concrete columns under cyclic loading (Ali and El-salakawy 2015; Elshamandy et al. 2018; Kharal and Sheikh 2020; Naqvi and El-Salakawy 2016; Tavassoli et al. 2015). The studies concluded performance as stable as that of steel bars as well as a higher lateral drift ratio, affirming the efficiency of GFRP as lateral reinforcement. It should be noted, however, that the amount and detailing of the GFRP transverse reinforcement influenced the deformability of the GFRP-reinforced columns (Elshamandy et al. 2018; Tavassoli et al. 2015). Increasing the axial load level—regardless of column cross section—drastically affected the deformability of the GFRP-reinforced columns with rapid deterioration of concrete core (Elshamandy et al. 2018; Tavassoli et al. 2015).

The lack of experimental data on different variables and the limited number of test specimens could explain the restrictions in design codes on FRP-reinforced structural

members. ACI 440.1R (2015) do not recommend the use of FRP bars as main longitudinal reinforcement in compression members. CSA S806 (2012) recognizes FRP bars as longitudinal members but neglects their contribution in compression. Current FRP design codes and guidelines such as ACI 440.1R (2015), CSA S806 (2012), and CSA S6 (2019) do not have considerable seismic provisions for the design of the FRP-reinforced columns subjected to seismic loads. ACI 440.IR (2015) and CSA S806 (2012) do not offer any procedures to determine the ductility/deformability factor of FRP-reinforced columns. Elshamandy et al. (2018) reported that the increasing the longitudinal bar size of GFRP-reinforced column increases the strain in GFRP transverse reinforcement beyond 6000 $\mu\varepsilon$ strain limit in accordance with CSA S806 (2012). Thus, the effect of longitudinal bar size on FRP longitudinal and transverse reinforcement under simulated seismic loading needs further investigation.

4.2 RESEARCH SIGNIFICANCE

The current study is the part of extensive research to produce a database on GFRP-reinforced concrete columns subjected to combined quasi-static cyclic load and constant axial load. This paper reports the experimental results for eight full-scale columns. The effect of parameters such as longitudinal bar size and transverse reinforcement spacing and size on strength, deformability, inelastic deformation, and plastic-hinge length were addressed. The deformability index of the GFRP-reinforced columns and strain efficiency of the GFRP lateral reinforcement were also investigated. The results reported in this manuscript represent a significant contribution to the relevant literature and provide end users, engineers, and code committees with much-needed data and recommendations to advance the use of GFRP reinforcement in RC columns.

4.3 EXPERIMENTAL INVESTIGATION

4.3.1 Details of test specimens

The experimental program included the casting and testing of eight full-scale rectangular columns having a cross section of 400 × 400 mm (15.8 × 15.8 in.) with an effective height of 1650 mm (65 in.) and an overall height of 1850 mm (72.8 in.). The lateral load was applied at an effective height of 1650 mm (65 in.) from the column–stub interface with a displacement-controlled hydraulic actuator. The columns were supported on a footing (stub) measuring 600 mm (23.6 in.) high and 1200 × 1200 mm (47.2 × 47.2 in.) in cross section. The test specimens typify a full-scale column measuring 3700 mm (145.6 in.) high, representing the column between the footing and mid-height of the first story, i.e., the assumed point of column contraflexure.

Glass FRP bars were used to reinforce the columns in both the longitudinal and transverse directions. The parameters studied were the size of longitudinal reinforcement and the size and spacing of transverse reinforcement. The columns were reinforced with 12 longitudinal bars 15.9 mm (0.6 in.) in diameter and 19.1 mm (0.7 in.) in diameter. Spirals and cross ties measuring 9.5 mm (0.4 in.), 12.7 mm (0.5 in.), and 15.9 mm (0.6 in.) in diameter were used as transverse reinforcement. The stubs in all the specimens were reinforced at the top and bottom with M20 steel bars. The longitudinal reinforcement extended 550 mm (21.6 in.) within the stub, which satisfies the development-length requirement in CSA S806 (2012). The clear concrete cover of 25 mm (1 in.) was maintained in all the columns. Figure 4.1 shows the reinforcement details of the specimens. Rectilinear spirals (Fig. 4.1(b)) were used as the outer transverse reinforcement and cross ties (Fig. 4.1(c)) as the inner transverse reinforcement.

The specimens were subjected to cyclic lateral loading and constant axial loading. The lateral load was applied with a displacement-based hydraulic actuator at a height of 1650 mm (65 in.) from the column–stub interface. A constant axial load of 20% the capacity of the column was maintained throughout the test in all the columns. The constant axial load

was calculated as $0.2A_g f_c^{'}$, where A_g is the gross cross-sectional area of the column and $f_c^{'}$ is the concrete compressive strength.

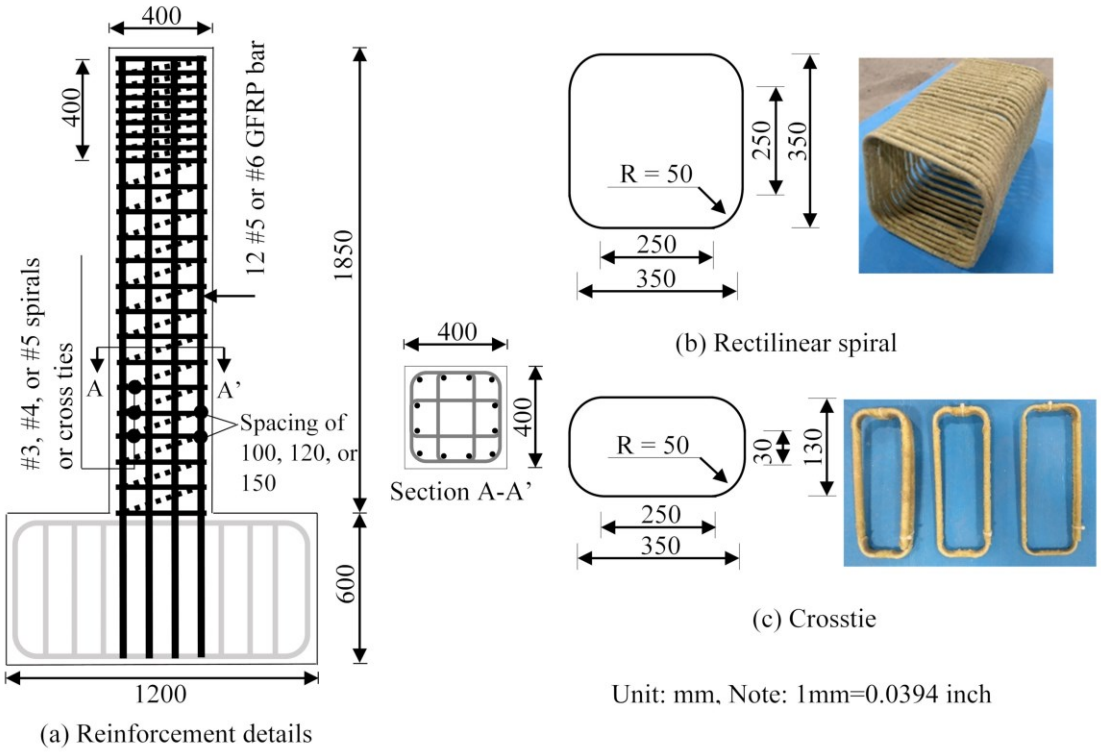

Figure 4.1- Specimen details

The nomenclature pattern for the test specimens G#X-#Y-Z, where, G#X represents the size of the GFRP longitudinal reinforcement bar (#5 and #6), as designated by the manufacturer. The second part (#Y) represents the size of the transverse reinforcement bar (#3, #4, or #5). The third part (Z) stands for the spacing of the transverse reinforcement (100, 120, or 150). Table 4.1 provides the reinforcement details of the test specimens.

Table 4.1- Reinforcing details of test specimens

	Longitudinal Reinforcement			Transverse Reinforcement			
Specimen	Bar no.*	d_b (mm)	ρ_l (%)	Bar no.*	Bar size (mm)	Spacing (mm)	ρ_{sv} (%)
G#5-#3-100	15M (#5)	15.9	1.48	10M (#3)	9.5	100	0.71
G#5-#4-100	15M (#5)	15.9	1.48	12M (#4)	12.7	100	1.27
G#5-#4-120	15M (#5)	15.9	1.48	12M (#4)	12.7	120	1.06
G#5-#4-150	15M (#5)	15.9	1.48	12M (#4)	12.7	150	0.85
G#6-#4-100	20M (#6)	19.1	2.14	12M (#4)	12.7	100	1.27
G#6-#5-100	20M (#6)	19.1	2.14	15M (#5)	15.9	100	1.98
G#6-#4-120	20M (#6)	19.1	2.14	12M (#4)	12.7	120	1.06
G#6-#4-150	20M (#6)	19.1	2.14	12M (#4)	12.7	150	0.85

*Numbers in parentheses are the manufacturer's bar designation. Notes: d_b is the nominal bar diameter; ρ_l is the longitudinal reinforcement ratio; ρ_{sv} is the transverse reinforcement ratio; 1 mm = 0.094 in.

4.3.2 Specimen design

The specimen design was based on CSA S806 (2012) recommendation and accumulating recent research on FRP-reinforced concrete columns (Ali and El-salakawy 2015; Elshamandy et al. 2018; Tavassoli et al. 2015). Based on clause 8.2.1 in CSA S806 (2012), the column section was designed as an over-reinforced section to prevent sudden failure due to FRP rupture. In other words, the failure of the FRP-reinforced concrete section should be initiated by concrete crushing in the compression zone. To ensure compressive concrete failure, the longitudinal reinforcement ratio (ρ_{frp}) on the tension side of the column should be greater than the balanced reinforcement ratio (ρ_{frpb}). The plane-section analysis was performed for flexural failure at a distinct axial load to generate the moment–axial load interaction curve based on strain profiles, assuming a maximum strain in the concrete compression fiber of 0.0035, in accordance with CSA S806 (2012). The compressive strength of the GFRP longitudinal bars was ignored in the analysis. Table 4.2 provides the computed theoretical lateral capacities from the moment–axial load

interaction diagram using a concrete compressive strength of 34 MPa (4931 psi) for all the columns.

Table 4.2- Theoretical and experimental lateral load capacities

Specimen ID	f_c' (MPa)	V_{theo} (kN)	$V_{\exp}$ (kN)	$\frac{V_{\exp}}{V_{theo}}$
G#5-#3-100	32.6	141	192	1.36
G#5-#4-100	31.6	141	250	1.77
G#5-#4-120	34.2	141	232	1.64
G#5-#4-150	33.5	141	196	1.39
G#6-#4-100	34.4	151	251	1.66
G#6-#5-100	34.4	151	300	1.98
G#6-#4-120	34.7	151	260	1.72
G#6-#4-150	34.1	151	221	1.46

Note: f_c' is the concrete compressive strength; $V_{\exp}$ is experimental lateral load capacity in kN; V_{theo} is computed theoretical lateral load capacity in kN; 1 MPa = 145 psi; 1 kN = 0.225 kip.

According to CSA S806 (2012) clause 12.7.3.4, the spacing of transverse reinforcement should not exceed the minimum of one-quarter of the smallest column dimension, six times the diameter of the smallest longitudinal bar, and 150 mm (5.9 in.). Thus, three different spacings of 100 mm (3.9 in.), 120 mm (4.7 in.), and 150 mm (5.9 in.) were selected in compliance with the seismic code provision.

4.3.3 Material properties

The ready-mix normal-weight concrete with target compressive strengths of 30 MPa (4350 psi) and 50 MPa (7250 psi) after 28 days were used to cast the columns and stubs, respectively. Table 4.2 gives the average compressive strength of concrete for each specimen determined by testing at least three standard cylinders measuring 100 × 200 mm (3.94 × 7.87 in.) on the day of specimen testing. The GFRP reinforcing bars in the present study were Grade III high modulus, sand-coated bars (CSA S807 2019). The longitudinal bars were #5 and #6; the transverse reinforcement consisted of #3, #4, and #5 bars

(rectilinear spirals and cross ties). The tensile properties of the straight bars were determined by testing five samples in compliance with ASTM-D7205 (2011); the bent bars were tested according to ASTM D7914 (2014). Table 4.3 lists the material properties of the GFRP reinforcing bars.

Table 4.3- Reinforcement material properties

Bar Type	Bar No.	A_f (mm^2)	A (mm^2)	E_{frp} (GPa)	f_{frpu} * (MPa)	ε_{fu} (%)
Straight	#5	197.9	229	67.2	1433	2.13
	#6	285	323	64.7	1399	2.16
Spirals and cross ties	#3	71.3	95	56.2	1232	2.19
				-	691†	-
	#4	126.7	151	63.2	1570	2.48
				-	801†	-
	#5	197.9	234	60.1	1488	2.48
				-	749†	-

* Guaranteed tensile strength: average value-3 x standard deviation (ACI Committee 440 2015).
†Strength of bent portion of GFRP spirals and cross ties.
Note: A_f is the nominal cross-sectional area; A is cross-sectional area experimentally measured based on Annex A of CSA S806 (2012); E_{frp} is modulus of elasticity; f_{frpu} is guaranteed tensile strength; ε_{fu} is ultimate strain; 1 mm^2 = 0.00155 $in.^2$; 1 MPa = 145 psi.

4.3.4 Instrumentation

All the test specimens were instrumented with electrical strain gauges and linear variable differential transducers (LVDTs) to monitor deformations. Sixteen strain gauges were installed on the longitudinal bars (12 strain gauges were installed above the column–stub interface and four were installed below the column–stub interface), nine on the rectilinear spirals, and six on the cross ties, as shown in Figure 4.2. Four LVDTs were mounted horizontally at different column heights to measure column lateral displacement. Three LVDTs were installed on either side of the columns perpendicular to the loading direction

to monitor concrete strain. One LVDT was installed to check for sliding between the footing and laboratory strong floor.

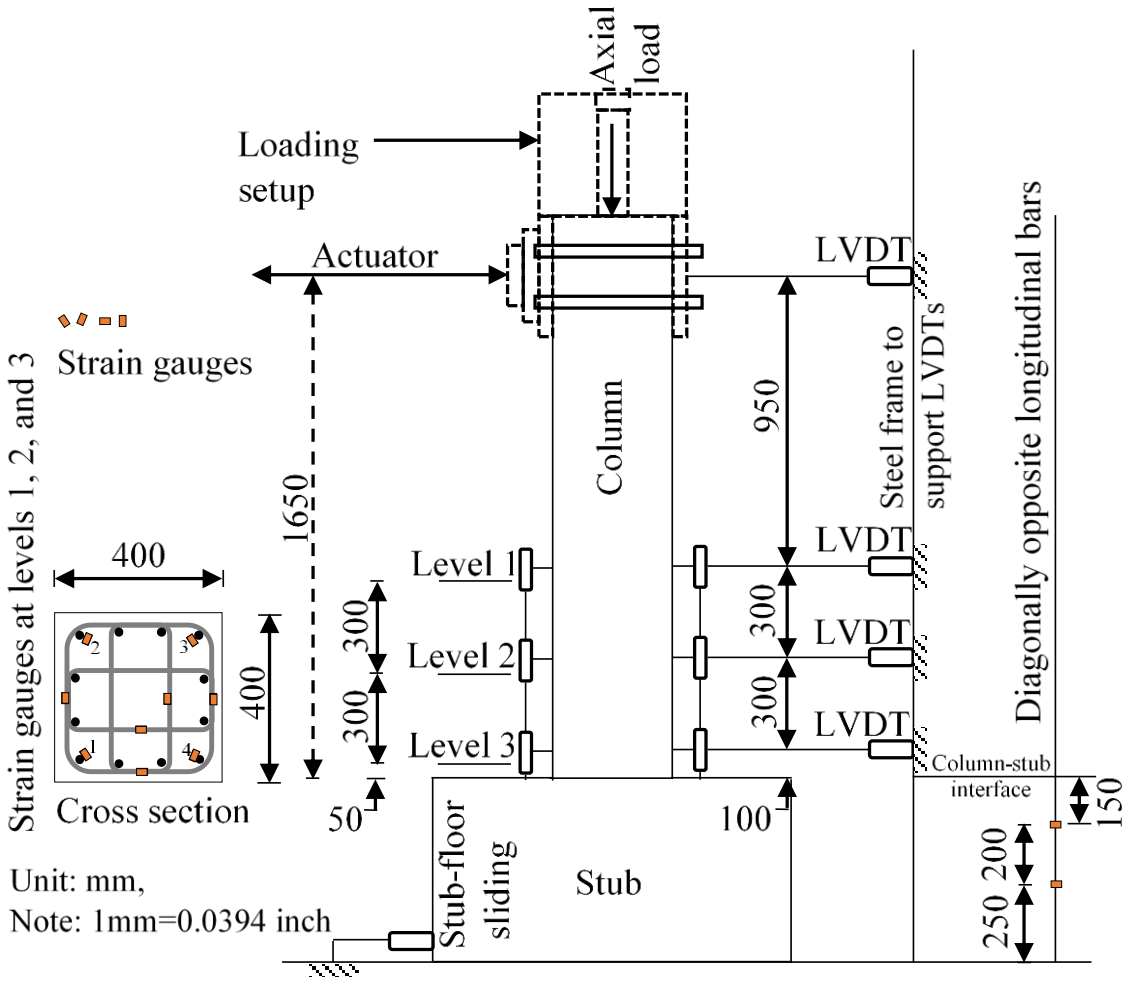

Figure 4.2- Specimen instrumentation

4.3.5 Test setup and loading procedure

The specimens were tested in a vertical position at the structural laboratory of the University of Sherbrooke, as shown in Figure 4.3. The simulated earthquake load was created by concurrently applying a constant axial load to the top of the columns with two

hydraulic jacks and a lateral cyclic load, applied with an MTS actuator. Two DYWIDAG steel bars connected the two hydraulic jacks to the bottom steel beams, while the lower sides of bar were hinged to the bottom steel beams with spherical-shaped head nuts on both sides to allow the specimens to freely rotate throughout the test while maintaining the constant axial load, as shown in Fig. 4.3. More details of the test setup can be found in the literature (Elshamandy et al. 2018). Once the predetermined axial load was applied and maintained constant; the specimen was subjected to displacement-based quasi-static cyclic loading at a rate of 2 mm/min. (0.08 in./min.). Each drift cycle was repeated twice until the specimen failure, as illustrated in Figure 4.4.

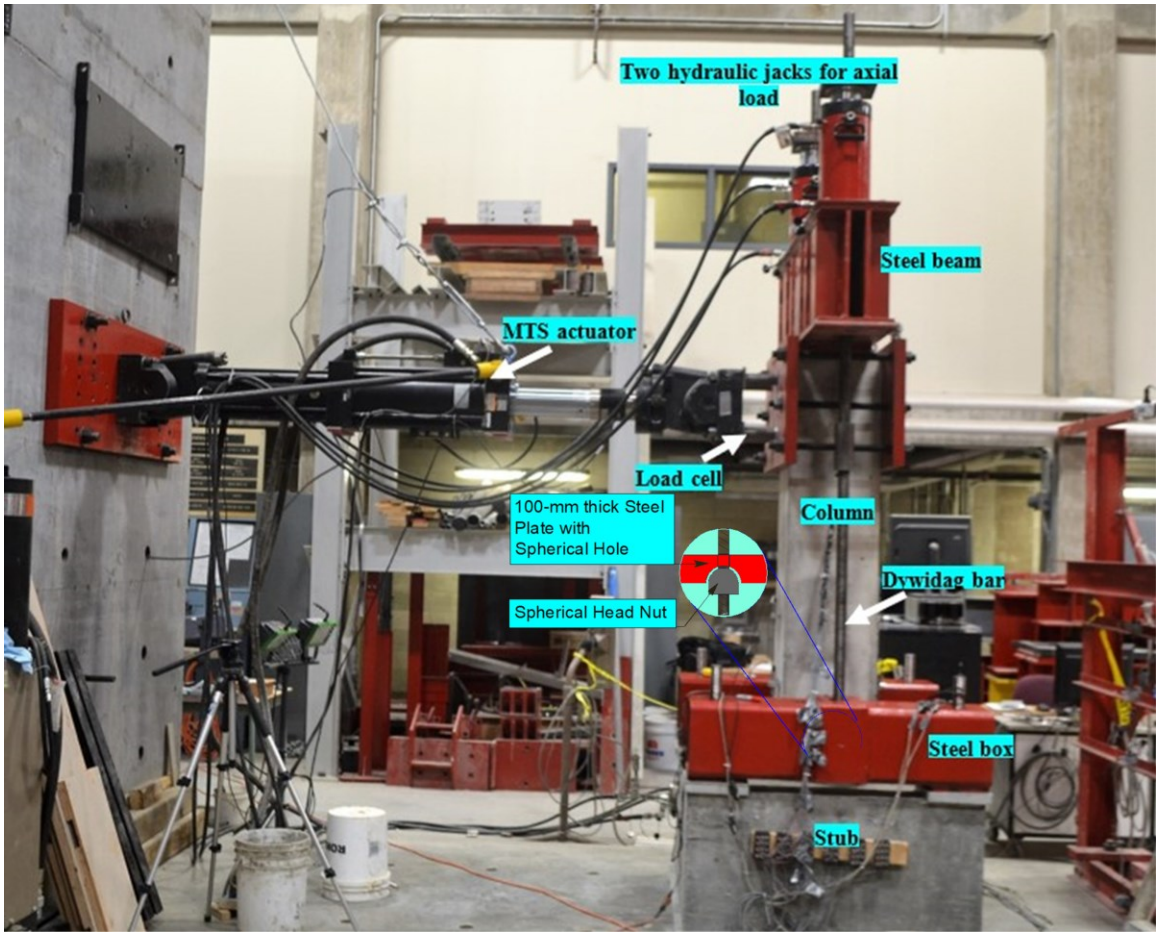

Figure 4.3- Test setup

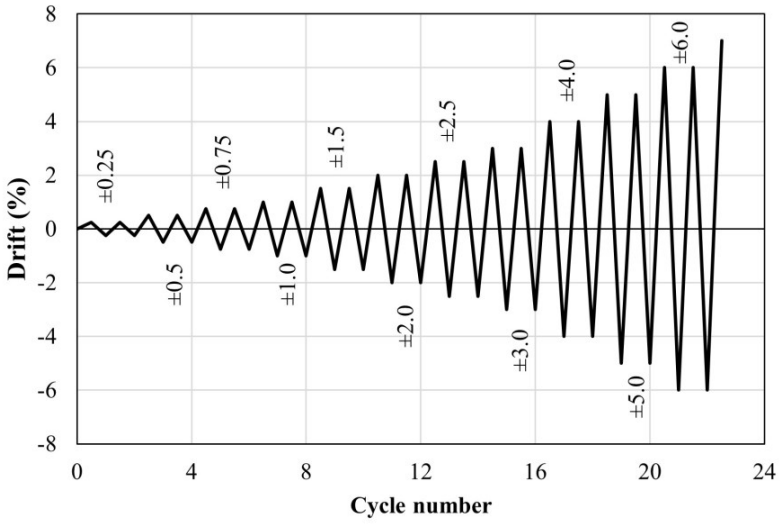

Figure 4.4- Load history

4.4 TEST RESULTS AND DISCUSSION

4.4.1 General behavior

The second loading excursion at the same drift ratio followed the same path as the first loading excursion with reduced stiffness. Thus, the second loading path was removed from the hysteresis curve for simplicity. The occurrence of significant events—such as the beginning of initial cracking, spalling of concrete cover, and concrete crushing—are indicated in the lateral load versus drift hysteresis response, as shown in Figure 4.5.

The initial behavior change in all columns was due to the development of flexural cracks on the actuator face and the front face of the column. The initial cracks mainly occurred at lateral drifts ranging from 0.20% to 0.30%. Subsequently, more flexural cracks developed and propagated at a distance equal to the spacing of the lateral ties. Under increased displacement, the flexural cracks continued to develop up to 50% to 70% of the effective column height (1650 mm [65 in.]), measured above the column–stub interface.

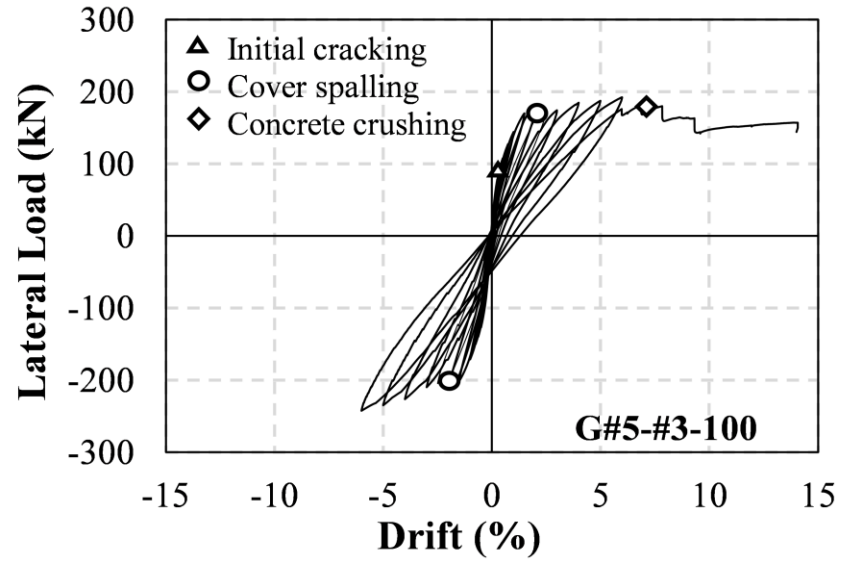

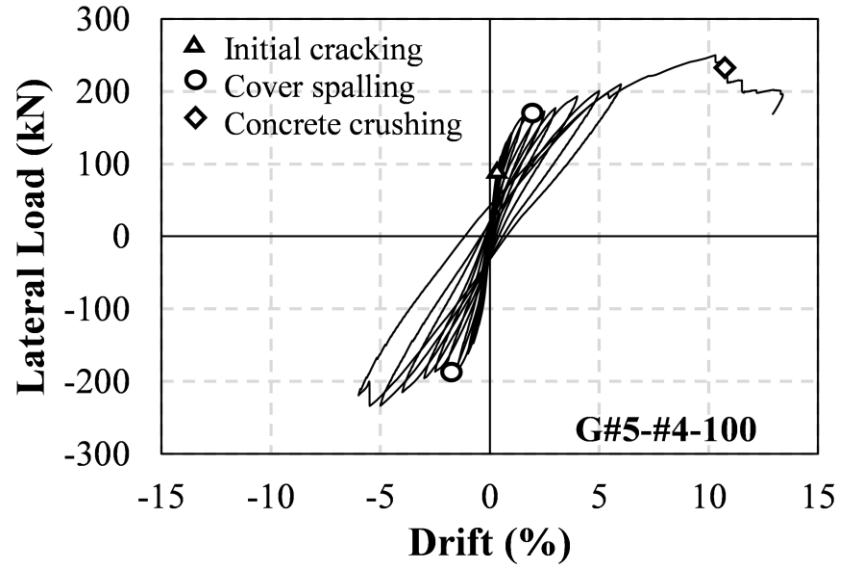

Figure 4.5- Hysteresis response

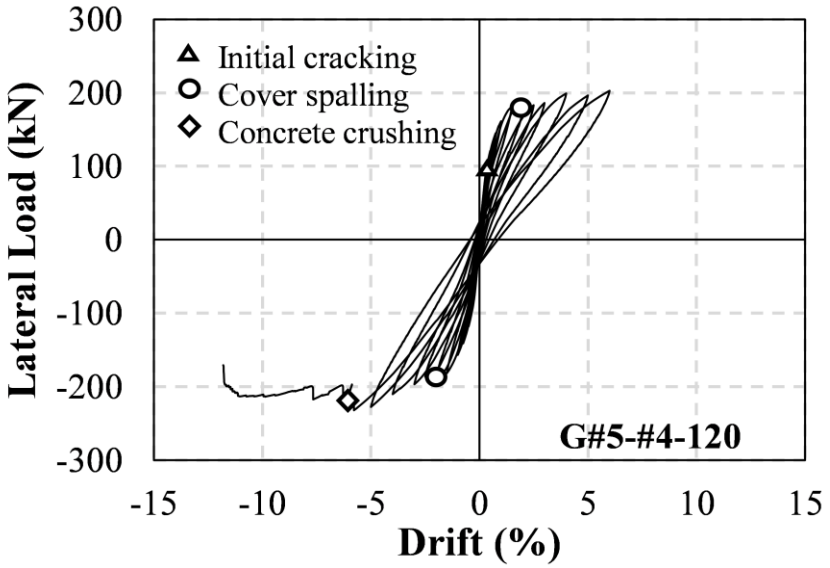

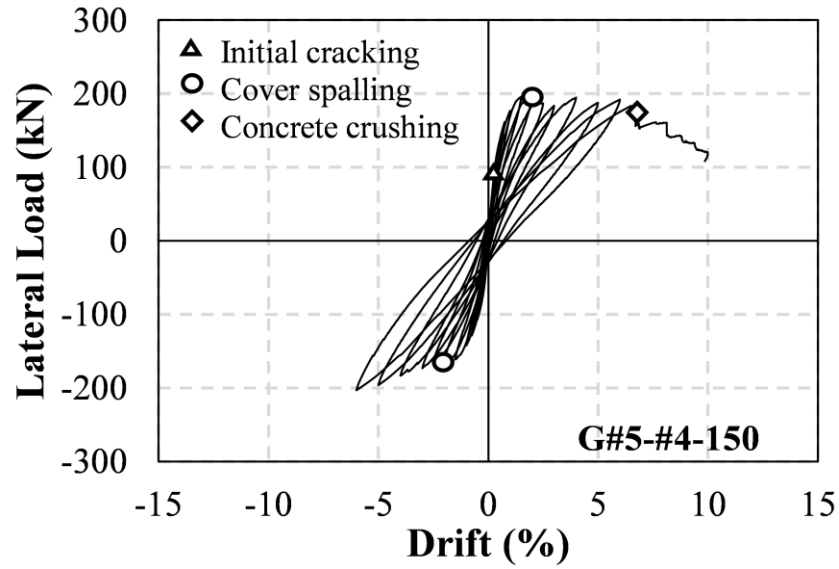

Figure 4.5- Hysteresis response (continued)

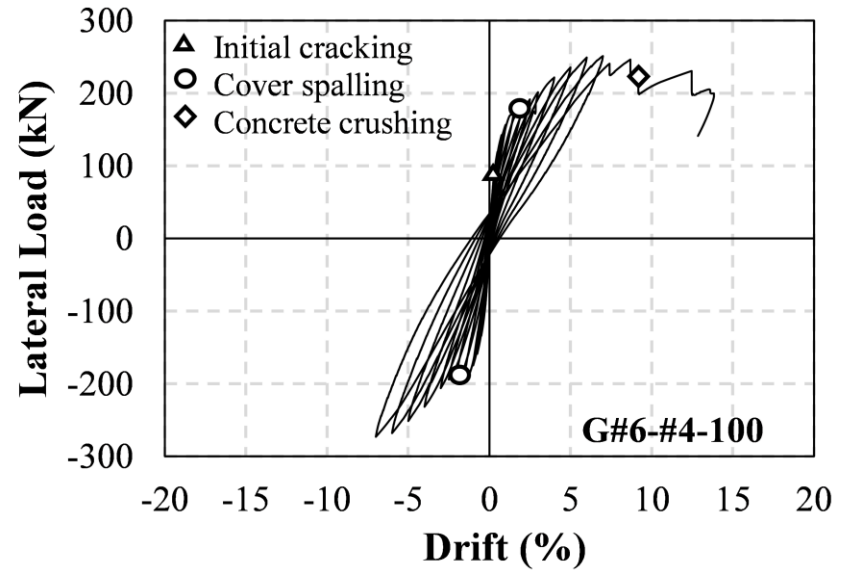

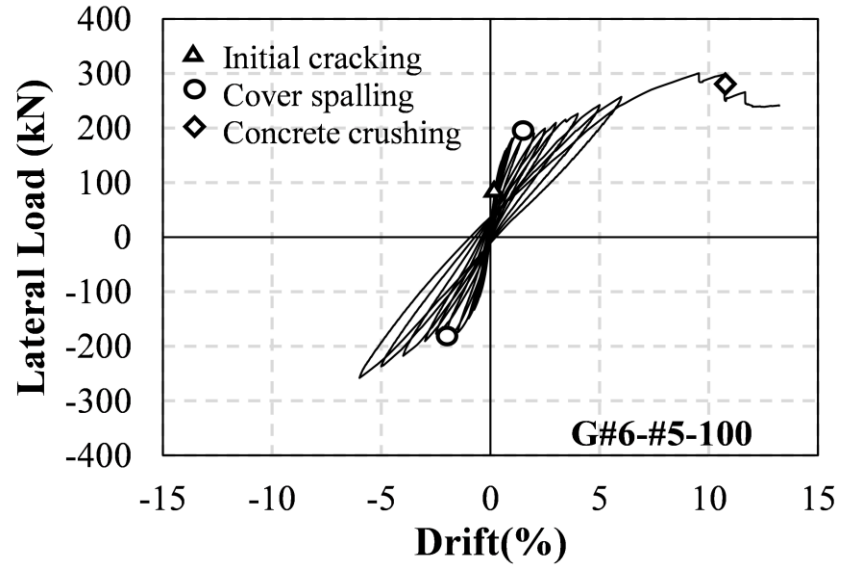

Figure 4.5- Hysteresis response (continued)

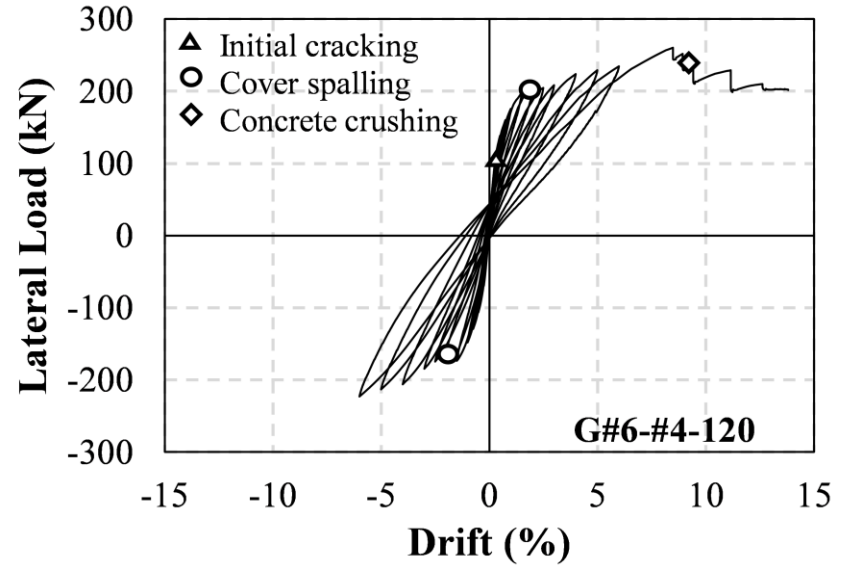

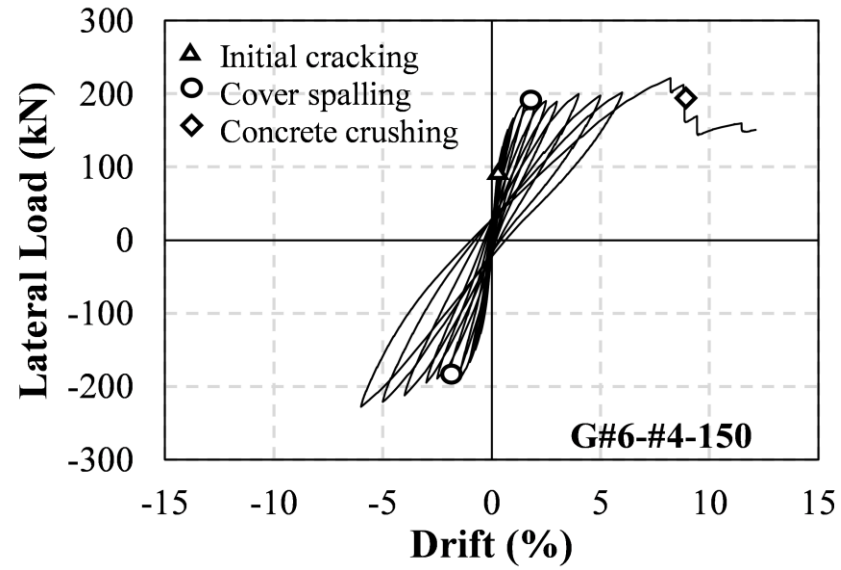

Figure 4.5- Hysteresis response (continued)

Further application of the drift cycle resulted in vertical splitting cracks at the corners of the column compression side, as shown in Figure 4.6(a). The next key observation was strength degradation due to the continuous loss of concrete cover, which occurred in all specimens within a range of 1.5 to 4.0% lateral drift. The concrete cover spalling (Fig. 4.6(b)) first occurred in the front faces in drift cycles between 1.5% to 2.0%, moving towards the side faces in later drift cycles. Depending on the test variables, two different behaviors were observed. Strength gain and a second peak were observed after a lateral load plateau in all well-confined columns with a transverse reinforcement spacing of 100 mm (3.9 in.) and 120 mm (4.7 in.), as shown in the plotted lateral load versus drift envelope curve (Fig. 4.7). Other researchers observed similar behavior in past experimental studies of GFRP-reinforced columns (Elshamandy et al. 2018). The columns with low confinement exhibited no significant changes in strength after concrete cover spalling, as observed with columns G#5-#4-150 and G#6-#4-150. All the columns had stable behavior with large deformability; the applied constant axial load was maintained until failure. In the final drift cycle, the maximum capacity of the columns resulted in crushing of compression bars, as shown in Figure 4.6(c), and a drop in the applied axial load.

The failure of all columns occurred in the test regions (virtual plastic-hinge zone), mainly due to crushing of the longitudinal GFRP bars in compression, accompanied by deterioration of the core concrete (Fig. 4.6(d)). No spiral damage or rupture was observed, even after column collapse. In case of specimens G#5-#3-100 and G#6-#5-100, cross tie rupture was observed in the test zones or most damaged regions, as shown in Figure 4.6(e).

The dominant form of failure for all the specimens was flexural, as shown in Figure 4.8. The well-confined columns had larger damaged regions or larger plastic hinge zones compared to those with lower levels of confinement. The most damaged section was 200 to 260 mm (7.9 to 10.2 in.) above the column–footing interface. Similar behavior were observed in other experimental studies (Ali and El-salakawy 2015; Elshamandy et al.

2018). This resulted mainly from the confinement provided by the footing to the column section at the column–footing interface.

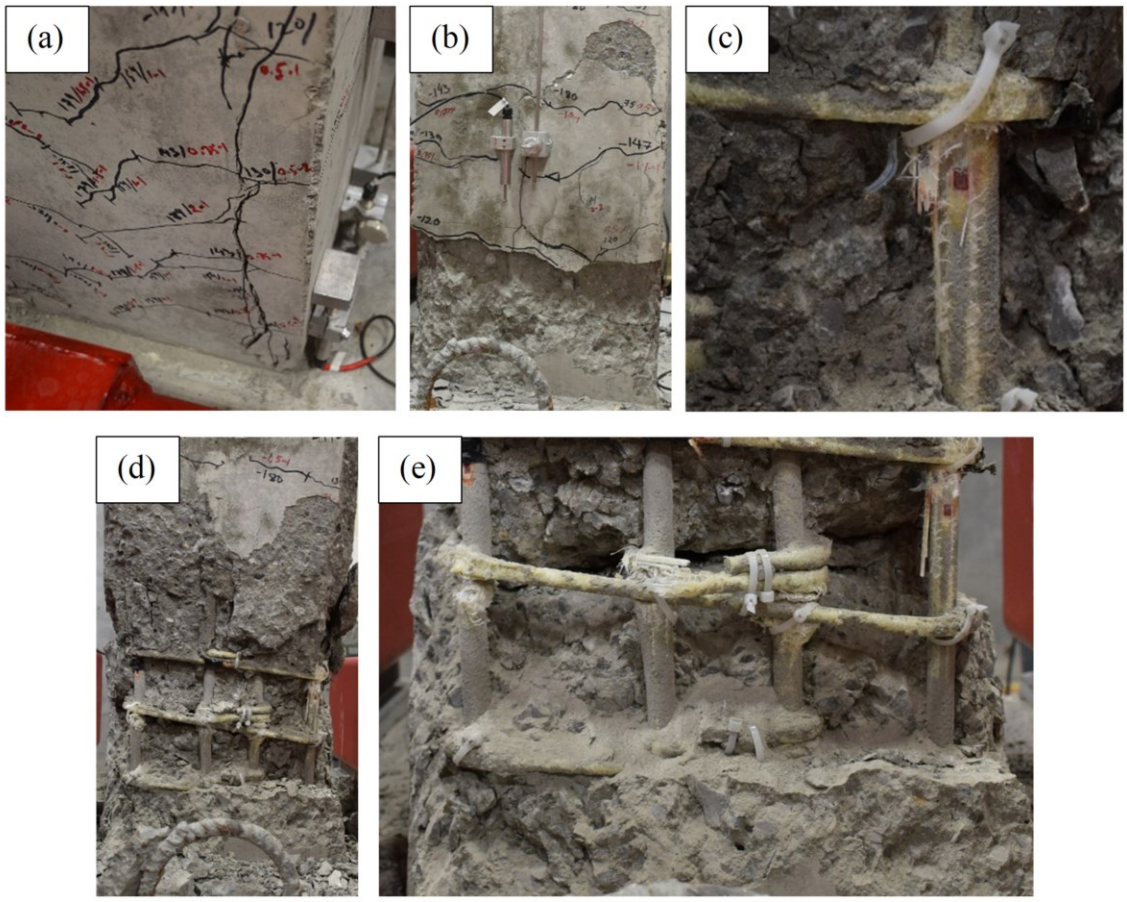

Figure 4.6- Failure progression of GFRP-reinforced columns: (a) vertical splitting; (b) concrete cover spalling; (c) fracture of longitudinal bars; (d) core concrete crushing; and (e) rupture of cross ties.

The ratio of experimental lateral capacity to computed theoretical lateral load capacity of the columns ($V_{\exp}/V_{theo}$) is listed in Table 4.2. The experimental lateral capacity was found to be 36-98 % more than the computed value. This could be attributed to the neglected compressive contribution of FRP bars in the calculation. The lateral load prediction is discussed in more details below.

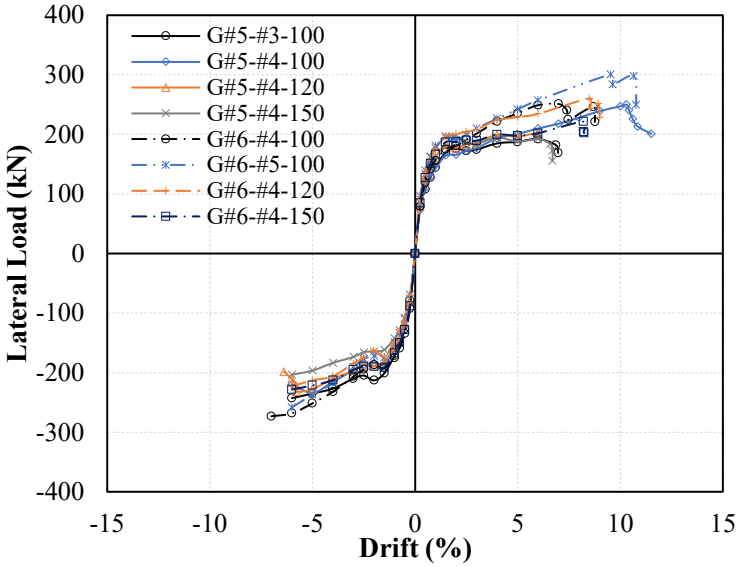

Figure 4.7- Envelope curve of hysteretic response

4.4.2 Deformability index

Deformability is the ability of a structure to support load without failure given a certain amount of deformation. The deformability factor is defined as the ratio of ultimate deformation to yield deformation. The yield deformation is the point at which a structure's behavior changes from elastic to inelastic. Steel rebars yield, but GFRP bars do not. So, an explicit point shifting the behavior of GFRP-reinforced concrete columns from elastic to inelastic deformation should be investigated as ACI 440.1R (2015) and CSA S806 (2012) do not offer any procedures for evaluating the deformability factor of FRP-reinforced concrete structures.

GFRP-reinforced concrete columns show inelastic behavior once the concrete starts to deteriorate in compression (Elshamandy et al. 2018; Mohamed et al. 2014c). The inelastic behavior imparted by concrete deterioration in the GFRP-reinforced columns began at a concrete compressive strain of $\varepsilon_c = 0.003$, when the concrete cover started to split and spall at the compressed end. Therefore, the transition point from elastic to inelastic in our study

is defined as $\varepsilon_c = 0.003$ (Fig. 4.9) and called elastic deformation (Δ_e) or the virtual yield-deformation point (Mohamed et al. 2014c).

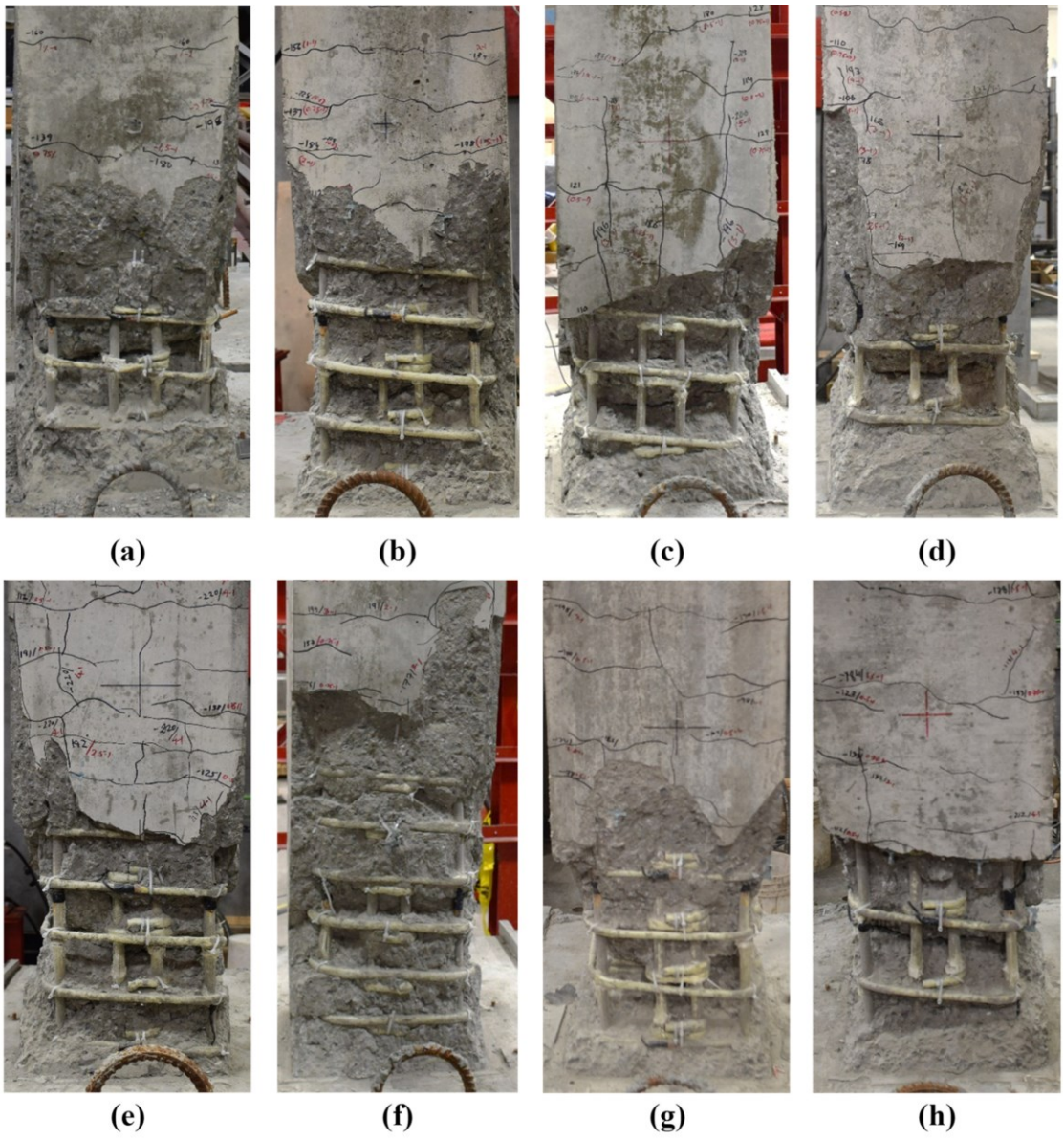

Figure 4.8- Virtual plastic hinge zone at failure (a) G#5-#3-100; (b) G#5-#4-100; (c) G#5-#4-120; (d) G#5-#4-150; (e) G#6-#4-100; (f) G#6-#5-100; (g) G#6-#4-120; and (h) G#6-#4-150

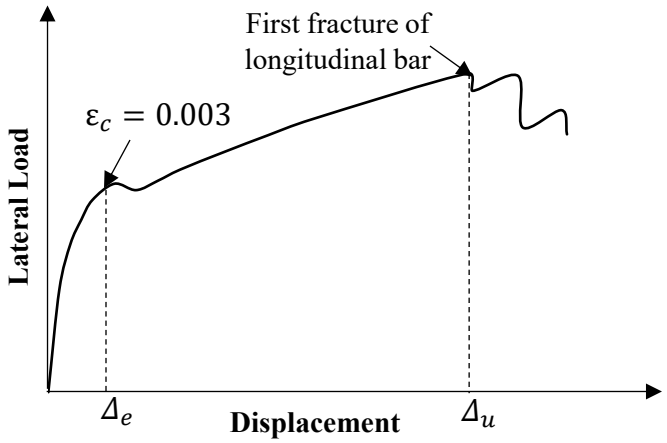

Figure 4.9- Elastic and ultimate displacement definition

The maximum available deformation or ultimate deformation (Δ_u) has been adequately estimated for experimental steel-reinforced structures (Park 1989). It can be based on (a) the limiting value of concrete compression strain, (b) displacement at the ultimate load of the envelope curve, (c) post-peak displacement with a minor reduction in the ultimate load, and (d) displacement corresponding to reinforcement fracture or buckling. The hysteretic response (Fig. 4.5) in our study shows a stable response after the deterioration of the concrete cover in the most damaged areas (Fig. 4.8). The columns started to regain strength until the failure of the longitudinal GFRP bars in compression (Fig. 4.7). Thus, the displacement at which crushing of the first longitudinal bar in compression occurs with a reduction in lateral load is defined herein as the ultimate deformation (Δ_u) (Fig. 4.9). So, the displacement deformability (μ_Δ) is as follows.

$$\mu_\Delta = \frac{\Delta_u}{\Delta_e} \tag{4.1}$$

The maximum drift δ_u is defined based on the ultimate displacement (Δ_u) at the failure of the first GFRP longitudinal bar in compression as $\delta_u = \Delta_u / h_e$, where h_e is the effective height of the test specimen. Table 4.4 gives the calculated deformability indexes and drifts.

The deformability index was influenced by the spacing and size of the GFRP transverse reinforcement. Column G#5-#4-100, confined with 12.7 mm (0.5 in.) lateral GFRP bars, achieved 43% more deformability than column G#5-#3-100, confined with 9.5 mm (0.4 in.) transverse GFRP bars. Similarly, the deformability of column G#6-#4-100, confined with 12.7 mm (0.5 in.) transverse reinforcement, was 10% lower than that of column G#6-#5-100, reinforced with 15.9 mm (0.6 in.) lateral GFRP bars. Thus, increasing the size of the transverse GFRP reinforcement improved the deformability index of the tested columns. The spacing of the transverse reinforcement in columns G#6-#4-100, G#6-#4-120, and G#6-#4-150 were 100, 120, and 150 mm (3.9, 4.7 and 5.9 in.), respectively. Column G#6-#4-100 achieved 23% and 27%, respectively, more deformability index than columns G#6-#4-120 and G#6-#4-150. Given that, column deformability could be improved by decreasing the spacing of the transverse reinforcement.

Table 4.4- Deformability index

Specimen ID	δ_u (%)	Δ_e (mm)	Δ_u (mm)	μ_Δ
G#5-#3-100	7.0	21.5	115	5.3
G#5-#4-100	10.1	22.0	166.6	7.6
G#5-#4-120	5.8	20.8	95.5	4.6
G#5-#4-150	6.6	21.0	108.7	5.2
G#6-#4-100	7.4	17.5	122	7.0
G#6-#5-100	9.5	20.4	157.4	7.7
G#6-#4-120	8.5	24.4	140	5.7
G#6-#4-150	8.2	24.5	135.5	5.5

Note: δ_u is maximum drift; Δ_e is elastic displacement; Δ_u is ultimate displacement; μ_Δ is displacement deformability index; 1 mm = 0.0394 in.

4.4.3 Energy dissipation

Energy dissipation of reinforced concrete structures is one of the important parameters in withstanding severe earthquakes (Paulay and Priestley 1992). It is defined as the area under the lateral force–displacement curve of a drift cycle. The cumulative energy dissipation in each cycle for the tested columns was computed by summing the dissipated energy in successive cycles and plotted against the drift ratio, as shown in Figure 4.10. Regardless of the different reinforcement parameters, the energy dissipated in each drift cycle was similar. The columns that exhibited higher drift cycles dissipated more energy up to failure, depending on the confinement level. Slight difference in cumulative dissipated energy was noted in columns confined with different transverse GFRP reinforcement size as shown in Figure 4.11.

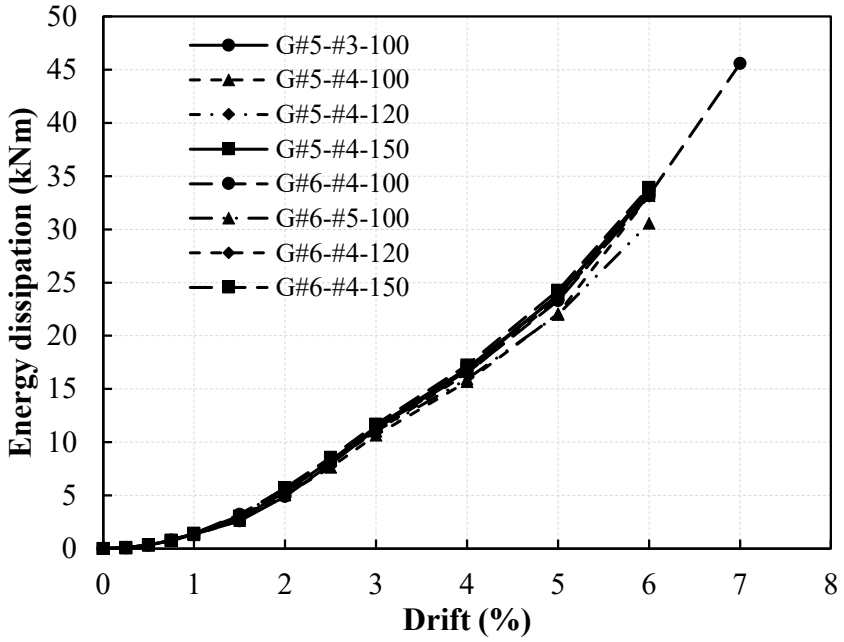

Figure 4.10- Cumulative dissipated energy in all columns

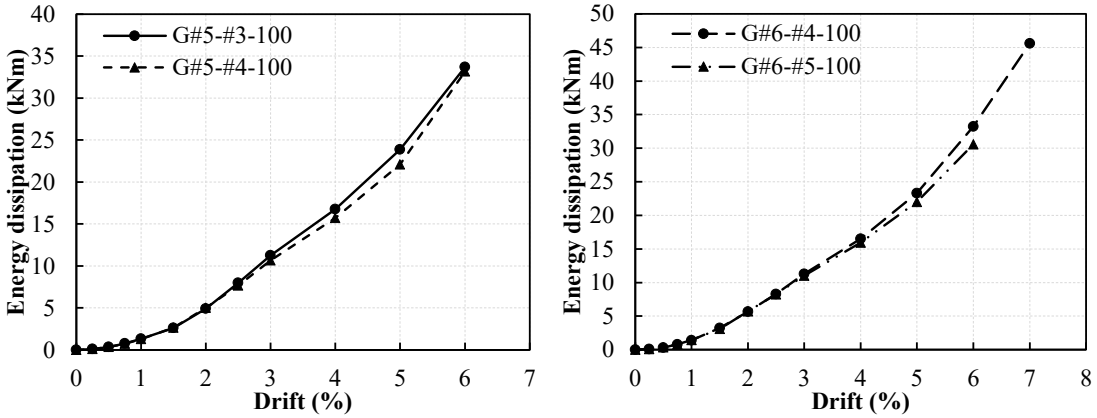

Figure 4.11- Cumulative dissipative energy- comparison of lateral reinforcement bar size

As shown in Fig. 4.5, columns G#5-#4-100 and G#6-#5-100—with larger-diameter lateral GFRP bars—developed narrower hysteresis loops than columns G#5-#3-100 and G#6-#4-100, respectively. This was due to the contribution of the elastic behavior of the larger lateral GFRP bars. Thus, columns G#5-#4-100 and G#6-#5-100 exhibited lower cumulative dissipated energy than columns G#5-#3-100 and G#6-#4-100, respectively, as shown in Fig. 11.

4.4.4 Effect of longitudinal bar size

Specimens G#5-#4-100 and G#6-#4-100 were reinforced with longitudinal reinforcement ratios of 1.48% and 2.14%, respectively. As shown in Figure 4.7, specimen G#6-#4-100 had higher lateral resistance than specimen G#5-#4-100 at each drift cycle until specimen failure, although the achieved drift was 10.1% and 7.4% for specimens G#5-#4-100 and G#6-#4-100, respectively. Thus, increasing the longitudinal reinforcement ratio enhanced the lateral load capacity but affected the drift capacity of the column specimens. This did not hold true for specimen pairs G#5-#4-120 and G#6-#4-120 and G#5-#4-150 and G#6-#4-150 when the spacing of the transverse reinforcement was increased. In these cases, both strength and drift capacity were enhanced in comparison to columns with lower longitudinal GFRP reinforcement ratio.

The longitudinal bars in specimen G#5-#4-100 had higher maximum measured strain at each drift ratio than those in specimen G#6-#4-100, as shown in Figure 4.12. At 4% drift, the maximum strain in the longitudinal bars in specimens G#5-#4-100 and G#6-#4-100 was 56.5% and 48.5% of the ultimate strain of the #5 and #6 GFRP bars, respectively. The higher longitudinal bar strain supports the increased deformability in specimen G#5-#4-100. Similar behavior was obtained for specimen pairs G#5-#4-120 and G#6-#4-120 and G#5-#4-150 and G#6-#4-150, in which the columns with the larger GFRP bars had experienced less maximum strain at each drift ratio (Fig. 4.12).

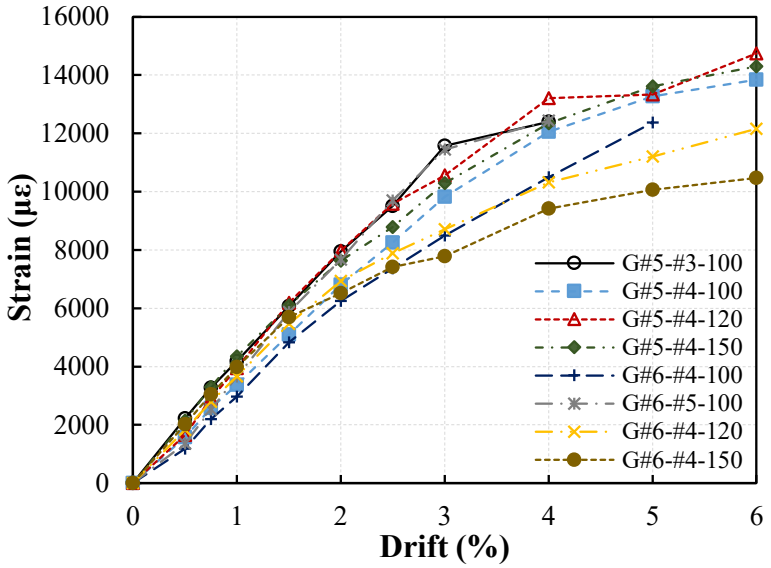

Figure 4.12- Maximum strain developed in longitudinal bars vs. drift ratio.

Figure 4.13 shows the longitudinal bar strain profile along specimen height. The positive and negative strain values define tensile and compressive strains in the longitudinal bar, respectively. Clearly, specimens G#5-#4-100, G#5-#4-120, and G#5-#4-150 reinforced with smaller longitudinal GFRP bars developed more strain in the longitudinal reinforcement than did specimens G#6-#4-100, G#6-#4-120, and G#6-#4-150, respectively, at each drift cycle. At a drift ratio of 4.0%, specimens G#5-#4-100, G#5-#4-120, and G#5-#4-150 had 1.6 to 2.3 times more strain in the longitudinal reinforcement

embedded 150 mm (5.9 in.) below the column-stub interface compared to columns G#6-#4-100, G#6-#4-120, and G#6-#4-150. In all the test specimens, the strain gauges located 350 mm (13.8 in.) below the column–stub interface recorded strains of approximately zero. Thus, the embedded length of 550 mm (21.6 in.) in the stub was sufficient for the longitudinal bars.

4.4.5 Effect of transverse reinforcement

Various transverse reinforcement ratios were selected to check the confinement level based on spacing and size of the lateral GFRP bars (Table 4.1). Based on the hysteresis response (Figure 4.5), specimen G#5-#4-100 showed an increase of 8% and 27.5% in lateral load capacity compared to specimens G#5-#4-120 and G#5-#4-150, respectively. The drift ratio for specimen G#5-#4-100 at failure was about 60% higher than that of the columns with wider transverse reinforcement spacing. This indicates that closer spacing of the transverse reinforcement improved column strength and deformability. In the case of columns with higher longitudinal reinforcement ratios, however, specimen G#6-#4-100 exhibited lateral load capacity similar to specimen G#6-#4-120 but showed a 13% increase in strength compared to specimen G#6-#4-150. The first longitudinal GFRP bar in specimen G#6-#4-100 crushed at 7.4% drift ratio with a lateral load capacity of 251 kN (56.4 kips), even though the column's lateral load increased afterwards reaching 247 kN (55.5 kips) at 8.7% drift and 230 kN (51.7 kips) at 12.5% drift (Fig. 4.5). The drift capacity achieved by specimens G#6-#4-120 and G#6-#4-150 was 8.5% and 8.2%, respectively. Thus, the spacing of transverse reinforcement did not significantly affect the drift capacity of columns with larger longitudinal bar sizes. Further, column G#5-#4-150 achieved 1.14 times more drift than column G#5-#4-120 (Table 4). This demonstrates that the maximum spacing of transverse reinforcement governed by CSA S806 (2012) for seismic designs (least of one-quarter of minimum member dimension, 150 mm (5.9 in.), or six times the diameter of the smallest longitudinal bar) is restrictive. Although, according to clause 8.4.6 in CSA S806 (2012), the maximum spacing of transverse reinforcement for all specimens were found to be 189 mm (7.4 in.).

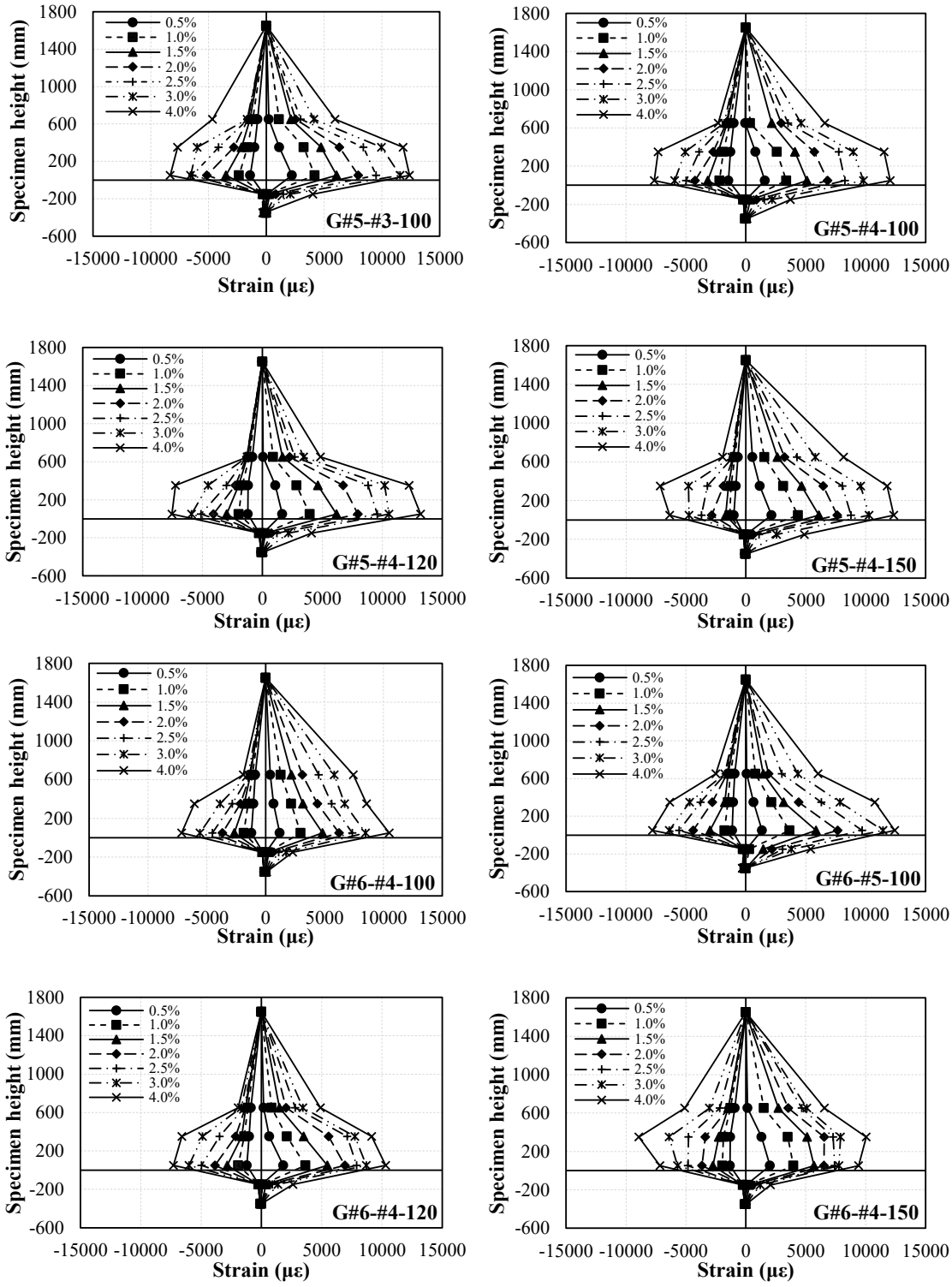

Figure 4.13- Longitudinal bar strain profile along the height

The transverse reinforcement ratio of specimens G#5-#3-100 and G#5-#4-100, based on the size of the lateral reinforcement, was 0.71% and 1.27%, respectively. Specimen G#5-#4-100 had 30% higher lateral capacity than specimen G#5-#3-100 due to its larger transverse reinforcement, with a 45% increase in drift capacity (Fig. 4.5). Specimens G#6-#5-100 and G#6-#4-100 were reinforced with 15.9 mm (0.6 in.) and 12.7 mm (0.5 in.) lateral GFRP bars, respectively. Specimen G#6-#5-100 had lateral strength and drift capacity that were 19.5% and 29% higher than that of G#6-#4-100 (Fig. 4.7) due to the larger size of its transverse reinforcement bars. Thus, increasing the confinement ratio by increasing the size of transverse reinforcement bars enhanced both strength and drift capacity of the column. Specimens G#5-#4-100 and G#6-#5-100 yielded tapered hysteresis loops compared to specimens G#5-#3-100 and G#6-#4-100 (Fig. 4.5). This could be due to the additional confinement provided by the larger GFRP transverse spirals and cross ties. Thus, specimens G#5-#3-100 and G#6-#4-100 showed comparatively higher cumulative energy dissipation than specimens G#5-#4-100 and G#6-#5-100, respectively (Fig. 4.11).

Figure 4.12 shows the relationship between the maximum strain in the longitudinal bars versus drift ratio. At lower drift levels, the longitudinal bars in the specimens with closer spacing—G#5-#4-100 and G#6-#4-100—achieved lower strains than those in specimens G#5-#4-120 and G#6-#4-120, respectively. The columns with wider transverse reinforcement spacing had higher applied lateral stress on the longitudinal bars at the lower drift level due to the lateral expansion of the concrete core. The narrower spacing of the lateral reinforcement effectively confined the concrete core, improving the lateral load capacity and yielding lower strain in the longitudinal bars. The virtual plastic hinge zones of the tested columns are consistent with the above statement. Specimens G#5-#4-100 and G#6-#4-100 had larger damaged zones than specimens G#5-#4-150 and G#6-#4-150 (Fig. 4.8).

4.4.6 Lateral reinforcement strain efficiency

Figure 4.14 plots the strain developed in the transverse reinforcement in specimens G#5-#3-100 and G#5-#4-100 during testing. Given the same drift ratio, the strain developed in

the rectilinear spiral and cross ties at the strain gauge in specimen G#5-#4-100 with the highest strain was comparatively higher than that of specimen G#5-#3-100. This demonstrates the effective confinement provided by the higher lateral reinforcement ratio in specimen G#5-#4-100, which explains the increase in the lateral load of specimen G#5-#4-100 after the concrete cover spalled, as shown in Figure 4.5. The maximum strain developed in the rectilinear spiral and cross ties in specimen G#5-#4-100 was 9% and 24% more than that of specimen G#5-#3-100, respectively.

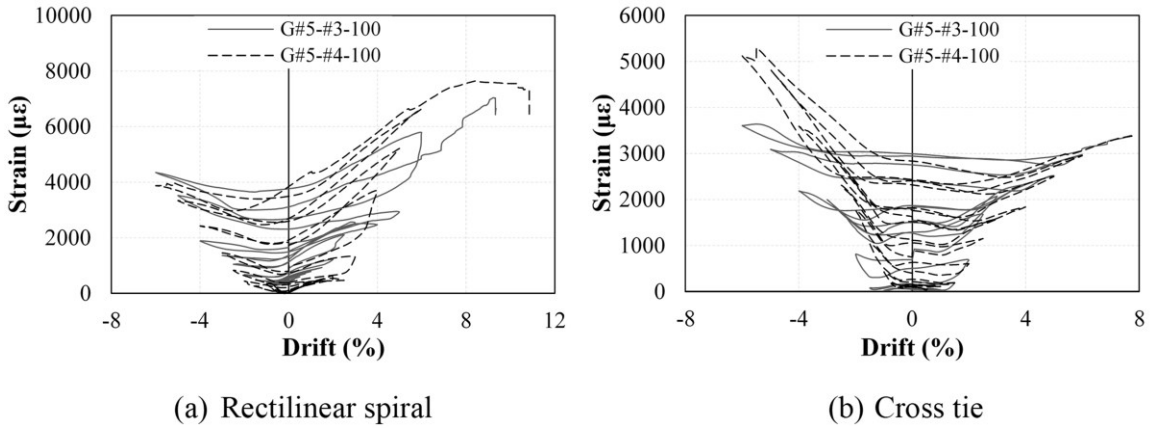

Figure 4.14- Maximum strain developed in spiral and cross tie.

Table 4.5 gives an outline of recorded maximum strain in the rectilinear spirals and cross ties at a 4% drift cycle and just before failure. At the 4% drift cycle, the strain in both the rectilinear spirals and cross ties was less than 6000 $\mu\varepsilon$, which satisfies the hoop strain requirement in CSA S806 (2012). The increase in the lateral load capacity of the tested columns after the load plateau (Fig. 4.7) due to concrete cover deterioration indicates the effective confinement provided to the column core by the lateral GFRP reinforcement. The lateral reinforcement efficiently limited the lateral expansion of the concrete core, thus delaying crushing of the core. This can be seen in the hysteresis response of the tested columns (Fig. 4.5). The maximum strain at failure in the straight portion of the GFRP

spirals and cross ties was, however, considerably less than the ultimate strain of the lateral reinforcement, as listed in Table 5.

Table 4.5- Strain developed in rectilinear spiral and cross tie

Specimen	Ultimate Strain ε_{fhu}, με	Maximum Strain at 4% Drift, $\varepsilon_{fh4\%}$, με		Maximum Strain ε_{fh}, με		$\frac{\varepsilon_{fh}}{\varepsilon_{fhu}}$ *
		Spiral	Cross tie	Spiral	Cross tie	
G#5-#3-100	21900	2519	2337	7040	4265	0.32
G#5-#4-100	24800	3697	3592	7643	5300	0.31
G#5-#4-120	24800	2242	2350	3883	3484	0.16
G#5-#4-150	24800	5238	3700	9628	7473	0.39
G#6-#4-100	24800	4050	2856	6976	6152	0.28
G#6-#5-100	24800	3488	2408	7408	4743	0.30
G#6-#4-120	24800	3588	3798	4272	4366	0.18
G#6-#4-150	24800	4125	4327	5379	5480	0.22

* ε_{fh} is the largest of rectilinear spiral or cross tie strain.

4.5 LATERAL LOAD PREDICTION

A detailed plane-section analysis was conducted to predict the lateral load capacity of the tested columns applying the nominal axial load–moment (P-M) interaction diagram. The analysis was based on the code provisions for FRP-reinforced concrete structures (CSA S806 2012; CSA S6 2019). The assumptions considered for the plane-section analysis based on the provisions in CSA S806 (2012) and CSA S6 (2019) were: (a) the strain in the concrete and GFRP bars at any level is proportional to the distance from the neutral axial; (b) the maximum available strain in concrete compression fiber is $\varepsilon_{cu} = 0.0035$ and the tensile strength of concrete is ignored; (c) a perfect bond exists between the concrete and the GFRP reinforcement; (d) GFRP has a linear elastic stress–strain relationship until failure; (e) the elastic moduli of GFRP bars in tension and compression are equal (Deitz et al. 2003); and (f) all resistance and reduction factors are equal to unity.

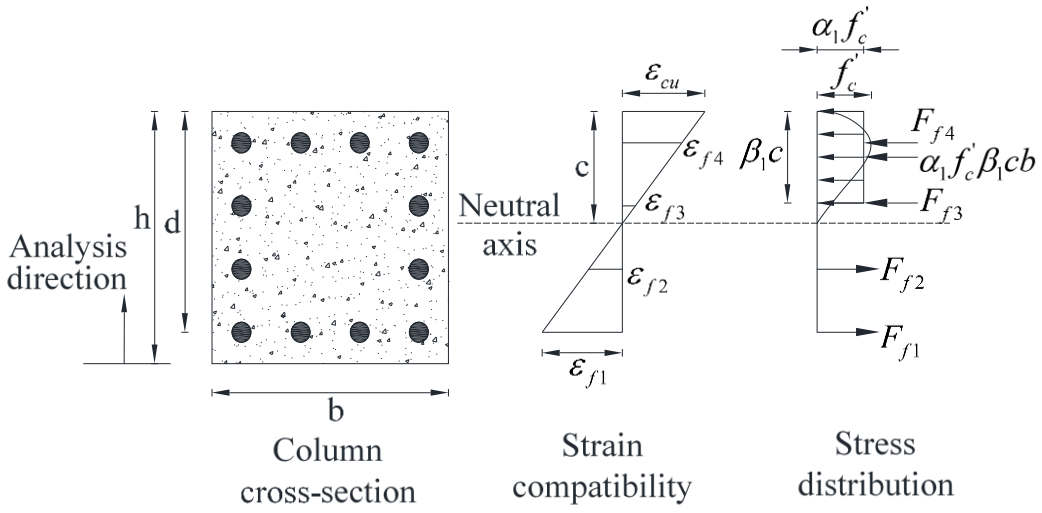

Figure 4.15- Stress and strain distribution for sectional analysis

Figure 15 shows the plane-sectional analysis of the studied GFRP-reinforced concrete columns. The plane-section analysis was conducted by implementing the strain compatibility and equilibrium of forces with and without considering the contribution of the longitudinal GFRP bars in compression. CSA S806 (2012) does not consider the contribution of FRP bars in compression, whereas CSA S6 (2019) recommends the compressive strength of FRP bars should be limited to a stress corresponding to a strain of 2000 με. The literature reports that the compressive strength of a GFRP bar based on coupon tests is half of its tensile strength (Tavassoli et al. 2015). The results for the tested columns show that the maximum compressive strain of the GFRP bars varied between 0.39 and 0.64 times the ultimate tensile strain (ε_{fu}) before the failure of the GFRP bars in compression or a malfunction of the strain gauges, as shown in Fig. 16. The considered maximum compressive strain (ε_{fc}) of the GFRP bars was 0.002 as per CSA S6 (2019) and 0.0035 equivalent to the assumed maximum available compressive strain in the concrete. An equivalent concrete stress block was used with reduced compressive strength of concrete, as shown in Fig. 15. Factors α_1 and β_1 in Fig. 15 are the ratio of the average

stress in the rectangular compression block to a specified concrete strength and the ratio of the depth of the rectangular compression block to the depth of the neutral axis, respectively. Both factors are the function of concrete compressive strength (CSA S806 2012; CSA S6 2019). The concrete compressive strength used in the analysis was 34 MPa.

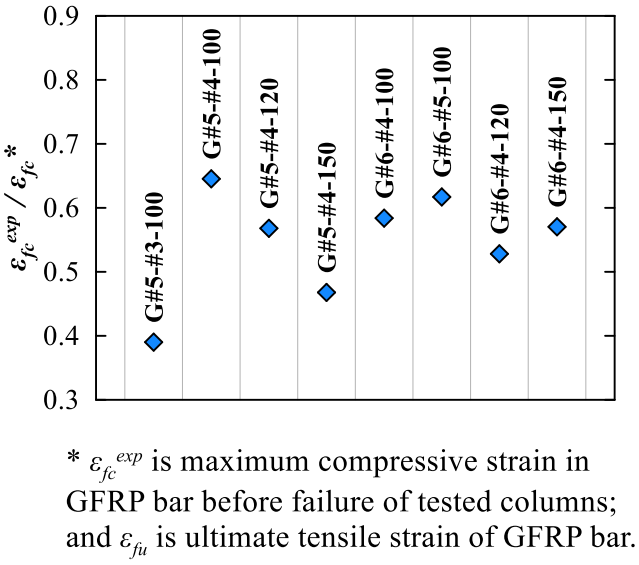

Figure 4.16- Maximum compressive strain in GFRP bar in tested columns before fracture of first longitudinal bar

Figure 17 shows the axial load–moment interaction diagram computed based on the mentioned assumption and sectional analysis. The inclusion of GFRP-bar compressive strain in the calculation of the P–M interaction curve yielded higher values than those neglecting the contribution of the GFRP bars in compression. When the GFRP-bar compressive strain increased from 0.002 to 0.0035, the axial load and moment increased, as shown in Fig. 17. At the lower depth of the neutral axis [$c \leq 120$ mm (4.7 in.)], however, both the axial load and moment remained same. This was due to strain compatibility (Fig. 15): as the depth of the neutral axis decreased, the compressive strain (ε_{f4}) in the GFRP bars near the compression fiber decreased, and at the lower depth of the neutral axis, the

compressive strain in the GFRP bars, ε_{f4} contributed equally to the moment and axial load independent of the assumed maximum compressive strain in the GFRP bars (ε_{fc}).

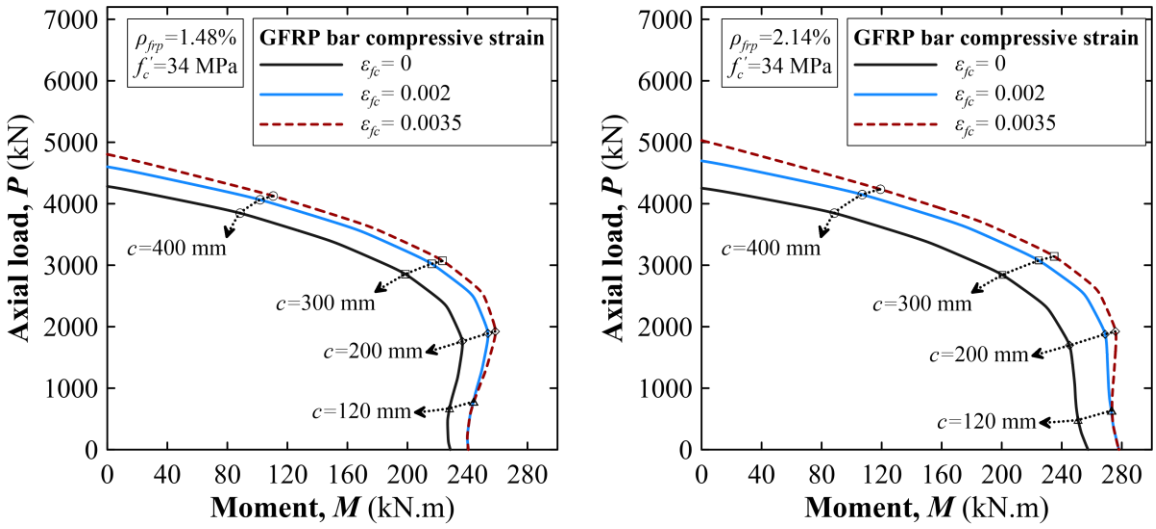

Note: c= depth of neutral axis; 1 mm=0.0394 in.

Figure 4.17- Axial load-moment interaction curve for GFRP-reinforced concrete columns

Table 6 lists the lateral load capacity computed from the P–M interaction curve (Fig. 17) corresponding to the axial load, $P = 0.2A_g f_c'$. The predicted lateral load capacity neglecting the contribution of the GFRP bars in compression was very conservative. The predicated capacity improved by considering the contribution of the GFRP bars in compression, although the values of $V_{\exp}/V_{theo}$ were still higher, as shown in Table 6. As shown in Fig. 15, the value of ε_{f4} in sectional analysis will always be lower than the maximum assumed compressive strain in concrete ($\varepsilon_{cu} = 0.0035$) due to strain compatibility, even if the compressive strain of the GFRP bars is increased. Thus, a confined-concrete model should be developed based on a large set of experimental data on GFRP-reinforced concrete columns subjected to simulated seismic loads in order to accurately predict the lateral load capacity.

Table 4.6- Comparison of predicated and experimental lateral load capacities

Specimen ID	V_{exp} (kN)	V_{theo} [a] (kN)	V_{theo} [b] (kN)	V_{theo} [c] (kN)	$\frac{V_{exp}}{V_{theo}}$ [a]	$\frac{V_{exp}}{V_{theo}}$ [b]	$\frac{V_{exp}}{V_{theo}}$ [c]
G#5-#3-100	192	141	150	151	1.36	1.28	1.27
G#5-#4-100	250	141	150	151	1.77	1.67	1.65
G#5-#4-120	232	141	150	151	1.64	1.55	1.54
G#5-#4-150	196	141	150	151	1.39	1.31	1.30
G#6-#4-100	251	151	164	166	1.66	1.53	1.51
G#6-#5-100	300	151	164	166	1.98	1.83	1.81
G#6-#4-120	260	151	164	166	1.72	1.58	1.57
G#6-#4-150	221	151	164	166	1.46	1.35	1.33

[a] Lateral load predicted neglecting the contribution of GFRP bar in compression (CSA S806 2012).

[b] Lateral load predicted considering the contribution of GFRP bar in compression, $\varepsilon_{fc} = 0.002$ (CSA S6 2019)

[c] Lateral load predicted considering the contribution of GFRP bar in compression, $\varepsilon_{fc} = 0.0035$

Note: V_{exp} is experimental lateral load capacity in kN; V_{theo} is predicted lateral load capacity in kN; 1 kN = 0.225 kip.

4.6 SUMMARY AND CONCLUSIONS

To check the effectiveness of longitudinal and transverse GFRP reinforcement, eight concrete columns were tested under simulated quasi-static cyclic load and constant axial load. The experimental results are presented in the form of hysteretic response, deformability, and strain in GFRP longitudinal and lateral reinforcement. The following conclusions can be drawn from this study.

1. The well-confined GFRP-reinforced concrete columns showed stable hysteretic response achieving a second peak after strength degradation due to deterioration of the concrete cover.

2. There was no significant difference in the energy dissipation of the tested columns, regardless of longitudinal or transverse reinforcement ratio.

3. The transition between the elastic and inelastic zone of the GFRP-reinforced columns was referred to as elastic deformation (Δ_e), and defined at a concrete compressive strain, $\varepsilon_c = 0.003$. The ultimate deformation (Δ_u) was defined as corresponding to the displacement upon the crushing of the first longitudinal GFRP bar in compression.

4. The well-confined columns with lower longitudinal reinforcement ratio showed increased strength and drift capacity compared to the specimens with less reinforcement, with drift capacity based on first longitudinal GFRP bar failure. This did not hold true for the columns with more longitudinal reinforcement where the spacing of the lateral reinforcement did not significantly affect drift capacity.

5. Increasing the longitudinal bar size decreased the drift capacity of the well-confined column but improved both strength and drift capacity of the columns with less confinement based on drift capacity defined at the first longitudinal GFRP bar failure. The well-confined column G#5-#4-100 reinforced with longitudinal reinforcement ratio of 1.48% developed more strain in the longitudinal bar than column G#6-#4-100 with longitudinal reinforcement ratio of 2.14%, which supports the increased deformability in specimen G#5-#4-100.

6. GFRP spirals and cross ties restrained the lateral expansion of concrete core in the case of the columns with lower spacing, which effectively improved the horizontal load resistance with lower maximum strain in the longitudinal bars.

7. The column reinforced with more lateral spirals and cross ties developed more strain, which helped enhance the strength and deformability of the specimen compared to columns with fewer lateral spiral and cross ties.

8. The maximum strain developed in the spiral and cross ties at a 4% drift ratio in all the specimens was less than 0.006, which is the maximum strain allowed in CSA S806 (2012). The spirals and cross ties effectively limited the expansion of the concrete core after the cover spalled. The maximum strain developed in the straight

portion of the lateral reinforcement at failure was, however, significantly lower than its rupture strain.

9. Including the contribution of GFRP bars in compression in predicting the load capacity improved the $V_{\exp}/V_{theo}$ ratio. In contrast, the predicted values of the lateral load capacity were too conservative. Thus, a confined-concrete model should be developed based on larger number of experimental data on GFRP-reinforced concrete column subjected to simulated seismic loads to accurately predict the lateral load capacity.

Chapter 5
BEHAVIOR OF RC COLUMNS WITH HYBRID REINFORCEMENT (STEEL/GFRP) UNDER REVERSED CYCLIC LOAD

Comportement de colonnes en béton armé d'armature hybride (acier-PRFV) constituée d'armature longitudinale en acier et d'armature transversale en PRFV sous charge cyclique inversée

Foreword

Authors and affiliation:

- **Girish Narayan Prajapati**, Ph.D. Candidate, Department of Civil Engineering, Université de Sherbrooke, Sherbrooke, QC, Canada, J1K 2R1.
- **Ahmed Sabry Farghaly,** Research Associate, Department of Civil Engineering, Université de Sherbrooke, Sherbrooke, QC, Canada, J1K 2R1.
- **Brahim Benmokrane**, **FACI**, Professor of Civil Engineering and Tier-1 Canada Research Chair in Advanced Composite Materials for Civil Structures and NSERC Research Chair in Innovative FRP Reinforcement for Concrete Structures, Department of Civil Engineering, Université de Sherbrooke, Sherbrooke, QC, Canada, J1K 2R1.

Journal: ACI Structural Journal

Status: Submitted May 2021

Abstract

This paper presents the results of laboratory testing of four full-scale concrete columns reinforced with hybrid reinforcement consisting of longitudinal steel bars and transverse glass fiber-reinforced polymer (GFRP) spiral and cross ties. The columns had an overall height of 1850 mm (72.8 in) and cross section of 400 × 400 mm (15.8 × 15.8 in.). The reinforcement parameters were transverse reinforcement ratio (1.27%, 1.06% and 0.85%) and longitudinal steel bar size (No. 5 and No. 6). The columns were subjected to constant axial load and reversed cyclic loading with increase amplitude until failure. Test results show that column failure depended on the amount of reinforcement. All the columns achieved drift values consistent with the requirements of the relevant design codes. The strain profile of the GFRP spirals and cross ties during the test show their effectiveness in providing confinement after the steel yielded. Spacing of the transverse reinforcement affected column drift capacity. The test results show strength values consistent with North American design codes. The measured lateral effective stiffness was close to the required values in ACI 318 and ASCE/SEI 41. Moreover, the test results provide reliable evidence about the best approach for optimally combining the two structural materials (steel and GFRP).

5.1 INTRODUCTION

Aggressive environments corrode steel reinforcement in conventionally reinforced concrete structures, which substantially reduces their service lives. The harsh winter in northern countries leads to the extensive use of deicing salt. That reduces concrete alkalinity, which leads to corrosion of the steel reinforcement (Lounis and Daigle 2008). Corrosion costs directly impact a country's economy, such as in the United States where they account more than 3% of the gross domestic product (Koch et al. 2002). Estimates for repairing infrastructure damage due to corrosion in United States and Canada run into billions of dollars (Koch et al. 2002; Renew Canada 2014). These high costs have led contractors to seek out more efficient and corrosion-resistant solutions. Fiber-reinforced

polymers (FRPs) represent one such solution that both improves structure service life while reducing repair costs (ISIS Canada 2007). Research on the behavior of FRP as internal reinforcement in reinforced concrete members has fueled its use in bridge slabs and beams (El-Salakawy et al. 2005; Kassem et al. 2011). The behavior of this kind of reinforcement under seismic loading is questionable due to the linear elastic behavior of FRP materials.

Mohamed et al. (2014) tested concrete walls reinforced solely with GFRP bars under reversed cyclic loading. They reported sufficient drift capacity without reduction in the walls' flexural capacities. Recent research by various investigators on concrete columns reinforced longitudinally and transversely with FRP bars and subjected to simulated seismic load showed that such columns exhibited a more stable response with achievable drift ratios than their counterpart steel-reinforced concrete columns (Ali and El-salakawy 2015; Elshamandy et al. 2018; Sharbatdar and Saatcioglu 2009; Tavassoli et al. 2015). Nevertheless, the linear behavior of GFRP bars caused GFRP-reinforced columns to dissipate lower energy than their counterpart steel-reinforced columns (Ali and El-salakawy 2015; Tavassoli et al. 2015). Studies on FRP-reinforced beam–column connections reported lower strength due to the low stiffness of GFRP bars (Mady et al. 2011). Thus, in an effort to achieve sufficient inelasticity to structures, Tavassoli and Sheikh (2017) conducted research on combining steel and GFRP bars, in which steel could provide the required inelasticity and GFRP ties could provide effective confinement.

Concrete columns reinforced with hybrid longitudinal steel and transverse GFRP reinforcement have shown acceptable behavior (Tobbi et al. 2014a) and provided better corrosion resistance (Pantelides et al. 2013). Research on hybrid-reinforced concrete columns under reversed cyclic loading—either circular cross sections with GFRP spirals (Tavassoli and Sheikh 2017) or square cross sections with GFRP ties (Kharal and Sheikh 2018)—exhibited behavior identical to steel-reinforced columns. Research on concrete columns reinforced with hybrid reinforcement consisting of steel and FRP reinforcement is, however, limited and requires intensive study to provide design recommendations for use in seismic design.

ACI 440.1R (2015) contains no provisions for the design of concrete members with hybrid reinforcement, whereas CSA S806 (2012) has clauses on the design of concrete members reinforced with hybrid reinforcement (steel/FRP) subjected to seismic load. Thus, the present study assessed the behavior of concrete columns reinforced with hybrid reinforcement consisting of steel longitudinal bars and GFRP spirals and ties under lateral cyclic load. Moreover, this study compares the obtained experimental results to the relevant North American design codes.

5.2 RESEARCH SIGNIFICANCE

Experimental research is required to verify the relevance of reinforced concrete structure individual member reinforced with hybrid longitudinal steel and lateral GFRP reinforcement under different loading conditions, especially under simulated seismic loading. There is a need for new noncorroding structural materials for the construction of parking structures and highway bridge columns to reduce infrastructure deterioration due to steel corrosion while providing the required inelastic behavior during seismic events. Laboratory tests have been conducted to investigate the behavior of concrete columns reinforced with hybrid reinforcement consisting of longitudinal steel and transverse GFRP reinforcement subjected to quasi-static reversed cyclic loading. Our study examined the feasibility of using GFRP transverse reinforcement in reinforced concrete structures to develop more economical and durable alternatives to steel-reinforced structures from a perspective of seismic performance. Test results are summarized, showing the effectiveness of GFRP spirals and cross ties in terms of ductility, energy dissipation, and effective stiffness. The results reported in this paper represent a significant contribution to the relevant literature and provide designers, engineers, and members of code committees with much-needed data and recommendations to advance the use of hybrid reinforcement (steel/GFRP) in concrete columns. Moreover, the promising results of this study represent a further step toward the use of hybrid reinforcement (steel/GFRP) for concrete columns.

5.3 EXPERIMENTAL INVESTIGATION

5.3.1 Test specimens

Column specimens had an overall height of 1850 mm (72.8 in.) and cross-sectional dimensions of 400 × 400 mm (15.8 × 15.8 in.). The specimens portray a full-scale column of 3300 mm (145.6 in.) high, representing a column between the footing and the point of contraflexure with an effective height of 1650 mm (65 in.). The column is supported by stub of 600 mm (23.6 in.) height and cross-sectional dimensions of 1200 × 1200 mm (47.2 × 47.2 in.) (Fig. 5.1). A clear cover of 25 mm (1 in.) was maintained. Columns were reinforced with twelve longitudinal steel bars: three with No. 5 (15.87 mm [0.6 in.]) rebar and one with No. 6 (19.05 mm [0.7 in.]) rebar. The transverse reinforcement for each column were No. 4 (12.7 mm [0.5 in.]) GFRP spiral and cross tie. Stub were reinforced at top and bottom layer with No. 6 steel rebar.

The notations S#5-#4-100, S#5-#4-120 and S#5-#4-150 denotes that the columns reinforced with No. 5 longitudinal steel rebars and transverse reinforcement spaced at 100, 120 and 150 mm (3.94, 4.72, and 5.91 in.), respectively. Spacing of transverse reinforcement selected based on clause 12.7.3.4, CSA S806 (2012), which state that the spacing of lateral reinforcement should not exceed the minimum of one-quarter of least column dimension, $6d_b$ (d_b is diameter of longitudinal bar), and 150 mm (5.9 in.). The notation S#6-#4-100 denotes that the column is reinforced with No. 6 longitudinal reinforcement and transverse reinforcement spaced at 100 mm (3.94 in.).

5.3.2 Material properties

The specimens were cast in two stages; first, the bottom stub was cast using the ready-mix normal weight concrete with a target compressive strength of 50 MPa (7.2 ksi), then the column was cast using 30 MPa (4.3 ksi) target compressive strength. Concrete strength was measured prior to testing of column using three standard cylinders of size 100 × 200 mm (3.94 × 7.87 in.). The average compressive strength for the column concrete were 34.28

MPa (5.05 ksi) for S#5-#4-100, 34.59 MPa (5.02 ksi) for S#5-#4-120, 34.63 MPa (5.02 ksi) for S#5-#4-150, and 35.58 MPa (5.16 ksi) for S#6-#4-100.

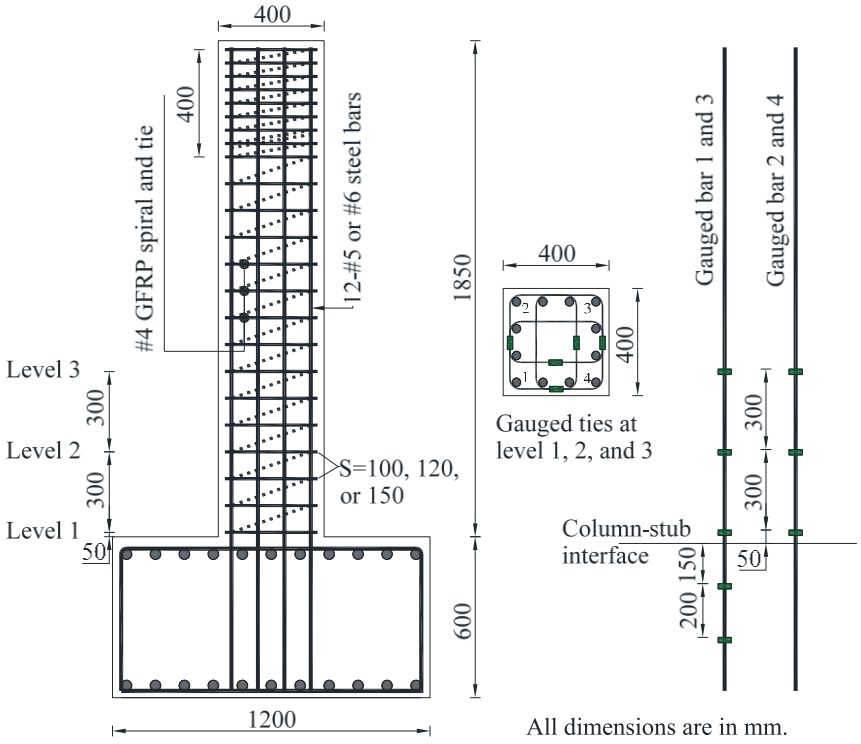

Figure 5.1- Reinforcements details and strain gauge locations

Steel rebar Grade 60 No. 5 and No. 6 were used as the longitudinal bars to construct the column specimens. The properties of Grade 60 steel rebar were provided by the manufacturer as elastic modulus (E_s) of 200 GPa (29007.5 ksi), yield strength (f_y) of 414 MPa (60 ksi) and yield strain (ε_y) of 0.002. Grade III high modulus, sand coated No. 4 GFRP spiral and cross ties (CSA S807 2010) were used as transverse reinforcement. Five samples were tested for tensile properties in straight portion per ASTM D7205/D7205M (2016) and in bent bars per ASTM D7914 (2014). The average elastic modulus, ultimate tensile strength in straight portion and ultimate strain were 63.2 GPa (9166 ksi), 1570 MPa

(228 ksi), and 2.48%, respectively. Average tensile stress in bent portion was 801 MPa (116 ksi).

5.3.3 Instrumentation

The test specimens were instrumented to measure the surface deformations and strains in reinforcing bars. Strain gauges were installed on the longitudinal bars over a length that cover expected plastic hinge regions. Four strain gauges were attached to longitudinal bars below the column-stub interface. About fifteen strain gauges were installed on the GFRP spiral and cross ties in the potential plastic hinge region. Concrete strains were monitored using six linear variable differential transducers (LVDTs) installed either side of the column face. Figure 5.1 and Figure 5.2 illustrate the position of all the instruments used in the study.

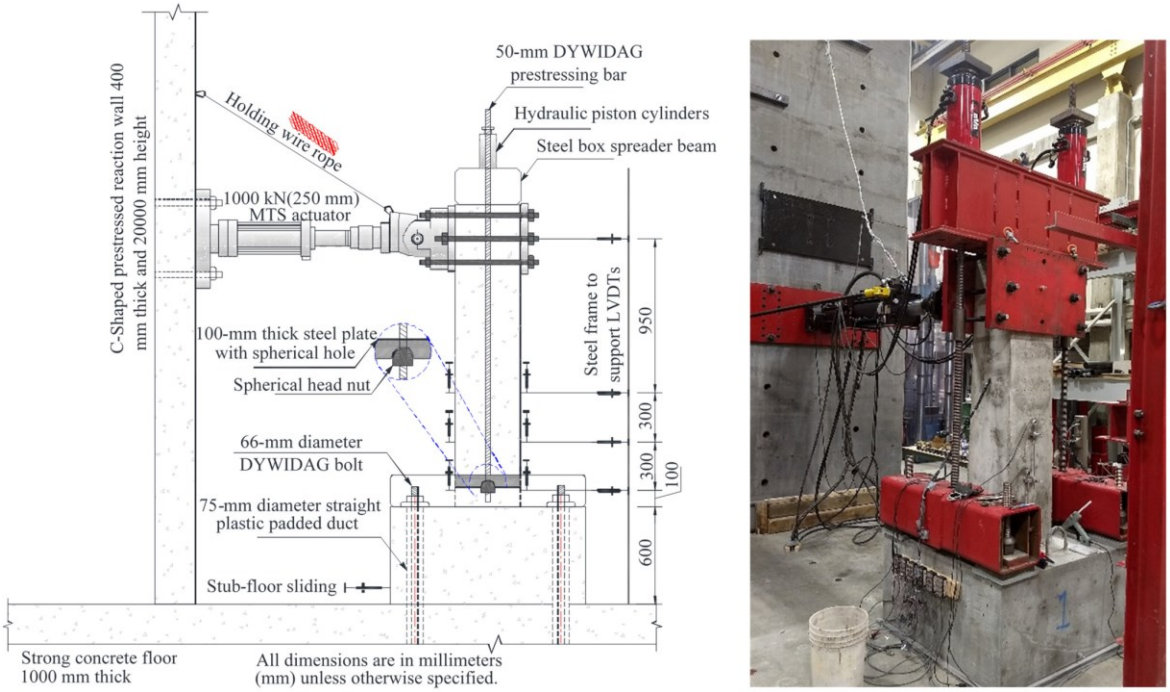

Figure 5.2- Test setup and LVDTs location

5.3.4 Test setup and procedure

Specimens were tested under combined constant axial compression and quasi-static cyclic loading. The stub was connected to the strong floor using four DYWIDAG steel bars. Two hydraulic jacks applied a constant axial load. The resulting axial load on columns was calculated using same day concrete strength to achieve the same axial load of $0.2A_g f_c^{'}$; where A_g is the gross cross-sectional area and $f_c^{'}$ is the concrete compressive strength. Two reversed lateral cycles at increasing drift were applied by a horizontal MTS actuator attached to column tip and another end to laboratory reaction wall (Fig. 5.2). Displacement-based quasi -static cyclic loading was followed at a constant rate of 2 mm/min. (0.08 in./min.) with lateral drift ratios (ratio of lateral displacement to columns effective height) as 0.25%, 0.50%, 0.75%, 1.0%, 1.5%, 2.0%, 2.5%, 3.0%, 4.0%, 5.0%, 6.0% and 7.0%.

Table 5.1- Failure progression for each specimen

	S#5-#4-100		S#5-#4-120		S#5-#4-150		S#6-#4-100	
	Drift ratio, %	Lateral load, kN	Drift ratio, %	Lateral load, kN	Drift ratio, %	Lateral load, kN	Drift ratio, %	Lateral load, kN
FTC*	+0.18	+70.3	+0.19	+73.4	+0.21	+79.9	+0.20	+82.4
FLBY	+0.66	+175.7	+0.74	+164.6	+0.75	+164.7	+0.89	+212.1
VSC	+0.92	+198.7	+1.13	+189.5	+0.86	+173.7	+1.25	+246.6
PLL	+1.19	+203.5	-1.26	-200.2	+1.27	+192.0	-1.38	-250.5
CCS	+1.50	+201.5	+1.45	+185.4	+1.05	+186.6	+1.58	+230.1
LBB	+4.00	+183.7	-3.00	-166.6	+3.00	+143.3	+5.00	+209.6
LBF	+4.90	+144.9	-5.15	-103.9	-	-	-	-
GTRF	-	-	-	-	-	-	+6.50†	+180.3†
DC	6.17	162.8	4.00	160.2	2.69	153.6	6.07	200.4

***** Acronyms: FTC is first tensile crack; FLBY is first longitudinal bar yield; VSC is vertical splitting crack; PLL is peak lateral load; CCS is concrete cover spalling; LBB is longitudinal bar buckling; LBF is longitudinal bar failure; GTRF is GFRP transverse reinforcement failure; and DC is drift capacity.

† Failure of GFRP ties in Column S#6-#4-100. Note: 1kN=0.225 kip

5.4 TEST RESULTS AND DISCUSSION

5.4.1 Crack progress and failure mode

Table 5.1 gives the significant behavioral change for all columns and is indicated on the hysteresis response (lateral load-drift ratio), as shown in Figure 5.3. At the same drift ratio, the second cycle followed a path similar path to the first cycle with reduced strength. Therefore, the second cycle has been removed from the hysteresis response. All columns showed predominantly flexure behavior. The horizontal flexural cracks developed and propagated at the distance equal to transverse reinforcement spacing in columns S#5-#4-120 and S#5-#4-150. These cracks, however, developed at twice the spacing of lateral reinforcement above 500 mm (19.7 in.) from the column-stub interface in columns S#5-#4-100 and S#6-#4-100 (see Fig. 5.4(a)). Horizontal flexural cracks developed up to about same height in all the columns until 1.0% drift cycle. After that, the increased lateral drift caused corner concrete cover to split in the compression face. At a 2.0% drift ratio, as shown in Figure 5.4(b), vertical splitting crack at corner in column S#5-#4-150 developed up to 1100 mm (43.3 in.) in height measured above column-stub interface. Degradation of the concrete cover started at first excursions at a 1.5% drift ratio in columns with No. 05 steel longitudinal reinforcement and at the next drift ratio in column S#6-#4-100. The cover spalling was rapid in the columns with wider transverse reinforcement spacing at the 2.0% drift ratio.

All of the specimens exhibited spalling of concrete cover predominantly in the plastic hinge region within 500 mm from column-stub interface (Fig. 5.4(c)). At higher drift cycle, the core concrete between transverse reinforcement starts to deteriorate. This degradation of core concrete leaves longitudinal steel reinforcement unprotected, and it buckled at higher drift ratios. The lower transverse reinforcement ratio of column S#5-#4-150 caused buckling of the longitudinal bars earlier at a 3.0% lateral drift ratio compared to the other test columns. The spacing of the transverse reinforcement delayed the buckling of steel bar in columns S#5-#4-100 and S#6-#4-100. Due to the confinement provided by the heavy

reinforcement in the stub, the buckling of steel bar occurred at 150 to 240 mm above the column-stub interface. Figure 5.4(c) shows the buckled longitudinal bar in columns S#5-#4-100, S#5-#4-120 and S#5-#4-150 at a 4.0% drift ratio.

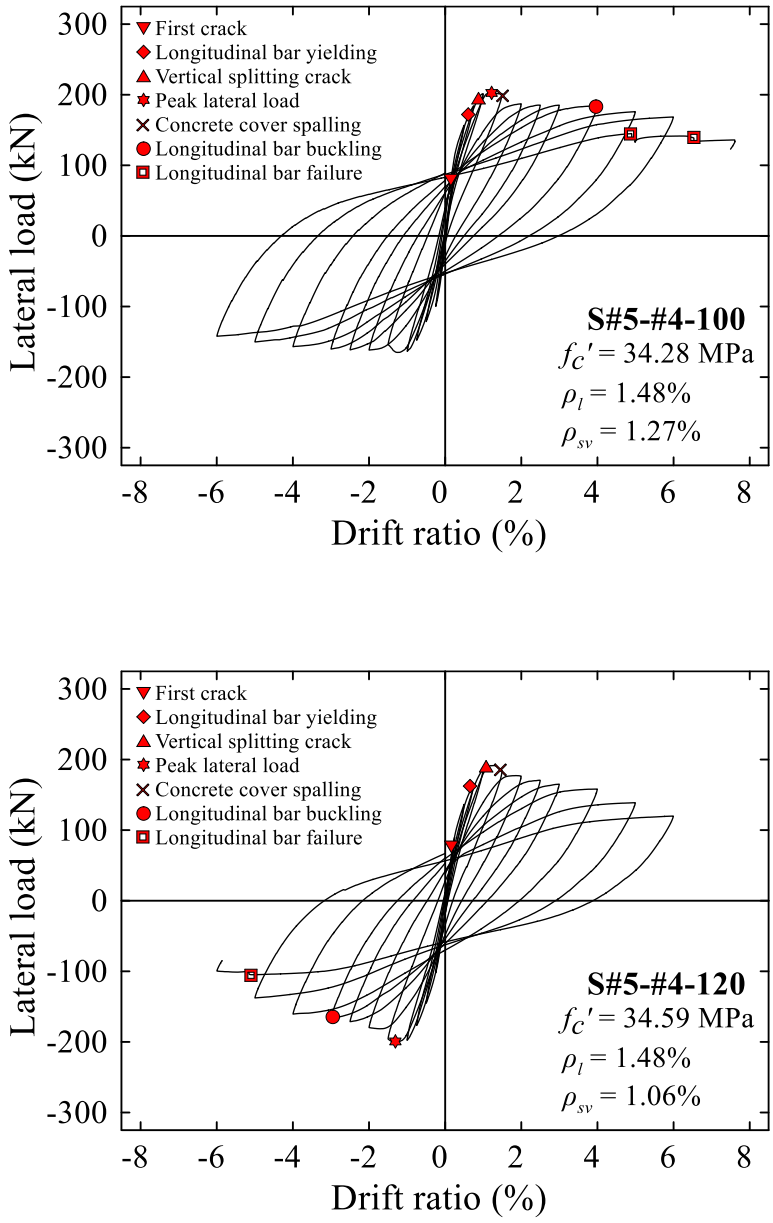

Figure 5.3-Hysteresis response

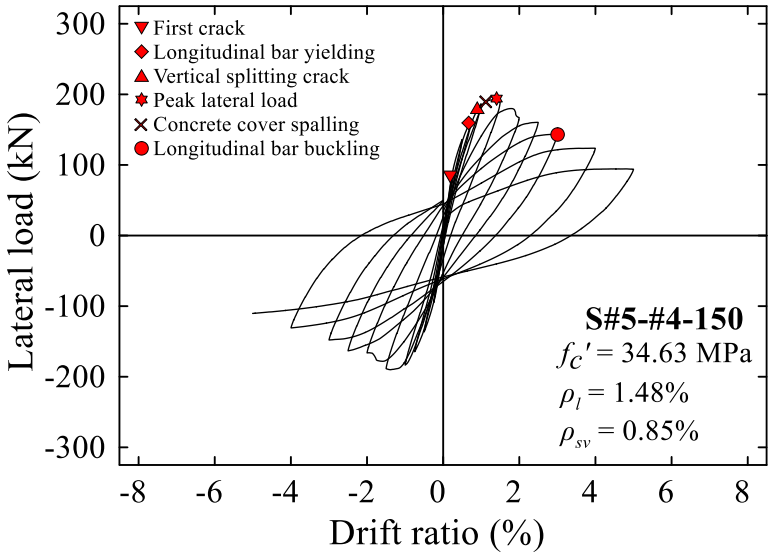

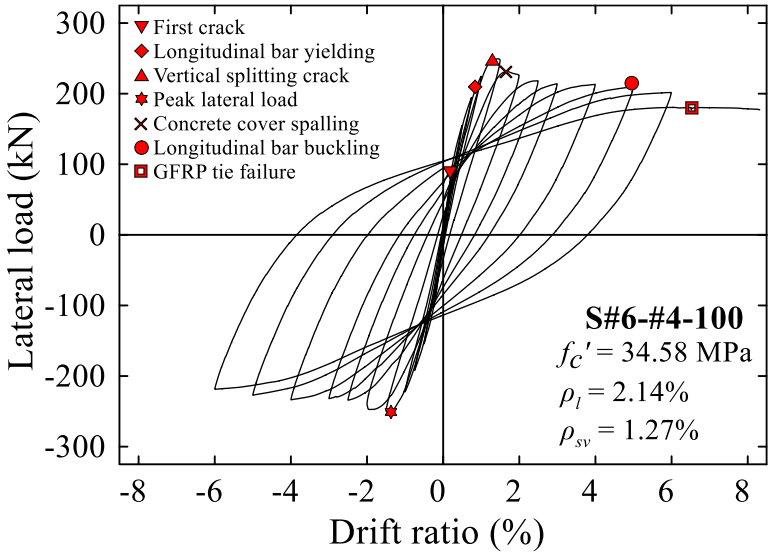

Figure 5.3- Hysteresis response (continued)

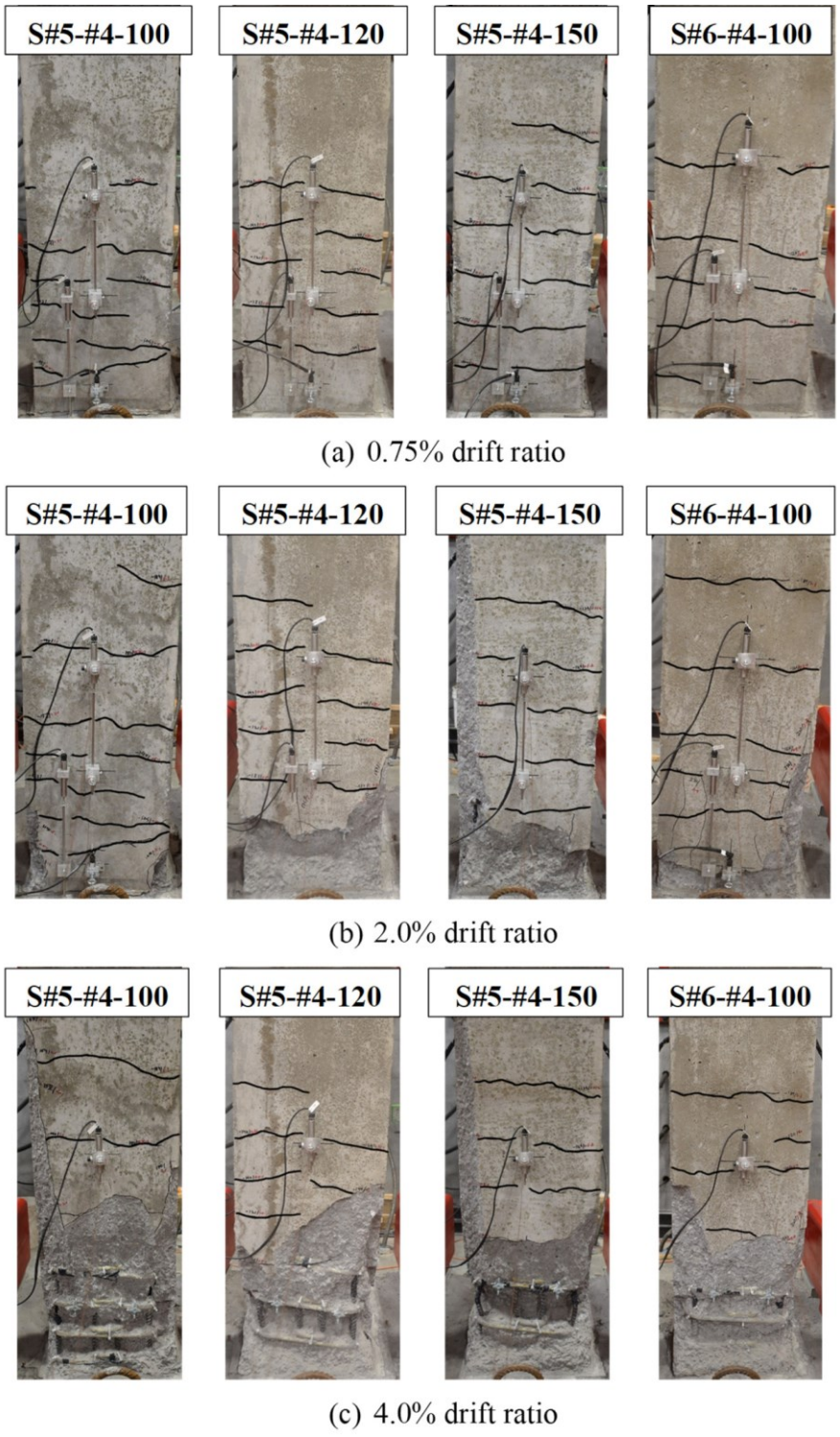

Figure 5.4- Crack progression in hybrid-reinforced concrete columns

Even after the buckling of longitudinal steel bars, all the columns sustained at least two more lateral drift cycles and with minimal strength degradation in case of Column S#5-#4-100 and S#6-#4-100 (Fig. 5.3). This shows that the increased confinement provided by the GFRP spiral and ties delayed the column failure. The role of GFRP spiral and cross ties is discussed in more details in the later section. Columns S#5-#4-100 and S#5-#4-120 experienced continued core concrete crushing and suffer significant buckling of steel bars and eventual fracture of longitudinal bar in the buckled zone (Fig. 5.5). All the longitudinal steel bars in column S#5-#4-150 buckled outwards accompanied by the crushing of the core concrete at final drift cycle, as shown in Figure 5.5. Column S#5-#4-150 was considered failed as the lateral strength degraded to 50% of the ultimate lateral load. The expansion of the concrete core caused the longitudinal reinforcement to buckle outward. Continuous outward buckling of steel bar in column S#6-#4-100 creates tension in the GFRP tie and led to its rupture (Fig. 5.5).

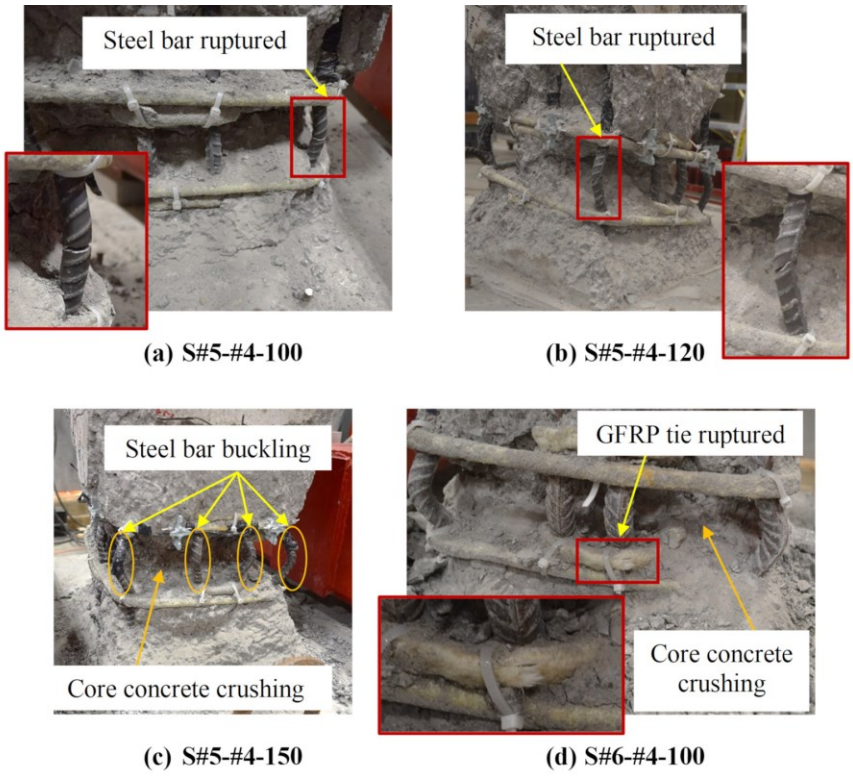

Figure 5.5- Failure modes of test columns

The drift capacity of the columns is defined as maximum drift ratio reached at 20% post-peak strength loss and listed in Table 5.1. There is no fixed goal for an adequate seismic performance. Stable behavior with minimal strength loss up to 4.0% drift ratio is, however, normally found to be satisfactory for preventing collapse at maximum considered earthquake according to most seismic design codes (FEMA-273 (2007), ASCE/SEI 41 (2017)). Columns S#5-#4-100, S#5-#4-120 and S#6-#4-100 satisfy this criterion. Accordingly, columns with hybrid reinforcement consisting of longitudinal steel and transverse GFRP reinforcement can be reviewed as being acceptable materials and designs for high seismic zones.

5.4.2 Displacement ductility

Ductility is the ability of a reinforced-concrete column to deform past the yielding of its longitudinal steel reinforcement. Table 5.2 provides the experimental column-tip displacement at the yielding of the first longitudinal bar Δ_y, at peak load Δ_{mu}, and at 80% of peak load at the post-peak stage $\Delta_{u,0.8}$. The displacement ductility (μ_Δ) in this paper is defined as the ratio of column top displacement at a specified point to displacement at the start of yielding of the longitudinal steel bars. This definition of μ_Δ is based on recorded experimental displacement without idealization of the load-displacement (F-Δ) curve. The calculated displacement ductility at peak load $\mu_{\Delta,mu}$, 2.5% drift ratio $\mu_{\Delta,2.5\%}$, 4.0% drift ratio $\mu_{\Delta,4\%}$, and post-peak 20% strength loss $\mu_{\Delta,0.8}$ are presented in Table 5.2.

The literature contains several discussions concerning the definition of displacement ductility of reinforced-concrete column confined with steel ties (Park and Paulay 1975; Paulay and Priestley 1992; Priestley et al. 1996; Sheikh and Khoury 1993). As Park (1988) and Priestley (2000) both mentioned, there is no uniform definition for the displacements at yield and ultimate loads. Nevertheless, many researchers have recommended idealized elastic-perfectly plastic bilinear curve to define the displacement ductility based on experimental data, using different methods to define the equivalent curve. Thus, to compare the columns in our study reinforced with hybrid reinforcement (steel/GFRP) to

conventional reinforced-concrete column confined with steel tie, we adopted the definition of idealized elastic-perfectly plastic bilinear curve from Park (1988), as illustrate in Figure 5.6. This method is based on equivalent elastic-plastic energy absorption. The area under the experimental load-displacement curve equates to the idealized bilinear curve for a chosen ultimate displacement and an initial stiffness equal to the secant stiffness measured at the first longitudinal bar yielding. Mathematically,

$$\frac{1}{2}F_{y,4\%}^{bc}\Delta_{y,4\%}^{bc}+\left(\Delta_{4\%}-\Delta_{y,4\%}^{bc}\right)F_{y,4\%}^{bc}=E_{F-\Delta,\mathrm{e}} \tag{5.1}$$

$$F_{y,4\%}^{bc}=K_y\Delta_{y,4\%}^{bc} \tag{5.2}$$

where; $F_{y,4\%}^{bc}$ and $\Delta_{y,4\%}^{bc}$ are yield load and displacement for elastic-plastic bilinear curve at maximum displacement $\Delta_{4\%}$ corresponding to 4.0% drift ratio; $E_{F-\Delta,\mathrm{e}}$ is the area under the experimental lateral load-displacement (F-Δ) curve; and K_y is the stiffness corresponding to first longitudinal bar yield.

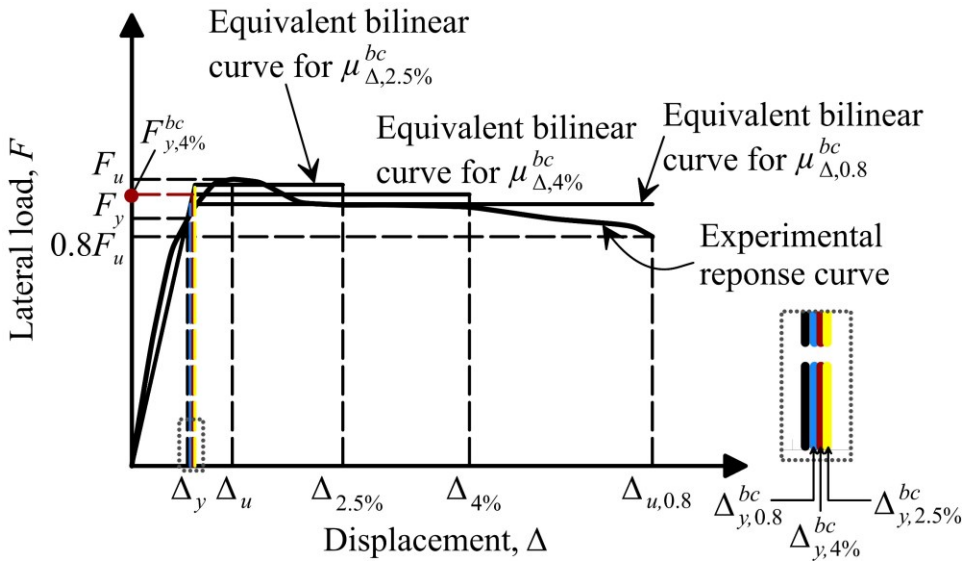

Figure 5.6- Idealized elastic-plastic bilinear curve

Table 5.2- Measured displacements and computed displacement ductility

Specimen	Direction	Measured displacements (mm)			Displacement ductility (μ_Δ)								
					At maximum load		At 2.5% drift		At 4.0% drift		At 20% strength loss		
		Δ_y	Δ_{mu}	$\Delta_{u,0.8}$	$\mu_{\Delta,mu}$	δ_{mu} (%)	$\mu_{\Delta,2.5\%}$	$\mu^{bc}_{\Delta,2.5\%}$	$\mu_{\Delta,4\%}$	$\mu^{bc}_{\Delta,4\%}$	$\mu_{\Delta,0.8}$	$\mu^{bc}_{\Delta,0.8}$	$\delta_{0.8}$ (%)
S#5-#4-100	Positive	10.86	19.63	101.7	1.81	1.19	3.80	3.34	6.08	5.54	9.37	8.86	6.17
	Negative	10.86	20.65	99.0[§]	1.90	1.25	3.80	3.11	6.08	5.1	9.12	7.92	6.00[§]
S#5-#4-120	Positive	12.15	20.72	70.2	1.71	1.26	3.40	2.96	5.43	5.05	5.78	5.42	4.25
	Negative	12.15	20.71	66	1.70	1.26	3.40	3.02	5.43	5.23	5.43	5.23	4.00
S#5-#4-150	Positive	12.32	20.98	44.4	1.70	1.27	3.35	2.97	—[†]	—[†]	3.6	3.24	2.69
	Negative	12.32	22.97	47.3	1.86	1.39	3.35	2.97	—[†]	—[†]	3.84	3.49	2.86
S#6-#4-100	Positive	14.74	23.87	100.1	1.62	1.45	2.80	2.41	4.48	4.12	6.79	6.5	6.07
	Negative	14.74	22.82	99.0[§]	1.55	1.38	2.80	2.28	4.48	3.83	6.72	5.91	6.00[§]

* Based on first longitudinal steel bar yielding.

[†] Specimen S#5-#4-150 drift ratio at 20% strength degradation was lower than 4.0% drift.

[§] Strength loss was less than 20% of maximum load. Maximum available drift ratio or displacement in negative direction.

Note: 1mm=0.0394 in.

Solving equation (5.1) and (5.2) to obtain the idealized elastic-perfectly plastic yield point ($F^{bc}_{y,4\%}$ and $\Delta^{bc}_{y,4\%}$). The idealized bilinear curve displacement ductility at 2.5% drift ratio $\mu^{bc}_{\Delta,2.5\%}$, 4.0% drift ratio $\mu^{bc}_{\Delta,4\%}$, and 20% post-peak strength degradation $\mu^{bc}_{\Delta,0.8}$ determined with this method are presented in Table 5.2. The average column lateral strength based on idealized bilinear curve at 2.5% drift ratio, 4.0% drift ratio, and 20% strength degradation are 99% [Coefficient of Variation (CV)=2%], 92.5% (CV=5%), and 93% (CV=2.8%) of experimental peak load, respectively. The average displacement ductility $\mu_{\Delta,2.5\%}$, $\mu_{\Delta,4\%}$, and $\mu_{\Delta,0.8}$ based on first longitudinal bar yield are, respectively, 16% (CV=3.6%), 8.3% (CV=6.4%), and 8.8% (CV=3.9%) higher than corresponding idealized bilinear curve displacement ductility $\mu^{bc}_{\Delta,2.5\%}$, $\mu^{bc}_{\Delta,4\%}$, and $\mu^{bc}_{\Delta,0.8}$, respectively. The literature indicates that reinforced concrete columns with steel ties should ensure a displacement ductility of more than four with limited strength degradation in seismic design (Park and Sampson 1972). In the present study, the columns reinforced with hybrid reinforcement— S#5-#4-100, S#5-#4-120 and S#6-#4-100— achieved displacement ductility greater than four at a post-peak 20% strength degradation with a flexure mode of failure.

It should be noted that a maximum drift of 2.5% is allowed in both American (ASCE/SEI 7 2016) and Canadian (NBCC 2015) building codes for normal importance building. For new moment-resisting frame members with hybrid reinforcement comprising of longitudinal steel bars and GFRP lateral reinforcement, CSA S806 (2012) design code requires minimum lateral drift ratios of 4.0% and 2.5% for columns in ductile and moderately ductile moment-resisting frame, respectively. The limit of 20% post-peak strength degradation is used in experimental studies to quantify the reasonable limit for sufficient performance of the structural element (AASHTO 2014; ATC 2009; Calvi et al. 2008). The drift achieved by columns reinforced with hybrid reinforcement (S#5-#4-100, S#5-#4-120 and S#6-#4-100) at 20% strength degradation was greater than the requirement for ductile moment-resisting frames (4.0%) by CSA S806 (2012). And drift achieved by column S#5-#4-150 was higher than 2.5% drift requirement for moderately ductile moment-resisting frames (CSA S806 2012).

5.4.3 Energy dissipation

Cumulative dissipated energy (E_{cum}) is evaluated up to failure drift at 20% post-peak strength degradation as

$$E_{cum} = \sum_{i=1}^{n} E_i \tag{5.3}$$

Where, E_i is dissipated energy in *i*th cycle as defined in Figure 5.7. Figure 5.8 shows the dissipated energy for individual cycle and cumulative dissipated energy of column S#5-#4-150 up to complete drift cycle recorded. Occurrences representing significant behavioral change inducing changes in dissipated energy (such as first longitudinal bar yielding, peak load, and longitudinal bar buckling) are indicated. The observed dissipated energy was higher in the first cycle compared to the second cycle with the same drift ratio. Damage induced by concrete cracking, splitting, and spalling in the first cycle caused loss of strength and stiffness, which lowered the dissipation capacity of the column in second cycle at the same lateral drift. Similar behavior was observed for other columns. The increase in the dissipated energy was higher at the loading cycle, when the columns attain peak load compared to preceding cycle, as shown in Figure 5.8.

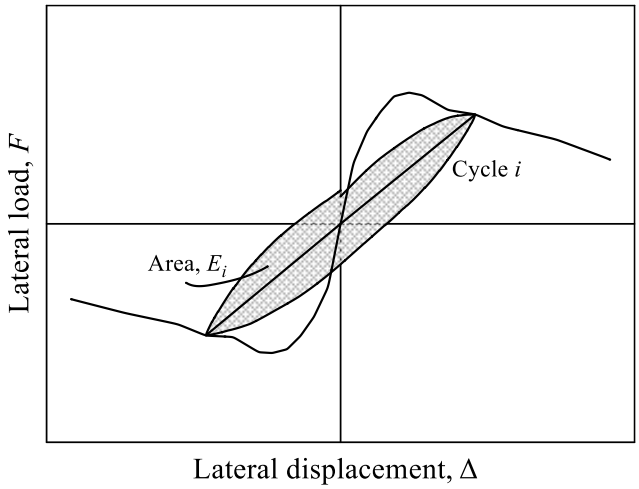

Figure 5.7- Definition of energy dissipation

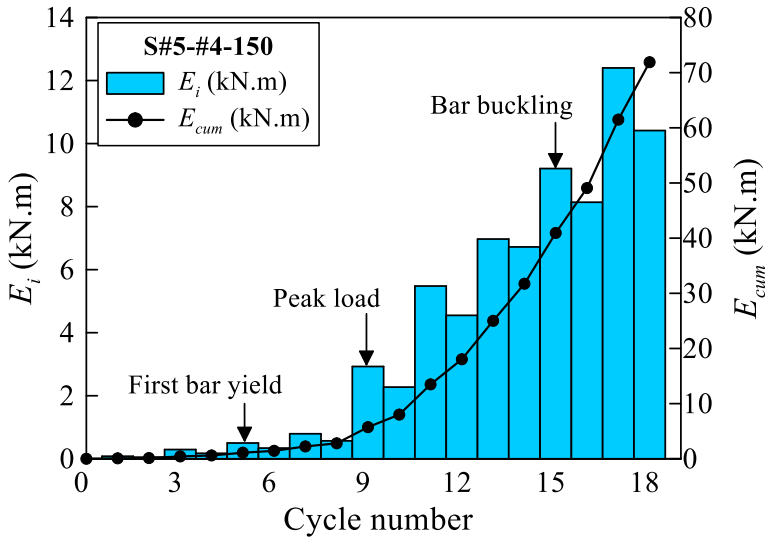

Figure 5.8- Dissipated energy per cycle and cumulative dissipated energy of column S#5-#4-150

Cumulative dissipated energy for each specimen versus loading cycle and residual drift (for first cycle of the same amplitude) is plotted in Figure 5.9 along with major behavioral change. As the amplitude of lateral drift cycle increases, the longitudinal bar yielded, the cover concrete deteriorates, and the longitudinal steel buckled, which induces plasticity in the hysteresis response. Thus, as the loading cycle increased, so did the cumulative dissipated energy increases, as in Figure 5.9(a). The level of spacing of transverse GFRP reinforcement does not impact the cumulative dissipated energy until failure. The column with wider spacing of lateral GFRP reinforcement achieved less drift than well-confined columns, thereby changing the final cumulative dissipated energy. Column S#5-#4-100 with transverse reinforcement at a pitch of 100 mm (3.94 in.) achieved about two and three times more cumulative dissipated energy than columns S#5-#4-120 and S#5-#4-150, respectively. As observed in Figure 5.9, the longitudinal reinforcement ratio affected the cumulative dissipative energy. Column S#6-#4-100 with longitudinal reinforcement ratio of 2.14% achieved greater cumulative dissipated energy than the other columns. Figure 5.9

indicates that the cumulative dissipated energy could be improved by increasing the transverse and longitudinal reinforcement ratio.

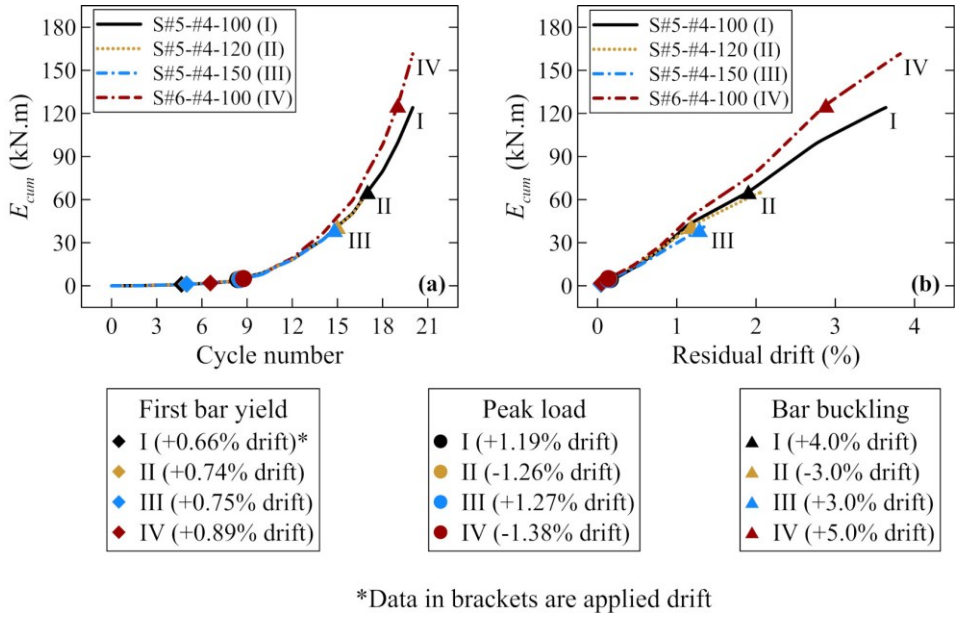

Figure 5.9- Cumulative dissipated energy versus (a) loading cycle; and (b) residual drift.

5.4.4 Longitudinal bar strain

Strain reading recorded from the strain gauges installed in the corner longitudinal steel bar are shown in Figure 5.10**.** The values are from strain gauges attached to steel bar located at 150 mm (5.9 in.) below column-stub interface; 50 mm (2 in.) and 350 mm (13.8 in.) above column-stub interface. The first longitudinal bar yielded at a strain of about $2000\mu\varepsilon$ occurring at the location near the column-stub interface. The recorded strains value escalated after the bar yield. The strains were almost same at 50 mm (2 in.) and 350 mm (13.8 in.) above column-stub interface until the yielding of steel bars in columns S#5-#4-120, S#5-#4-150 and S#6-#4-100.

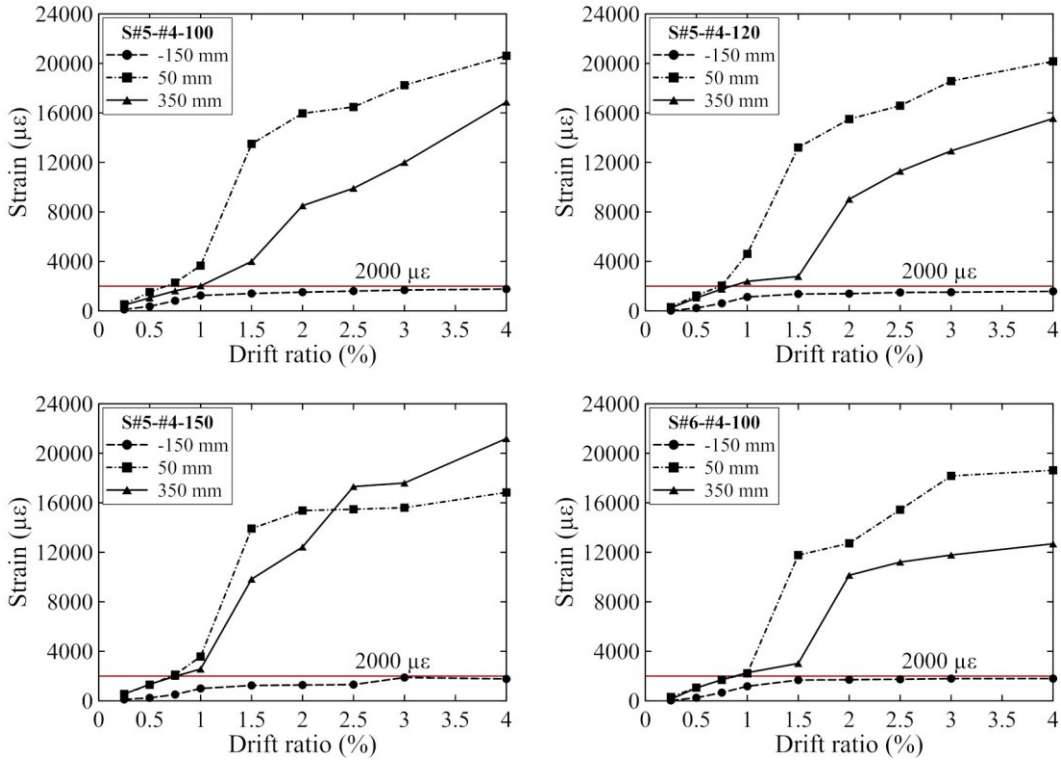

Figure 5.10- Strain developed in longitudinal steel bar

Figure 5.10 shows that the yielding of the longitudinal bar extended up to height of 350 mm (13.8 in.) before columns reaches its peak load. The strains in the gauges located at 50 mm (2 in.) from column-stub interface suddenly increased at a lateral drift ratio of 1.5%. Similar trend were observed in past research with concrete columns confined with steel ties (Wight 1973). At a 2.0% drift cycle, the strain hardening caused strains in longitudinal bar to redistributed away from the critical section. As seen in Figure 5.10, the strain values escalated in strain gauges located at 350 mm (13.8 in.) above column-stub interface, except for column S#5-#4-150. In this column, the strain values in the gauges located at both locations above column-stub interface increased at 1.5% lateral drift. The rate of increase in strain values began dropping off with increasing drift cycles after the 1.5% drift ratio in the strain gauges located at 50 mm (2 in.). In column S#5-#4-150, the strain gauge installed at 350 mm (13.8 in.) recorded greater strain than that in strain gauge installed at 50 mm (2 in.) from column-stub interface after 2.0% drift cycle.

The strain gauges installed at 150 mm (5.9 in.) below the column-stub interface recorded strains lower than $2000\mu\varepsilon$ up to 4.0% drift ratio. Strain value increased until 1.5% drift ratio after that plateau was observed in all specimens (Fig. 5.10). The measured longitudinal bar strain below the column-stub interface mirrored the typical behavior reported by Ali and El-Salakawy (2016) and Wight (1973) for column confined with steel reinforcement. Thus, the behavior of the longitudinal steel bar was unaffected by type of transverse reinforcement used (GFRP or Steel).

5.4.5 GFRP tie strain

Figure 5.11 provides the strain in GFRP rectilinear spiral and cross tie at level 2 (see Figure 5.1) for each specimen. Strain measurements are reported up to available drift ratios for each specimen as many strain gauges malfunctioned in the final drift cycles. At the initial stage of the drift cycles, the strain increased and then fell back to zero. After the yielding of first longitudinal steel bar, the strain in both GFRP spiral and cross tie increases with observable values at zero drift. More strain developed in the GFRP cross tie than in GFRP spiral when the cover concrete deteriorates and longitudinal bar yielding in the early stages of the lateral drift ratios. Once the cover had spalled, the core concrete's expansion was effectively resisted by GFRP rectilinear spiral, as shown by the increased strain after 1.5% drift ratio. A sharp increase in GFRP spiral strain was observed in each column at drift cycles causing bar buckling. The drift cycle at which the bar buckled for each specimen is marked in Figure 5.11. This shows that the GFRP cross tie is more effective up to the yielding of the longitudinal steel bars. And after the steel yielded, GFRP rectilinear spiral became more effective in controlling expansion of the core concrete.

All the test specimens withstood at least two more drift cycles before failure. This implies the effectiveness of GFRP transverse reinforcement in providing sufficient confinement, even in column S#5-#4-150 with its greater spacing and in preventing brittle mode of failure. Table 5.3 gives the strain developed at a peak of 4.0% and the maximum strain before the strain gauges malfunctioned. At the 4.0% drift ratio, the strain in GFRP rectilinear spiral was below $6000\mu\varepsilon$, as required by CSA S806 (2012), except for column

S#5-#4-150. The strain was, however, higher than steel tie yield strain of $2000\mu\varepsilon$. In addition, the strain was much lower than the rupture strain of the GFRP spiral. Thus, the GFRP spiral and cross ties provided more effective confinement to column core than steel ties. This statement, however, needs to be verified experimentally by considering an equivalent reinforced-concrete column confined with steel ties. Nevertheless, the confinement effectiveness of steel ties beyond yield strain was found to be inefficient and could jeopardize column behavior (Bayrak and Sheikh 1998). Similar observations appear in the literature (Kharal and Sheikh 2018) related to reinforced-concrete columns confined with GFRP ties having external plastic tube with ribbed surface.

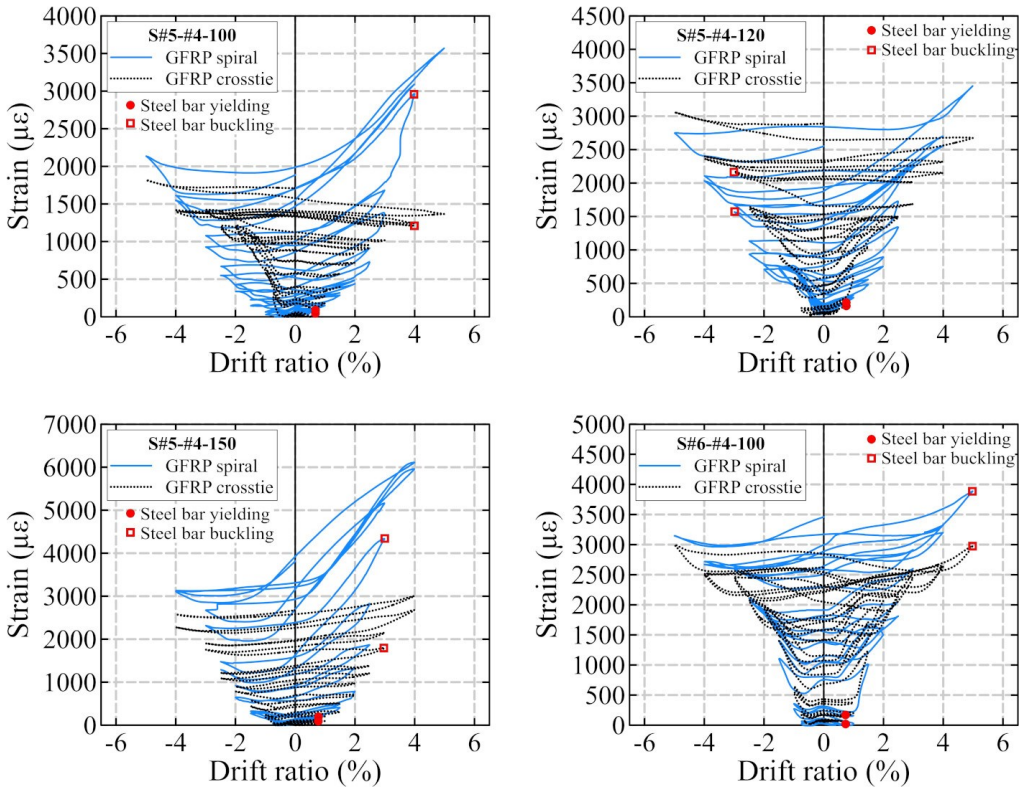

Figure 5.11- Strain developed in GFRP spiral and cross tie

Table 5.3- Strain developed in GFRP spiral and cross tie.

Specimen	Ultimate strain ε_{fhu}, με	Maximum strain at 4.0% drift, $\varepsilon_{fh,4\%}$, με		Maximum strain ε_{fh}, με	
		Spiral	Cross tie	Spiral	Cross tie
S#5-#4-100	24800	3094	1428	3779	1910
S#5-#4-120	24800	2702	2399	4138	3394
S#5-#4-150	24800	6113	3004	6113	3004
S#6-#4-100	24800	3322	2651	4161	3238

5.4.6 Effect of reinforcement parameters

The lateral load in column S#5-#4-100, with narrower tie pitch, increased by 2% and 6% compared to columns S#5-#4-120 and S#5-#4-150, respectively. The drift ratio (see Table 5.2) improved to 6.17% in column S#5-#4-100 compared to 4.25% and 2.86% in columns S#5-#4-120 and S#5-#4-150, respectively. Thus, spacing of the transverse reinforcement does not significantly affect the lateral load capacity. It did reduce the drift capacity of the columns with larger tie pitch by increasing post-peak strength degradation. Replacing the No. 5 longitudinal steel bar in column S#5-#4-100 with No. 6 steel bar in column S#6-#4-100 improved the lateral load capacity by 23% but did not increase the drift capacity.

5.5 COMPARISON WITH ANALYTICAL MODELS

5.5.1 Flexural strength

A maximum concrete compression strain (ε_{cu}) of 0.0035 and 0.003 is permitted in Canadian (CSA A23.3-19; CSA S806-12) and American (ACI 318-19; ACI 440.1R-15) design codes, respectively, although these codes use the equivalent concrete stress block with reduced compressive strength of concrete in plane-section analysis. The factor α_1 accounts for the concrete strength reduction is a function of specified concrete compressive

strength in Canadian codes, in contrast to American codes, which assumed it as a constant value. The decrease in the depth of nonlinear curve of concrete to form an equivalent rectangular stress block is accounted for by β_1, which is the ratio of rectangular block depth to neutral axis depth. Table 5.4 provides these factors. As the main reinforcement in the test specimens was steel, ACI 318 (2019) and CSA A23.3 (2019) were used to determine the flexure strength. The nominal flexural strength was obtained using manufacturer specified steel yield strength (f_y), and $1.25f_y$ to obtain probable flexural strength, as required by American (ACI 318-19) and Canadian (CSA A23.3-19) codes. Steel yield strain was evaluated as f_y / E_s. Concrete compressive strength measured on the day of specimen testing was used in the calculations. The flexural strength was computed with the mentioned assumption and corresponded to a concentric axial load of 20% of the compression capacity of column's gross section (see Table 5.5). Experimentally measured yield moment at the yielding of first bar and ultimate moment are also presented.

Table 5.4- Design code specifications (ACI 318-19; CSA A23.3-19)

	American code	Canadian code
α_1	0.85	$0.85-0.0015f_c^{'}>0.67$
β_1	$0.85-\frac{0.05\left(f_c^{'}-28\right)}{7}$, $28<f_c^{'}<55$ MPa	$0.97-0.0025f_c^{'}>0.67$
E_c	$4700\sqrt{f_c^{'}}$	$4500\sqrt{f_c^{'}}$

α_1 is the ratio of average stress in rectangular compression block to specified concrete strength; β_1 is the ratio of depth of rectangular compression block to depth of neutral axis; $f_c^{'}$ is the concrete compressive strength; and E_c is the elastic modulus of concrete. Note: 1 MPa = 145 psi.

Table 5.5 shows the discrepancies in flexural strength obtained using the provisions in the American (ACI 318-19) and Canadian (CSA A23.3-19) codes. Figure 5.12 gives the

plotted axial load-moment (P-M) interaction diagram. The different α_1 and β_1 factors in Table 5.4 were used to define the equivalent concrete stress block and assumed concrete compressive strain are the reasons for the differences in the obtained flexural strength.

Table 5.5- Experimental and calculated flexural strength of test columns.

Specimen	M_n^A	M_n^C	M_{pr}^A	M_{pr}^C	$M_{y,e}$	$M_{u,e}$	$\frac{M_{y,e}}{M_n^A}$	$\frac{M_{y,e}}{M_n^C}$	$\frac{M_{u,e}}{M_{pr}^A}$	$\frac{M_{u,e}}{M_{pr}^C}$
	kN.m									
S#5-#4-100	292	289	312	315	290	336	0.99	1.00	1.08	1.07
S#5-#4-120	292	289	312	315	272	330	0.93	0.94	1.06	1.05
S#5-#4-150	292	289	312	315	272	317	0.93	0.94	1.02	1.01
S#6-#4-100	349	346	374	380	350	413	1.00	1.01	1.10	1.09

M_n^A and M_{pr}^A are nominal and probable flexural strength computed based on assumption of ACI 318-19; M_n^C and M_{pr}^C are nominal and probable flexural strength computed based on assumption of CSA A23.3-19; $M_{y,e}$ and $M_{u,e}$ are experimentally recorded yield and ultimate flexural strength. Note: 1 kN.m=0.738 kip-ft.

Experimentally measured yield strength for well-confined columns S#5-#4-100 and S#6-#4-100 were equal to calculated nominal moment strength using both American (ACI 318-19) and Canadian (CSA A23.3-19) codes (Table 5.5 and Figure 5.12). The measured yield strength for columns S#5-#4-120 and S#5-#4-150 were only 6-7% lower than the computed nominal strength. The recorded ultimate moment strength was, on average, 6% (CV=3.4%) higher than the probable moment strength computed with both design codes. Thus, the estimation of probable moment strength could be supported by a factor of more than $1.25f_y$, considerably for the well-confined columns.

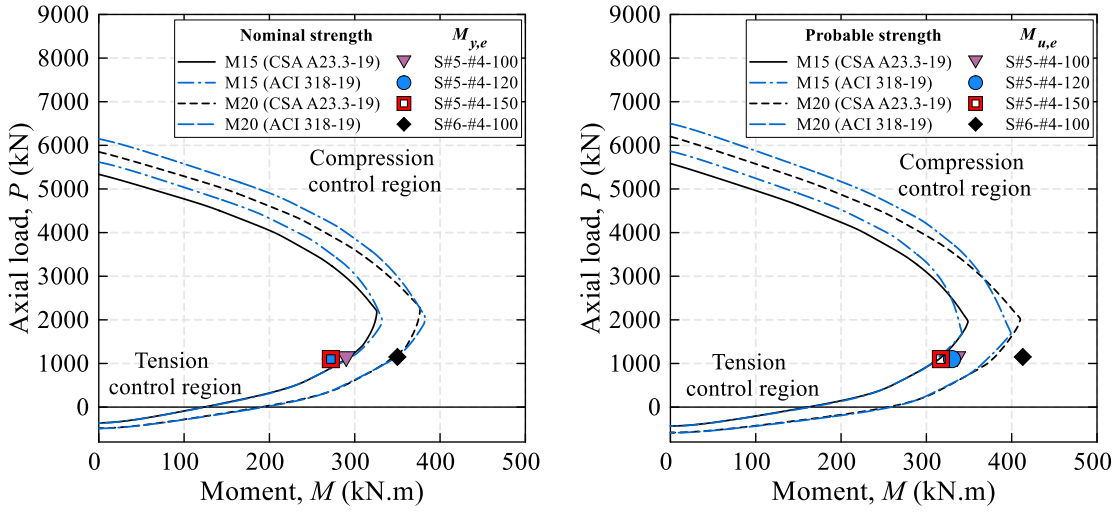

Figure 5.12- Comparison of P-M interaction with experimental data

5.5.2 Effective stiffness

Lateral secant stiffness of the yielding of the first longitudinal bar was calculated assuming the column as a cantilever and having a linear curvature variation over the effective height (H_e) before the first bar yielding. The experimentally recorded effective lateral stiffness $EI_{eff,e}$ of each column was computed as:

$$EI_{eff,e} = \frac{F_y H_e^3}{3\Delta_y} \tag{5.4}$$

where F_y and Δ_y are the applied load and corresponding displacement at first yield Table 5.1.

Stiffness values computed with Eqn. (4) were normalized to the column gross sectional stiffnesses ($E_c I_g$) (see Table 5.6). Table 5.4 provides the concrete elastic modulus, E_c taken from both code specification and calculated with the concrete compressive strength ($f_c^{'}$) on the day of testing of each column. Table 5.6 compares the normalized experimental

lateral stiffness ($EI_{eff,e}/E_cI_g$) computed according to both design codes to the values recommended in ACI 318 (2019) and CSA A23.3 (2019).

Table 5.6- Calculated and design code effective stiffness.

Specimen	$\frac{EI_{eff,e}}{E_cI_g{}^A}$ *	$\frac{EI_{eff,e}}{E_cI_g{}^C}$ †	EI_{eff}/E_cI_g		
			ACI 318-19, cl. A.8.4	ACI 318-19, cl. 6.6.3.1.1	CSA A23.3-19, cl. 10.14.1.2
S#5-#4-100	0.41	0.43			
S#5-#4-120	0.34	0.36			
S#5-#4-150	0.34	0.35			
S#6-#4-100	0.36	0.38	0.40	0.70	0.70

* E_c is elastic modulus of concrete based on ACI 318-19

† E_c is based on CSA S806-12

I_g is the moment of inertia of column gross section.

The updated design code ACI 318 (2019) from ACI 318 (2014) added an appendix A to verify the design using nonlinear analysis. The section on effective stiffness defined in ACI 318 (2019), clause A.8.4 are based on ASCE/SEI 41 (2017), clause 10.3.1.2.1. The effective lateral stiffness based on clause A.8.4 in ACI 318 (2019) and clause 10.14.1.2 in CSA A23.3 (2019), clause 10.14.1.2 are provided to determine the first-order lateral deflection based on elastic analysis. Elwood et al. (2007) recommended the Specification in clause 10.3.1.2.1 of ASCE/SEI 41 (2017) subsequent to their analysis of a database of 221 rectangular concrete columns confined with steel ties under reversed cyclic loading with axial loads lower than $0.67A_gf_c'$ (Elwood et al. 2007).

Effective stiffness is employed in modelling concrete ductile structural element to define the yield point or elastic limit of moment-curvature and load-deflection curve for bridge (AASHTO 2011; CSA S6-19) and buildings (ACI 318-19; ASCE/SEI 41-17; CSA A23.3-19). It can be established on experimental data or using recommendation of design codes. In our study, experimental effective stiffnesses were close to the estimated effective

stiffness values according to A.8.4 in ACI 318 (2019) and clause 10.3.1.2.1 in ASCE/SEI 41 (2017). This indicates that the behavior of columns with hybrid reinforcement consisting of steel bars and GFRP spiral and cross ties is similar in defining the effective stiffness. Clause 10.14.1.2 in CSA A23.3 (2019) overestimated the effective stiffness by 1.5 times the experimental effective stiffness for all test specimens, as there is no other specification is detailed.

5.6 CONCLUSIONS

Four full-scale columns with hybrid reinforcement consisting of longitudinal bars and GFRP spirals and ties were designed, constructed, and tested under simulated seismic loading with varying longitudinal and transverse reinforcement ratio. The fabricated and tested columns had an overall height of 1850 mm (72.8 in) and cross section of 400 × 400 mm (15.8 × 15.8 in.). The test results analysis and comparison were made in terms of crack propagation, hysteresis response, strain developed in longitudinal steel bars and transverse GFRP reinforcement (spirals and cross ties). Further, the experimental results were compared with the available North American codes and seismic design recommendations. Based on the test results, the following conclusions were drawn:

1. All the test specimens showed flexure behavior with concrete crushing and buckling of longitudinal steel bar. The column with adequate confinement provided by GFRP spiral and cross ties exhibited stable behavior, achieving drift more than 4.0% before the occurrence 20% strength degradation. Thus, the concrete columns with hybrid reinforcement could be reviewed as being acceptable material for use in new construction for high earthquake hazard zones.

2. At peak load, all the columns had a displacement ductility in excess of 1.50. The displacement ductility for the well-confined columns S#5-#4-100, S#5-#4-120, and S#6-#4-100 were 8.4, 5.3, and 6.2, respectively, with equivalent elastic-plastic bilinear curve at post-peak strength loss of 20%. This indicates that high ductility

can be achieved with transverse GFRP reinforcement. In addition, the achieved drift exceeded the requirement of CSA S806 (2012).

3. More energy dissipation was observed in the first cycle than in the second cycle for the same displacement amplitude. Narrower spacing of transverse GFRP reinforcement and higher longitudinal reinforcement ratio of steel is needed to improve the cumulative dissipated energy of such concrete columns.

4. The development of strain in the longitudinal steel bars of the concrete columns with hybrid reinforcement behaved similarly to the concrete columns totally reinforced with steel ties. The strain developed in transverse GFRP reinforcement indicates effective confinement provided by GFRP spiral and cross ties after the longitudinal reinforcement yielded. The GFRP cross ties provided an effective confinement up to and after yielding of longitudinal steel bars. As the core concrete expanded, the rectilinear GFRP spiral became more effective in confining the hybrid-reinforced concrete columns.

5. The drift capacity of the columns decreases as the pitch of the transverse GFRP reinforcement increased, without significantly affecting the lateral load capacity. The larger steel bar improved the lateral strength but did not increase column drift capacity

6. Probable flexural strength with $1.25f_y$ was 8% to 10% lower than the measured ultimate flexural strength of the well-confined columns. Thus, estimating the probable flexural strength estimated with a factor more than 1.25 could be justified, especially in the case of well-confined hybrid-reinforced columns.

7. The experimental effective stiffnesses at first yielding of longitudinal steel bar in the hybrid-reinforced columns was close to the prescribed effective stiffness in American codes (ACI 318-19; ASCE/SEI 41-17) for steel-reinforced concrete columns. The Canadian code (CSA A23.3-19), however, overestimate it by more than 1.5. Thus, effective stiffness recommended by American codes (ACI 318-19;

ASCE/SEI 41-17) can be used in defining the elastic point of load-deflection curve required in modelling ductile reinforced concrete structural element confined with GFRP spiral and cross ties.

8. This preliminary study on the hybrid-reinforced (steel/GFRP) concrete columns returned results similar to the requirements in North American building design code requirements for steel-reinforced concrete columns. Moreover, the transverse GFRP reinforcement was found to be very effective in confining the concrete core, reaching strains greater than the yield strain of steel ($2000\mu\varepsilon$).

The information presented in this paper improves understanding of how concrete columns reinforced with hybrid reinforcement consisting of steel longitudinal bars and transverse GFRP spiral and ties subjected to lateral cyclic load can be expected to behave. Much more experimental work is, however, required to investigate the seismic behavior of hybrid-reinforced columns. Moreover, the impact of different types of FRP reinforcement (such as carbon and basalt FRP) requires research. In addition, concretes such as fiber reinforced concrete (FRC), high strength concrete, and lightweight concretes (LWC) should be investigated.

Chapter 6

PERFORMANCE OF CONCRETE BRIDGE COLUMNS LONGITUDINALLY REINFORCED WITH STEEL AND GFRP BARS AND CONFINED WITH GFRP SPIRALS AND CROSS TIES UNDER REVERSED CYCLIC LOADING

Étude de la performances de colonnes de ponts en béton armé d'armature longitudinale d'acier et en PRFV et d'armature transversale constituée de spirales et d'épingles en PRFV sous chargement cyclique inversé

Foreword

Authors and affiliation:

- **Girish Narayan Prajapati**, Ph.D. Candidate, Department of Civil Engineering, Université de Sherbrooke, Sherbrooke, QC, Canada, J1K 2R1.
- **Ahmed Sabry Farghaly,** Research Associate, Department of Civil Engineering, Université de Sherbrooke, Sherbrooke, QC, Canada, J1K 2R1.
- **Brahim Benmokrane**, **FACI**, Professor of Civil Engineering and Tier-1 Canada Research Chair in Advanced Composite Materials for Civil Structures and NSERC Research Chair in Innovative FRP Reinforcement for Concrete Structures, Department of Civil Engineering, Université de Sherbrooke, Sherbrooke, QC, Canada, J1K 2R1.

Journal: Journal of Bridge Engineering, ASCE

Status: Submitted March 2021

Abstract

This paper reports the comparative results of an experimental study performed on concrete bridge columns with hybrid reinforcement (steel and GFRP) and GFRP reinforcement under quasi-static cycling loading. Four full-scale bridge columns were constructed with longitudinal steel rebars and confined with GFRP spirals and cross ties. Four other columns were constructed solely with GFRP reinforcement. The bridge columns had a cross section of 400 × 400 mm with a total height of 1850 mm. The columns were tested to failure under combined constant compressive axial load and quasi-static reversed cyclic loading. The columns were investigated in terms of longitudinal bar type, longitudinal reinforcement ratio, and transverse reinforcement ratio. The results show that the longitudinal reinforcement type significantly affected column performance in terms of important seismic parameters. The hybrid reinforced columns exhibited superior ductility and dissipated more energy than the GFRP-reinforced columns. Appropriately confined hybrid reinforced columns attained acceptable drift levels that meet the recommendations in most design codes. The failure mode of the GFRP-reinforced columns was more gradual with no strength degradation. The transverse reinforcement ratio and longitudinal reinforcement ratio patently influenced column behavior. The low elastic modulus of the GFRP bars compared to the steel rebars had a significant impact on the theoretical lateral capacity of the concrete columns.

6.1 INTRODUCTION

The main reason for the premature corrosion of steel rebars is an increase in the chloride concentration in concrete that eventually reduces its alkalinity. The presence of chloride ions in deicing salts—applied to roadways and bridges during the winter in countries such as Canada and in the snowbelt in the US—reaches the steel reinforcement through minor cracks in concrete. This causes the reinforcing steel to corrode and expand, which leads to cracking, delamination, and spalling of the concrete cover (Lounis and Daigle 2008). This reduces the load-carrying capacity of reinforced concrete structures such as bridge columns

leaving such structures vulnerable to natural calamities such as earthquakes. The cost to repair and rehabilitate bridges in North America has been estimated at hundreds of million dollars (Renew Canada 2014). This generates interest in using alternative materials like glass fiber-reinforced polymer (GFRP) as reinforcement in new reinforced concrete bridge structures due to its noncorroding properties (AASHTO, 2018).

Over the years, numerous studies have been conducted on the flexural behavior of reinforced concrete structures with GFRP as internal reinforcement (Kassem et al. 2011; Toutanji and Saafi 2000), which has led to its application in bridge slabs (El-Salakawy et al. 2005). Yet there is lack of research on GFRP-reinforced concrete members under compression. Nevertheless, recent studies on reinforced concrete columns under pure compression (Afifi et al. 2014; Alsayed et al. 1999; Karim et al. 2016; De Luca et al. 2010; Tobbi et al. 2012; Zadeh and Nanni 2012) and eccentric loading (Elchalakani et al. 2020; Hadhood et al. 2017; Hadi et al. 2016) have shown the viability of GFRP bars as longitudinal reinforcement. This research does not, however, demonstrate the practical behavior of reinforced concrete columns under reversed cyclic loading. The literature contains a few studies on the performance of GFRP-reinforced concrete walls, columns, and beam–column joints under combined axial and reversed lateral loads, which demonstrate the feasibility of GFRP bars.

Research on GFRP-reinforced concrete shear walls has indicated that appropriately designed and detailed walls with pure GFRP reinforcement could achieve their flexural capacities without a reduction in strength (Hassanein et al. 2019; Mohamed et al. 2014b). A drift ratio of more than 3% with any significant damage was reported from a test on lateral-resisting FRP-reinforced beam–column connections (Sharbatdar et al. 2011; Mady et al. 2011).

GFRP-reinforced concrete columns under simulated seismic loading have been shown to deliver stable performance and achieve higher levels of drift ratio than corresponding steel-reinforced columns (Ali and El-salakawy 2015; Elshamandy et al. 2018). The transverse reinforcement—either GFRP spirals (Elshamandy et al. 2018; Tavassoli et al. 2015) or

GFRP stirrups (Ali and El-salakawy 2015)—was able to provide increasing levels of confinement, delaying the crushing of the core concrete of the GFRP-reinforced concrete columns. However, GFRP-reinforced concrete columns showed linear-elastic behavior with lower residual deformations which resulted in reduced cumulative dissipated energy compared to steel-reinforced concrete columns (Ali and El-salakawy 2015; Elshamandy et al. 2018; Tavassoli et al. 2015). To prevent such situations, research is needed that considers the combination of steel and GFRP bars.

Hybrid columns with steel longitudinal reinforcement and GFRP transverse reinforcement under concentric loading were found to provide better resistance against the corrosion than a steel-reinforced column (Pantelides et al. 2013) while providing comparable compressive strength (Tobbi et al. 2014a). Little research on hybrid columns under simulated seismic loading has been reported. Tavassoli and Sheikh (2017) studied the behavior of circular hybrid reinforced columns confined with GFRP spirals and concluded that the strength and ductility of the columns were similar to that of a steel-reinforced column under reversed cyclic loading. It was also reported that the GFRP spiral effectively confined the concrete core at higher drift ratios. Research on square hybrid columns confined with GFRP ties indicates that properly designed and detailed columns provide satisfactory performance and are appropriate for seismic-based designs (Kharal and Sheikh 2018). Circular hybrid columns reinforced with GFRP spirals performed better than hybrid columns reinforced with GFRP ties (Kharal and Sheikh 2020). To date, no research has been performed on rectangular concrete columns reinforced longitudinally with steel bars and confined with GFRP rectilinear spirals, this merits research. The work on hybrid columns is limited. More experimental databases with varying test variables are required to recommend design provisions. The differences in behavior of GFRP-reinforced columns and steel-hybrid reinforced columns need to be investigated from the standpoint of seismic parameters.

6.2 RESEARCH SIGNIFICANCE

Our research aimed at experimentally determining the behavior of rectangular hybrid concrete bridge columns reinforced with longitudinal steel rebars and confined with GFRP spirals and cross ties subjected to simulated seismic loading. Response of the hybrid reinforced columns was compared to the counterpart GFRP-reinforced columns. Full-scale reinforced concrete columns were cast and tested to assess their seismic performance based on stiffness degradation, energy dissipation, and ductility. Parameters such as longitudinal bar type and longitudinal and transverse reinforcement ratios were also addressed. This study aimed at opening the way for further research to assess the feasibility of using GFRP lateral reinforcement in concrete structures and to initiate towards a more durable and economical alternative to steel-reinforced structures. This study is expected to open the way for further research to investigate the possibility of developing new applications for hybrid reinforcement (steel and GFRP) and GFRP bars and spirals, resulting in more durable, economic, and competitive reinforced concrete columns in seismic zones. Moreover, the experimental data provides the evidence required to include design provisions in the forthcoming AASHTO code on the use of hybrid reinforcement (steel and GFRP) and GFRP bars and ties as internal reinforcement in concrete bridge columns.

6.3 EXPERIMENTAL PROGRAM

6.3.1 Test specimens and Instrumentation

A total of eight full-scale specimens—each consisting of a 400 × 400 × 1850 mm rectangular column supported by a 600 × 1200 × 1200 mm stub—were cast and tested. Cyclic loading tests were conducted on a new earthquake bridge column and the reversed cyclic load was applied at an effective height of 1650 mm from the base of the column. Figure 6.1 shows the geometry of the test specimens. Four columns had GFRP as longitudinal and transverse reinforcement; four columns had steel as longitudinal

reinforcement and GFRP as transverse reinforcement (hybrid-reinforced columns). Figure 6.2(a) depicts the reinforcement cages for the GFRP-reinforced and hybrid columns. The hybrid columns had the same steel longitudinal reinforcement ratio as the GFRP-reinforced columns.

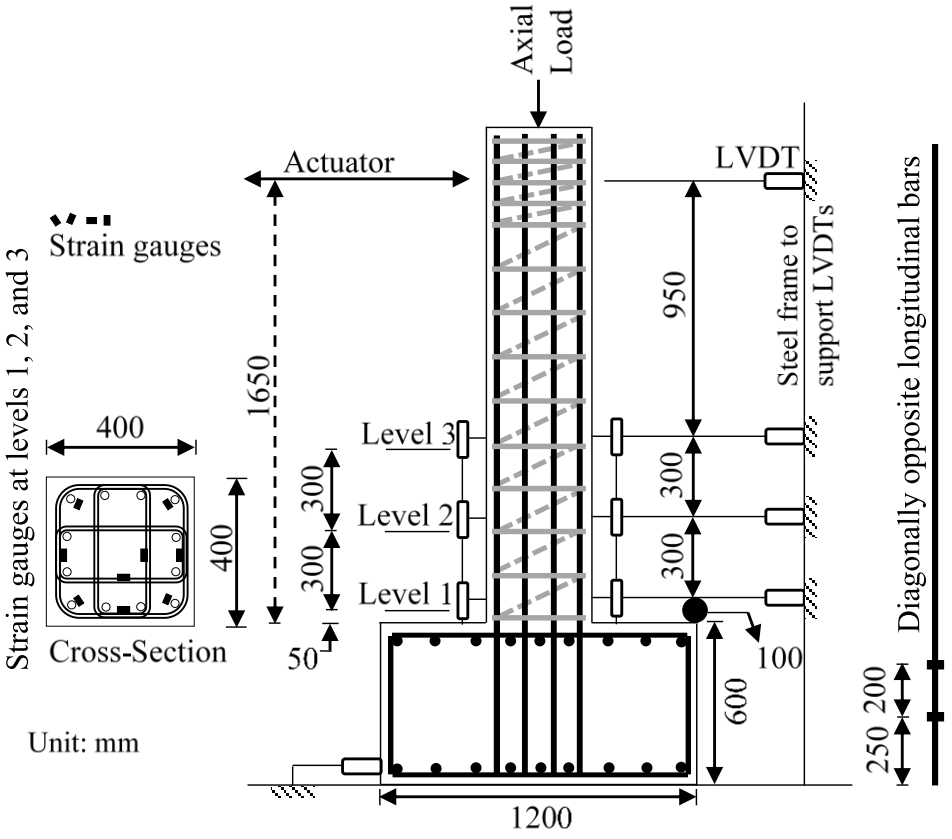

Figure 6.1- Test specimen details, strain gauges and LVDT locations

The study parameters were longitudinal bar type (steel or GFRP), longitudinal reinforcement size, and spacing of transverse reinforcement. Table 6.1 provides the details of the test specimens. All columns were reinforced with 12 number of longitudinal bars. Longitudinal bar size used in the study were 15.9 mm in diameter (#5) and 19.1 mm in diameter (#6) for both GFRP- and hybrid-reinforced columns. The area of the longitudinal reinforcement for all the columns were greater than the minimum requirement of $0.01A_g$ in bridge design codes AASHTO (2018) and CSA S6 (2019). All the columns were confined

with 12.7 mm (#4) GFRP spirals and cross ties. Figures 6.2(c) and 6.2(d) depict the GFRP spirals and cross ties used in the study, respectively. Spacing of the transverse reinforcement were selected based on requirements of AASHTO (2018), which say that the spacing of transverse reinforcement should not exceed the minimum of least dimension of the cross-section of the member, $6d_b$ (d_b is the diameter of the longitudinal bar), or 150 mm. In addition, according to AAHSTO (2018), the clear spacing between GFRP shear reinforcement elements should not be less than the greater of 1.33 times the maximum size of coarse aggregate or 25 mm. The longitudinal bars were extended 550 mm into the stub, satisfying the development-length requirement in CSA S806 (2012). M20 reinforcing steel bars were used to reinforce the stub in the top and bottom layers. An overall concrete cover of 25 mm was provided.

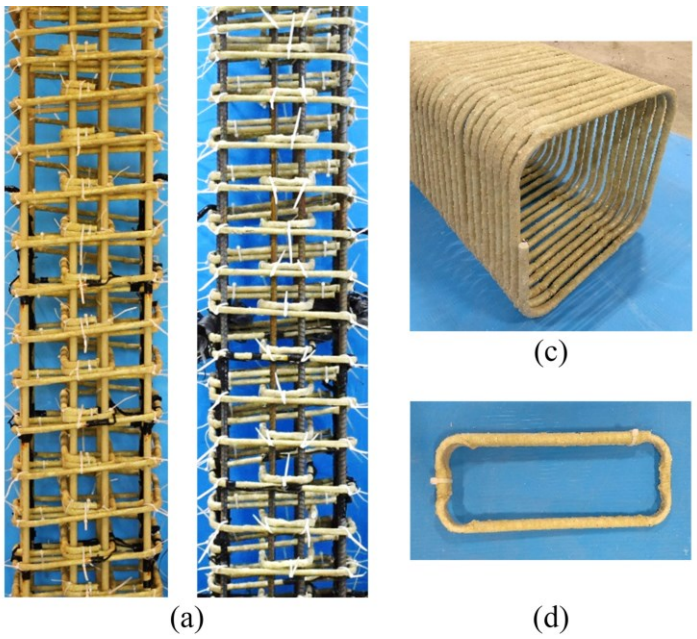

Figure 6.2- (a) Reinforcement cages; (c) GFRP spiral; and (d) GFRP cross tie

Table 6.1- Test specimen details and experimental results

Specimen	$f_c^{'}$ (MPa)	Longitudinal Reinforcement			Transverse Reinforcement		P_{th} (kN)	P_e (kN)	δ_u (%)	μ_Δ	$\frac{P_e}{P_{th}}$
		Bar no.*	d_b (mm)	ρ_l (%)	Spacing (mm)	ρ_{sv} (%)					
LG-15M-100	31.57	15M (#5)	15.87	1.48	100	1.27	138	250	10.1	7.56	1.81
LG-15M-120	34.23	15M (#5)	15.87	1.48	120	1.06	138	232	5.78	4.60	1.68
LG-15M-150	33.48	15M (#5)	15.87	1.48	150	0.85	138	196	6.59	5.17	1.42
LG-20M-100	34.42	20M (#6)	19.07	2.14	100	1.27	147	251	7.39	6.39	1.71
LS-15M-100	34.28	15M (#5)	15.87	1.48	100	1.27	175	204	6.16	9.89	1.17
LS-15M-120	34.59	15M (#5)	15.87	1.48	120	1.06	175	201	3.96	6.22	1.15
LS-15M-150	34.63	15M (#5)	15.87	1.48	150	0.85	175	192	2.68	4.01	1.10
LS-20M-100	35.58	20M (#6)	19.05	2.14	100	1.27	207	250	6.07	7.28	1.21

*Numbers in parentheses are the manufacturer's bar designation.

Notes: $f_c^{'}$ is the concrete compressive strength; d_b is the nominal bar diameter; ρ_l is the longitudinal reinforcement ratio; ρ_{sv} is the transverse reinforcement ratio; P_e is the experimental lateral load; P_{th} is the theoretical lateral load with ACI 440. 1R (2015), and ACI 318R (2019) provisions for columns reinforced with longitudinal GFRP and steel bars, respectively; δ_u is maximum drift; and μ_Δ is the displacement ductility index.

The cyclic transverse load was applied with a displacement-controlled hydraulic actuator. An axial load of 20% the column capacity was applied with two hydraulic jacks and maintained constant throughout the test. The constant axial load was defined as $0.2A_g f_c^{'}$, where A_g is the gross cross-sectional area of the column and $f_c^{'}$ is the compressive strength of the concrete. The pattern for identifying the test specimens is LX-xxM-nnn, where LX represents the type of longitudinal bar (LG for GFRP and LS for steel); xxM represents longitudinal bar size; and nnn represents the spacing of transverse reinforcement.

A total of 31 electrical strain gauges were used in each specimen to monitor the deformation. The four corner longitudinal bars, spiral, and cross ties were instrumented at three levels, as shown in Figure 6.1. Two strain gauges at two different locations on diagonally opposite longitudinal bars were installed below the column–stub interface to

measure the strain variation inside the stub. To measure the concrete strain, six linear variable differential transducers (LVDTs) were placed in both sides of the test column at three different levels above the column-stub interface perpendicular to loading direction as shown in Figure 6.1. Four LVDTs were installed horizontally at different positions along the column height to measure the lateral displacement of the column. One LVDT was installed to check for sliding between the stub and laboratory strong floor.

6.3.2 Material properties

The stubs were cast with ready-mix normal-weight concrete with a target compressive strength of 50 MPa after 28 days, whereas the columns were cast with a target strength of 30 MPa. At least 3 standard cylinders measuring size 100 × 200 mm were cast for each column to determine the average concrete compressive strength on the day of testing. Table 6.1 lists the average compressive strength of the concrete.

Table 6.2- Reinforcement material properties

Longitudinal Reinforcement					
	Bar no.	A_b (mm^2)	E_s (GPa)	f_y (MPa)	ε_y (%)
Steel rebars	15M (#5)	200	200	414	0.2
	20M (#6)	284	200	414	0.2
	Bar no.	A_b (mm^2)	E_{frp} (GPa)	f_{frpu} * (MPa)	ε_{fu} (%)
GFRP bars	15M (#5)	198 (229) †	67.2	1433	2.13
	20M (#6)	285 (323) †	64.7	1399	2.16
GFRP (#4) transverse reinforcement					
Straight portion		127 (151) †	63.2	1570	2.48
Bent portion		127 (151) †	-	801	-

* Guaranteed tensile strength: average value-3 x standard deviation (ACI Committee 440 2015).
†Values in parentheses are the cross-sectional area calculated based on Annex A in CSA S806 (2012).
Notes: A_b is the nominal cross-sectional area; E_s is the elastic modulus of steel; f_y is the steel yield strength; ε_y is the steel yielding strain; E_{frp} is the modulus of elasticity of FRP; f_{frpu} is the guaranteed tensile strength of FRP; and ε_{fu} is the ultimate strain of FRP.

Two diameters of longitudinal steel reinforcement were used in the column specimens: Grade 60 15M and 20M. Grade 60 20M reinforcing steel was used in the stub. Table 6.2 gives the properties of the steel bar as provided by the manufacturer. The GFRP bars used to reinforce the columns in both the longitudinal and transverse directions were grade III, high-modulus, sand-coated bars (CSA S807 2010). Bar sizes #5 and #6 were used as longitudinal reinforcement; bar size #4 was used as transverse reinforcement (rectilinear spirals and cross ties). The tensile properties of the straight bars and straight portions of the bent bars were determined as per ASTM D7205 (2016) and the bent bars according to ASTM D7914 (2014). Table 6.2 gives the material properties of the reinforcing bars.

6.3.3 Test setup and procedure

The test setup was built in the structural laboratory of University of Sherbrooke, as shown in Figure 6.3. The stub was fixed to the laboratory strong floor with two steel beams and four DYWIDAG bars (high strength steel bars) 66 mm in diameter to prevent lifting and sliding of the test specimen. The displacement-controlled hydraulic actuator was connected to the column tip through two plates and six high-strength threaded rods. The other end of the MTS actuator was attached to the laboratory strong reaction wall. Two 100-ton hydraulic jacks and a rigid steel beam at the top of column were used to apply the axial load. After reaching the axial load of 20% capacity of the column, the axial load was maintained constant throughout the test. Then, the test specimen was subjected to displacement control quasi-static cyclic loading at a rate of 2 mm/min. Two cycles were applied at each drift until specimen failure, as shown in Figure 6.4.

Figure 6.3- Column in position for testing

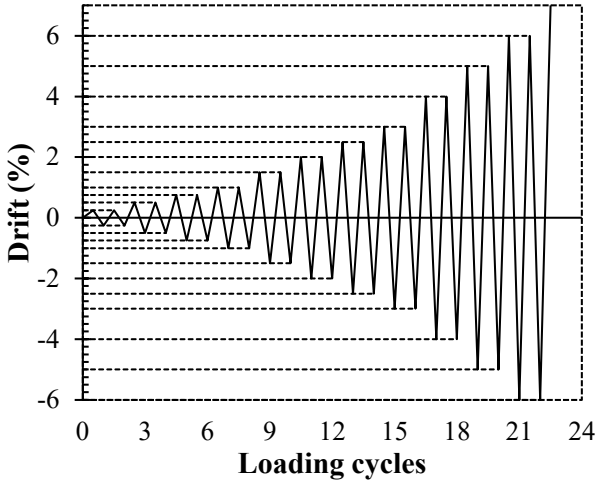

Figure 6.4- Applied loading history

6.4 TEST OBSERVATIONS

6.4.1 GFRP-reinforced concrete columns

The first distress in these columns occurred at a lateral drift ranging from 0.23% to 0.27% due to the appearance of flexural cracks. As those flexural cracks widened, more cracks appeared and propagated towards side faces of the column. The flexural cracks continued to develop up to a height equal to 70% to 75% of the effective height of the column (1650 mm) above the column–stub interface and were observed at a distance equal to the spacing of the transverse reinforcement. On further application of displacement, vertical splitting cracks developed at the corner of the column compression side (Fig. 6.5(a)). Spalling of the concrete cover (Fig. 6.5(b)) caused a strength degradation between 1.5% and 2.5% lateral drift in the GFRP-reinforced concrete columns. The well-confined columns LG-15M-100 and LG-20M-100 exhibited a second peak with increased strength after the strength degradation due to concrete cover spalling. The maximum capacity of the columns caused a drop in the applied constant axial load and crushing of the longitudinal compression bars (Fig. 6.5(c)). The failure of test columns was defined in the most-damaged region due to crushing of GFRP bars in compression with damage to the core concrete (Fig. 6.5(d)). No spiral damage or rupturing was observed in the GFRP-reinforced columns. Figure 6.6 shows the plastic hinge zone or most-damaged region of the column. Sparsely confined columns evidenced a shorter damaged zone compared to the well-confined columns.

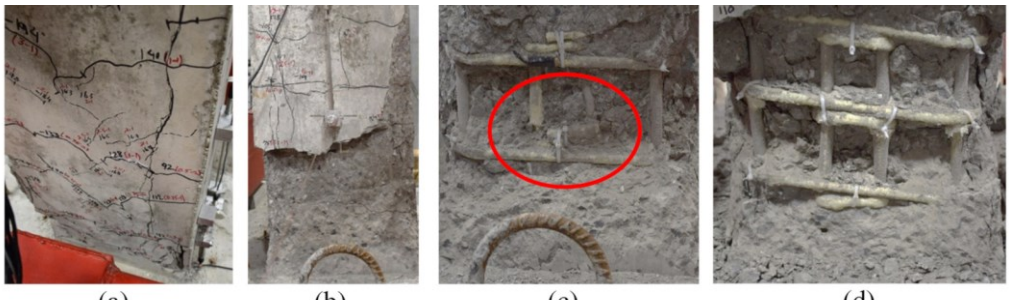

Figure 6.5- Failure progression of GFRP-reinforced concrete columns: (a) vertical splitting; (b) cover spalling; (c) longitudinal bar fracture; and (d) core concrete crushing

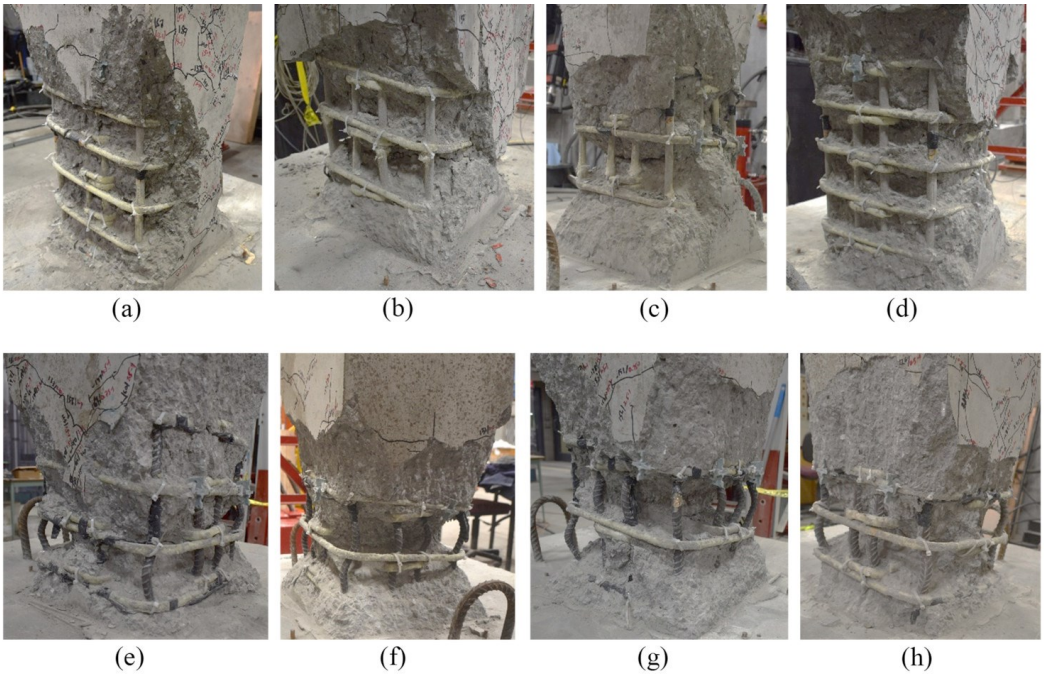

Figure 6.6- Images of the plastic hinge region: (a) LG-15M-100; (b) LG-15M-120; (c) LG-15M-150; (d) LG-20M-100; (e) LS-15M-100; (f) LS-15M-120; (g) LS-15M-150; and (h) LS-20M-100

6.4.2 Hybrid reinforced concrete columns

Failure of the hybrid reinforced columns proceeded more rapidly than that of the GFRP-reinforced columns. The initial flexural cracks appeared on the front face of the column between 0.19% and 0.22% lateral drift. As these flexural cracks widened; more cracks developed up to 55% of the effective height (1650 mm) of the column. The propagation of cracks towards the side face was greater in the most damaged section compared to the GFRP-reinforced columns, in which the cracks propagated slowly covering 70% of effective height of the column. Under increased drift cycle, the concrete cover started to split vertically at the corner (Fig. 6.7(a)). The next phenomenon—deterioration of concrete cover (Fig. 6.7(b))—was concentrated in the plastic hinge zone within 450 mm above the column–stub interface. The spalling of cover was rapid compared to that of the GFRP-reinforced columns. Further application of drift cycles critically damaged the concrete core and left the longitudinal steel reinforcement vulnerable to buckling. In general, the longitudinal rebars buckled outward in the space between two sets of spirals and cross ties.

Some rebar did buckle inwardly due to damage to concrete core between stirrups over the column length, as in columns LS-15M-120 and LS-20M-100 (Fig. 6.7(c)). Failure of the hybrid reinforced columns was due to the longitudinal steel reinforcement failing (Fig. 6.7(d)) accompanied with sudden drop in applied axial load, loss of confinement, and severe damage to concrete core. In contrast, column LS-15M-150 experienced damage to the core concrete and loss of confinement, reducing its lateral capacity to the point of causing its failure. No spiral or cross tie damage was observed other than in column LS-20M-100 (Fig. 6.7(e)).

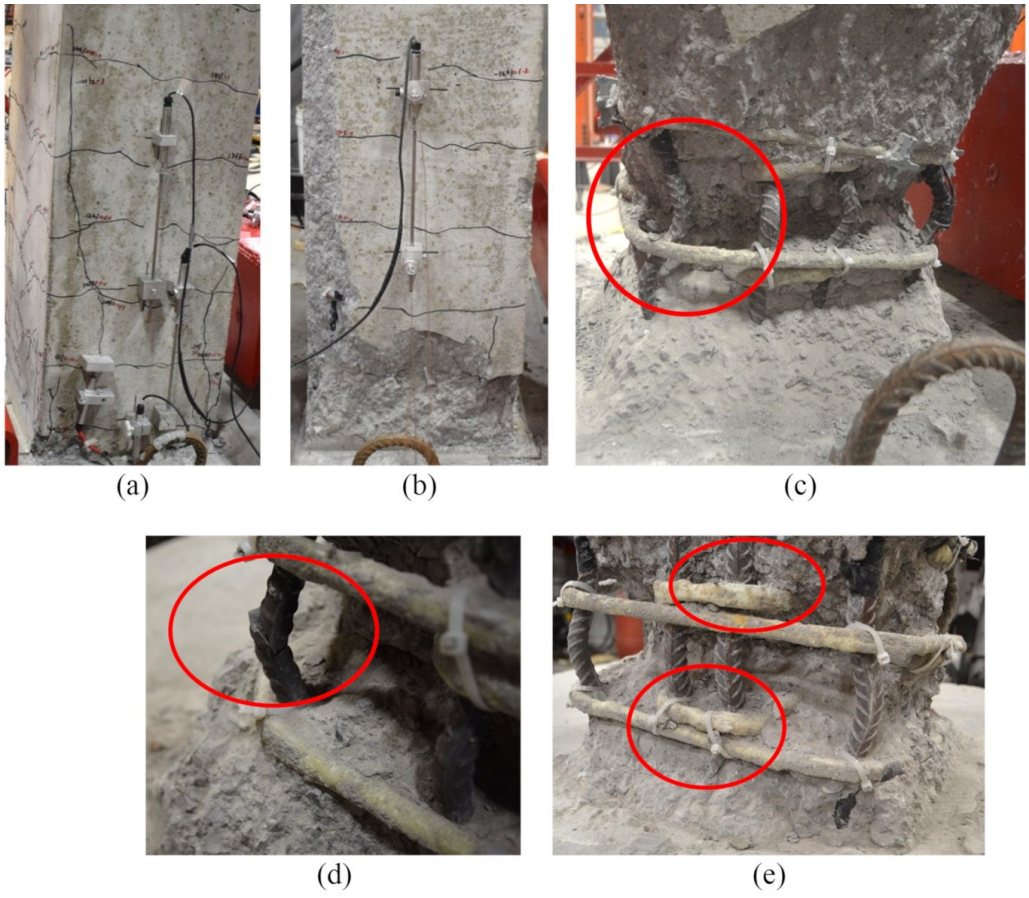

Figure 6.7- Failure progression of hybrid reinforced concrete columns: (a) vertical splitting; (b) cover spalling; (c) inward buckling of longitudinal rebar; (d) longitudinal steel rebar failure; and (e) rupture of GFRP cross tie

Like the GFRP-reinforced column, the well-confined hybrid column shows slightly larger plastic hinge region compared to lightly confined columns. Figure 6.6 contains close-up photographs of the plastic hinge region at failure. The most damaged region was 15 to 25 mm above the column–stub interface because of the confinement provided by the stub at the interface. This is consistent with similar research in the literature (Ali and El-salakawy 2015; Elshamandy et al. 2018; Sheikh and Khoury 1993).

6.4.3 Hysteresis response

The hysteresis response represents the relationship between the applied lateral load and the column tip drift ratio, as shown in Figure 6.8. The second excursion curve of the identical drift ratio has been removed for clarity since it followed a path similar to the first excursion with reduced stiffness. In the early stages of the drift cycle, the GFRP-reinforced columns had lower lateral capacity than the hybrid reinforced columns due to relatively low elastic modulus (lower stiffness) of the GFRP reinforcement compared to the steel. The GFRP-reinforced columns reached the first peak at 1.5% to 2.0% lateral drift before inelastic deformation occurred due to deterioration of the concrete cover. In contrast, the hybrid reinforced columns reached the peak load at about 1.25% drift. The structural hysteretic response is affected by changes in material behavior beyond the elastic range or by changes in the structural geometry. Examples of this include concrete cracks, cover splitting and spalling, buckling and rupture of bars, and failure of lateral reinforcement. Figure 6.8 illustrates the occurrence of such events. After the steel yielded in the hybrid reinforced columns—at a value close to the peak lateral load—the lateral capacity gradually decreased due to cover spalling and buckling of longitudinal steel rebars. The GFRP-reinforced columns experienced negligible degradation in strength; the well-confined columns reached a second peak load as observed in the hysteresis response.

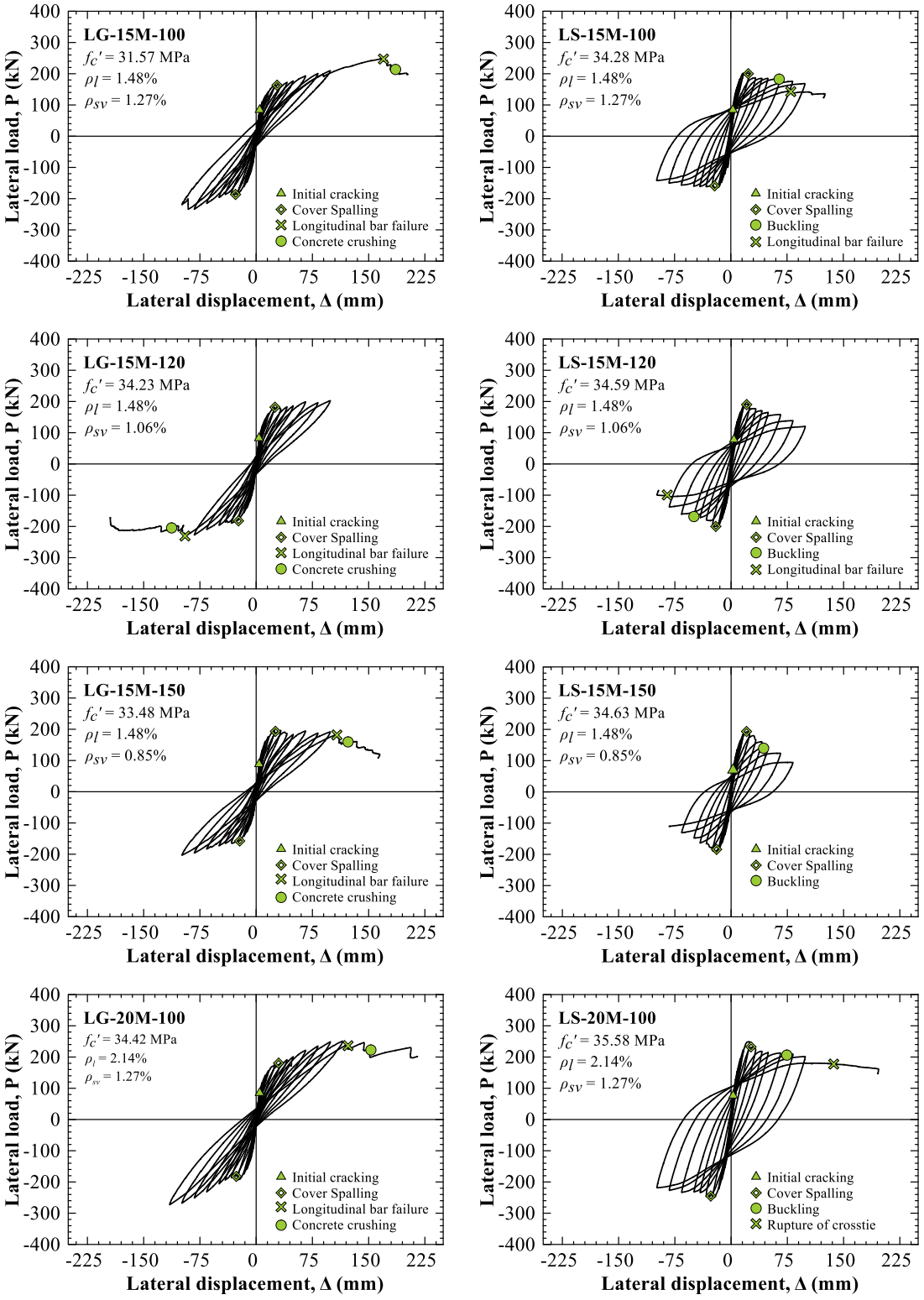

Figure 6.8- Hysteresis response

Due to the elastic behavior of the GFRP longitudinal bars up to failure, the unloading curve (descending part of the hysteresis response) nearly approaches the origin of the lateral load–drift ratio curve. The inelastic behavior in GFRP-reinforced columns was induced by open concrete cracks, extensive concrete damage, or failure of the longitudinal bars. In contrast, the hybrid reinforced columns exhibited significant plastic deformation due to extensive concrete damage or yielding of the reinforcement after the column yield point. Thus, larger residual deformation was observed in the hysteresis response for the hybrid reinforced columns than the GFRP-reinforced columns. The GFRP-reinforced columns achieved a longer load peak after virtual yielding (strength degradation due to severe concrete damage) (Mohamed et al. 2014c) before failure compared to the hybrid RC columns because of the low tangent modulus of the longitudinal steel rebars after yielding. Therefore, the longitudinal steel reinforcement in the hybrid RC column more likely buckled under compression, whereas the GFRP bars maintained their elastic modulus during the entire loading period. The hysteresis response of the GFRP-reinforced concrete columns displays reduced area under the hysteresis loop (Fig. 6.8), which indicates reduced energy dissipation compared to the hybrid reinforced columns.

6.5 TEST RESULTS AND DISCUSSION

6.5.1 Strain in longitudinal reinforcement

The maximum strain development at different locations, from the stub to the column's most damaged region was obtained to study the strain distribution along the column's longitudinal reinforcement. Figure 6.9 illustrates the strain development in the hybrid reinforced and GFRP-reinforced columns at different drift ratios. At 0.75% drift ratio, the strain in GFRP longitudinal bars was 13% to 56% higher than the steel rebars; the differences were greater for lightly confined columns (LG-15M-150 and LS-15M-150). Because the steel rebars in hybrid reinforced columns had not yielded at this drift level, the strain was close to the maximum strains of approximately 2000 με. When the hybrid

reinforced concrete columns yielded at the 1.5% drift cycle, the strain increased drastically in the strain gauge near the column–stub interface. The maximum strain developed in steel rebar at this drift level was about 2.4 times than that of the strain developed in GFRP longitudinal bars. In the later stage of the drift cycle, the concentrated plastic strain in the steel rebars at the 1.5% drift level began to propagate towards a height of 350 mm measured above the column–stub interface.

Noticeable plastic strain propagation was observed in column LS-15M-150 at 350 mm above the column–stub interface, where the strain in the steel rebars was 76% higher at the 2.5% drift ratio than at the 1.5% drift ratio. In contrast, the strain increases in the longitudinal steel rebar near the column–stub interface at the 2.5% drift ratio was only 11% higher than at the 1.5% ratio.

In the hybrid reinforced columns, the steel rebar strains were concentrated within the first two sets of strain gauge level (Fig. 6.1) above the column–stub interface. At the third level of strain gauges, the measured strains in the longitudinal rebars were close to 2000 με for each drift ratio and for all hybrid reinforced specimens. This is consistent with the damaged section observed in the hybrid reinforced columns (Fig. 6.6), where the deterioration of the core concrete and buckling of the longitudinal steel bar under compression occurred within 350 mm above the column–stub interface. The strain in the GFRP longitudinal bars increased uniformly and gradually at each drift ratio level. The strain in the GFRP bars strain approximately doubled between successive drift ratios (Fig 6.9). Unlike with the steel rebar, the strain in the GFRP bars spread throughout the column height, even inside the column base. For instance, the strain in GFRP bar at 150 mm below the column–stub interface was nearly 4000 με for columns reinforced with 15.9 mm bars, while the strain in the steel rebars was less than 2000 με in all the hybrid reinforced specimens. The uniformly distribution of longitudinal bar strain along the column height clarifies the increased plastic hinge zone in the GFRP-reinforced columns (Fig. 6.6). The maximum strain developed in the strain gauge near the stub–laboratory floor interface was close to zero, which suggests that the development length of the longitudinal bars within the stub was adequate.

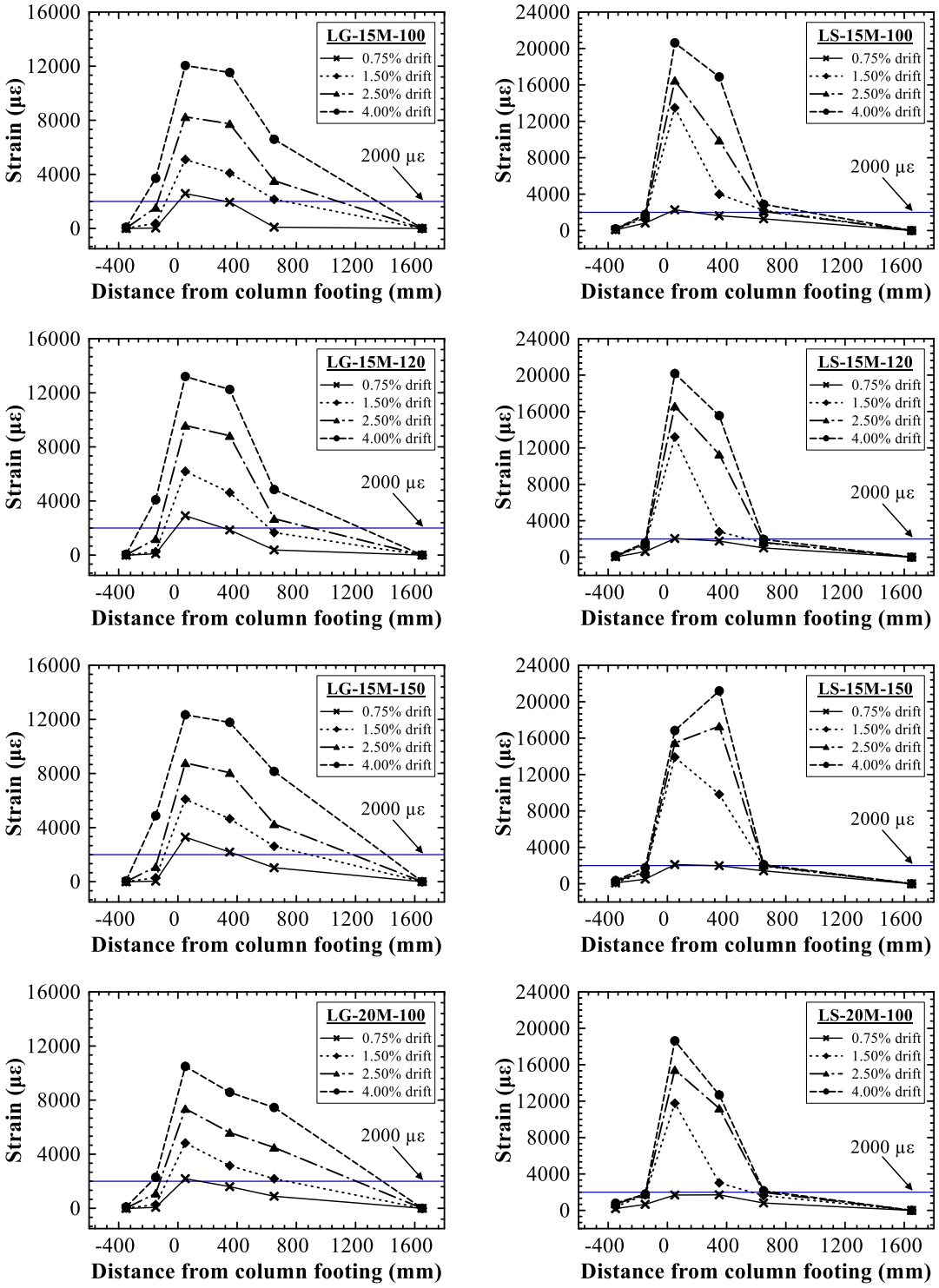

Figure 6.9- Longitudinal bar strain along the height

6.5.2 Energy dissipation

Energy dissipation is defined as the area under the lateral load–displacement curve for a drift cycle (Fig. 6.10). Figure 6.11 shows the plot of cumulative energy dissipation in each cycle by summing the dissipated energy in successive cycles versus the drift ratio. All the test specimens show similar cumulative energy dissipation up to the 0.50% drift cycle. The hybrid reinforced columns exhibited higher dissipated energy than the GFRP-reinforced columns because of the steel yielding at the 0.75% drift cycle. At the 2.0% drift ratio, the dissipated energy of hybrid reinforced columns was almost twice that of the GFRP-reinforced columns due to degradation of the columns resulted in significant dissipated energy. According to CSA S806 (2012), the moderate ductility occurs at the 2.5% drift level, the cumulated dissipated energy of the hybrid reinforced columns was more than 200% that of GFRP-reinforced columns because of excessive damage to the concrete cover and core concrete. The dissipated energy increased due to buckling of the longitudinal steel rebars and was 2.5 times higher in the hybrid reinforced column than the GFRP-reinforced column at the 4.0% drift cycle.

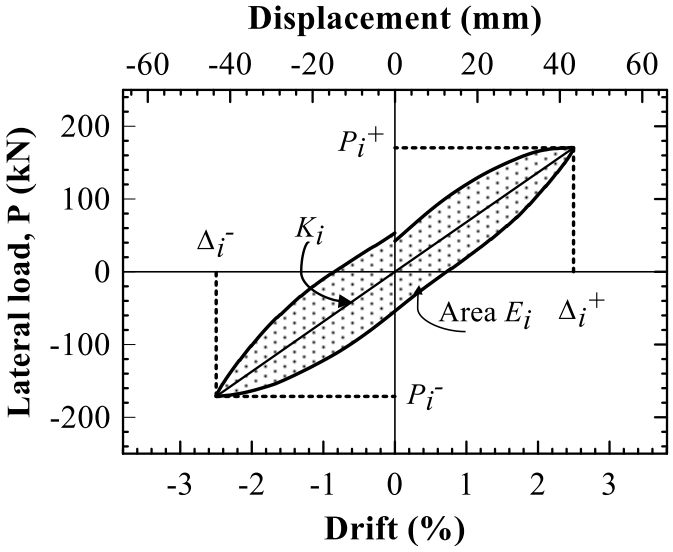

Figure 6.10- Definition of energy dissipation and secant stiffness at 2.5% drift for column LS-15M-150

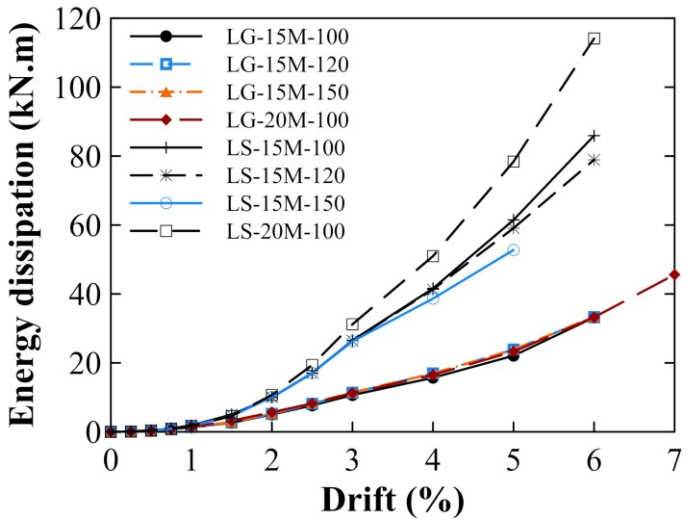

Figure 6.11- Cumulative energy dissipation

With respect to the GFRP-reinforced columns, Figure 6.11 shows similar levels of cumulative energy dissipation even with the use of different reinforcement parameters. Column LG-20M-100 exhibited higher drift cycle, allowing it to reach higher dissipated energy. The hybrid reinforced columns show different levels of dissipated energy at higher drift cycles. Column LS-20M-100 exhibits higher cumulative energy dissipation than the other specimens.

6.5.3 Evaluation of ductility parameter

Ductility is an important parameter in seismic zones where energy absorption is of prime concern. It is defined as a structure's ability to sustain inelastic deformation under stress for certain periods of time before failure. Two points are required to evaluate a structure's ductility: the yield deformation point, and the ultimate deformation point on the experimental load–displacement plot.

For hybrid reinforced columns, the yield deformation point (Δ_y) is defined at the point at which elastic behavior ends. The ultimate deformation point (Δ_u) is the maximum available displacement in the inelastic region. Sheikh and Khoury (1993) have clearly

defined the displacement ductility factor for steel-reinforced concrete columns and this factor was used in our study to determine the ductility of columns with longitudinal steel reinforcement. The yield point, Δ_y on the load–displacement plot was defined as the displacement equal to the maximum lateral load along the straight line that is secant to the real curve at 65% of the maximum lateral load P_{max} (Fig. 6.12(a)). The ultimate deformation point (Δ_u) can be established by (a) limitation of the concrete compression strain, (b) post-peak deformation with a reduced ultimate load, (c) displacement corresponding to ultimate load, or (d) displacement at fracture or buckling of the reinforcement (Park 1988). For hybrid reinforced columns, the ultimate displacement (Δ_u) was defined by limiting the post-peak load to $0.8P_{max}$ (Fig. 6.12(a)).

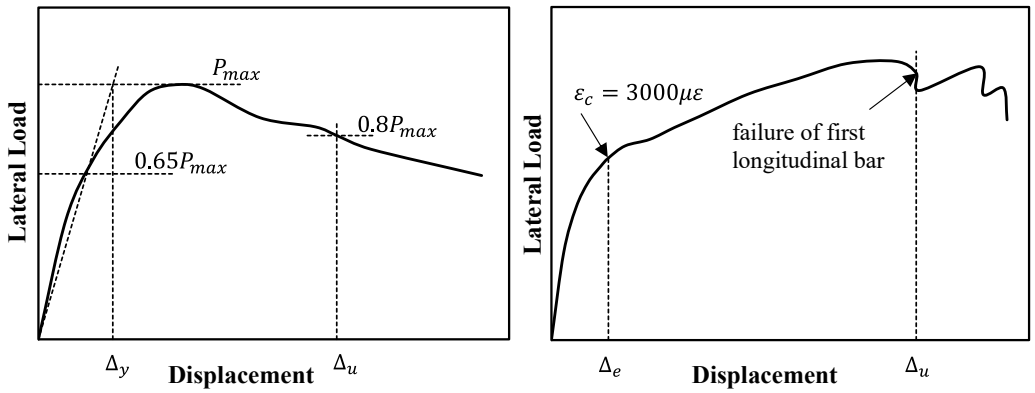

(a) Hybrid reinforced column (b) GFRP-reinforced column

Figure 6.12- Ductility definition

In hybrid reinforced columns, when the lateral capacity and the deflection exceed the column yield point, the steel undergoes plastic deformation. This increase in the deformation implies that the dissipated energy is increased due to the plasticity of the steel. The capability of energy dissipation is therefore implicitly included in the definition of ductility. The hysteresis response (Fig. 6.8) indicates that the dissipated energy for an individual drift cycle (for instance 4.0% drift) was higher in the hybrid reinforced columns than in the GFRP-reinforced columns (Fig. 6.11). Thus, even though GFRP-reinforced

columns experienced large deformation, the hysteresis response does not show high energy dissipation. Since GFRP bars behave linearly elastic up to failure, they do not have a yielding point. Therefore, the conventional definition of ductility, which is based on the yielding deformation and ultimate deformation points is not valid for GFRP-reinforced columns. Thus, the ductility of the GFRP-reinforced columns was found using two points: the virtual yield deformation point (start of severe damage to the concrete cover) and the ultimate deformation point. The GFRP-reinforced columns exhibited inelastic behavior due to severe damage to the concrete cover, which occurred at a concrete compressive strain of $\varepsilon_c = 3000\mu\varepsilon$. Considering a lower concrete compressive strain would most likely resulting in overestimating the displacement ductility μ_Δ. The lateral load in the GFRP-reinforced columns was observed to increase continuously after the concrete cover spalled until the failure of the specimen. Therefore, using $0.65P_{max}$ to obtain the elastic displacement-point resulted in large values for the well-confined columns as the point lying beyond the linear region. Thus, virtual yield deformation point (Δ_e) (Mohamed et al. 2014c) for the GFRP-reinforced columns was the displacement corresponding to concrete strain $\varepsilon_c = 3000\mu\varepsilon$ (Fig. 6.12(b)). The hysteresis response (Fig. 6.8) shows that the GFRP-reinforced columns started to regain their strength after the deterioration of the concrete cover up until the failure of the longitudinal GFRP bars in compression. Therefore, the ultimate displacement (Δ_u) corresponds to the displacement at which crushing of the first longitudinal bar occurs with the reduction in lateral load (Fig. 6.12(b)).

Thus, the displacement ductility (μ_Δ) is as follows:

For hybrid reinforced columns: $$\mu_\Delta = \frac{\Delta_u}{\Delta_y} \quad (6.1)$$

For GFRP-reinforced columns: $$\mu_\Delta = \frac{\Delta_u}{\Delta_e} \quad (6.2)$$

The columns' deformability levels were classified with the drift ratio δ_u. For hybrid reinforced columns, δ_u was defined as the ratio of the ultimate displacement (Δ_u) at the 80% peak load to the effective height (1650 mm) of the test specimen. For GFRP-reinforced columns, δ_u was defined as the ultimate displacement (Δ_u) at the first GFRP bar failure to the effective height. Table 6.1 lists the ductility parameters. The drift ratio δ_u for columns LS-15M-100 and LS-20M-100 were 6.16% and 6.07%, respectively, which is over the 4.0% drift recommended for ductility-based design in CSA S806 (2012).

6.5.4 Stiffness degradation

The secant stiffness was used to demonstrate the attribute of the stiffness degradation of the test specimens. The stiffness equation for each drift cycle is determined as follows (Fig. 6.10):

$$K_i = \frac{\left|P_i^+\right| + \left|P_i^-\right|}{\left|\Delta_i^+\right| + \left|\Delta_i^-\right|} \tag{6.3}$$

where, Δ_i^+ and Δ_i^- are the peak displacements in the *i*th cycle, and P_i^+ and P_i^- are the corresponding peak loads, as shown in Figure 6.10.

Figure 6.13 shows the variation of the normalized stiffness degradation with a maximum value with respect to the drift ratio of all the test specimens. The stiffness of each specimen constantly decreased as the drift ratio increased. The decrease in stiffness was more pronounced at the initial drift cycles; the stiffness degraded gradually at higher drift cycles. This is due to cracks in the concrete developing and widening in the initial drift cycles; longitudinal steel bars yielding; and the concrete cover splitting vertically at the corners and concrete cover spalling, causing the rapid stiffness degradation. After the 1.50% drift cycle, the core concrete confined with spiral and cross ties was activated. Thus, the test specimens still retained stiffness under the large drift cycles.

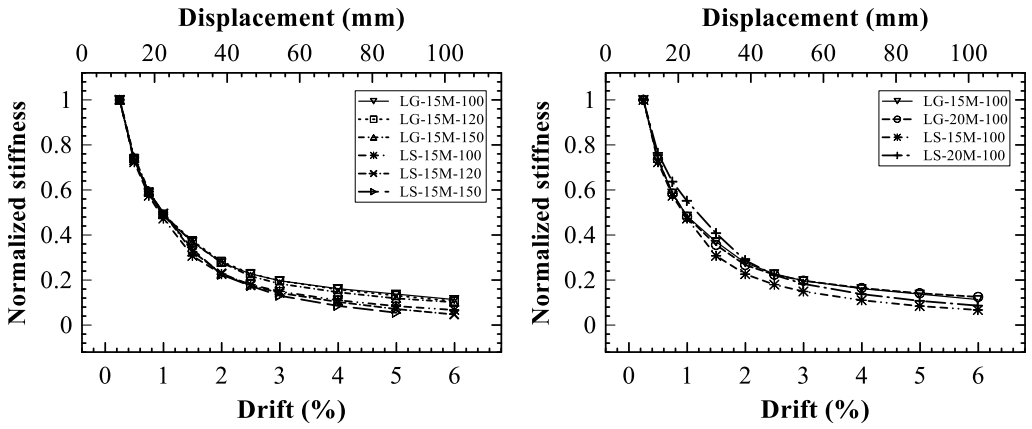

Figure 6.13- Normalized stiffness degradation of columns (a) with 15M longitudinal bars and (b) comparison of 15M and 20M longitudinal bars

As can be seen in Figure 6.13(a), the stiffness degradation for the all the columns was nearly the same until the 1.0% drift ratio. After that, stiffness degraded more rapidly in the hybrid reinforced columns with 15M longitudinal bars due to column yielding and excessive concrete spalling compared to the GFRP-reinforced columns. When the drift ratio was more than 1.5%, the decrease in normalized stiffness was noticeable in the hybrid reinforced columns (Fig. 6.13(a)). Due to the linear behavior of GFRP reinforcement, the stiffness degradation of the GFRP-reinforced columns was steadier than that of the hybrid reinforced columns after the 1.5% drift ratio. The GFRP-reinforced columns had about 29% more available stiffness than the hybrid reinforced columns at the 2.5% drift ratio. It increased to 47% to 71% with higher values for the lightly confined concrete columns (LG-15M-150 and LS-15M-150) at the 4.0% drift ratio. This is due to the deterioration of core concrete and buckling of the steel reinforcement in the hybrid columns. Due to crack stabilization after the 2.0% drift ratio, the stiffness gradually decayed in all the test specimens.

Spacing of the transverse reinforcement in GFRP-reinforced columns does not affect the stiffness degradation until 2.0% lateral drift. After the 2.0% drift ratio, LG-15M-100 had

greater normalized stiffness than the other two specimens. At 4.0% drift, column LG-15M-100 had normalized stiffness that was 5% and 11% higher than that of columns LG-15M-120 and LG-15M-150, respectively (Fig. 6.13(a)). In hybrid reinforced columns presented similar behavior in comparing the normalized stiffness of columns LS-15M-100, LS-15M-120, and LS-15M-150. At 4% drift, column LS-15M-100 had normalized stiffness that was about 7% and 29% higher than that of columns LS-15M-120 and LS-15M-150, respectively. The rate of stiffness degradation for columns LG-15M-100 and LG-15M-120 and for columns LS-15M-100 and LS-15M-120 was basically the same (Fig. 6.13(a)). This indicates that the effect of decreasing the stiffness degradation rate is not evident for higher transverse reinforcement ratios when the decrease in the spacing is small.

Figure 6.13(b) shows the normalized stiffness versus drift ratio for columns LG-20M-100 and LS-20M-100 with 20M longitudinal bars. The decay in stiffness for column LG-20M-100 was comparatively higher than that of column LS-20M-100 up until the 2.5% drift ratio. The increase was due to damage to the core concrete and buckling of longitudinal bars. The available stiffness for column LG-20M-100 was 20% and 45% more than that of column LS-20M-100 at the 4.0% and 6.0% drift ratios, respectively. Column LS-20M-100 exhibited nearly 20% more normalized stiffness than LS-15M-100 once the drift ratio was greater than 1.0% (Fig. 6.13(b)). Columns LG-15M-100 and LS-20M-100 had similar rates of stiffness decay despite the former being reinforced with 15M longitudinal GFRP bars and the latter with 20M longitudinal GFRP bars. That indicates that the change in the longitudinal GFRP reinforcement had no obvious effect on stiffness degradation.

6.5.5 Effect of longitudinal bars

The test results show that replacing GFRP longitudinal bars with steel reinforcement worsened the column's lateral load and drift capacity (Table 6.1). For instance, column LG-15M-120 was reinforced with 15M longitudinal GFRP bars and column LS-15M-120 with 15M longitudinal steel bars. Both columns were similar in all other details and were tested under similar loading conditions. Due to the non-yielding phenomenon and linearity of GFRP bars, the lateral load started to recover after the cover spalled, whereas the steel

rebars yielded and the tangential modulus decreased. This resulted in vulnerability to secondary effects and buckling of the rebars under compression. Thus, the lateral load and drift capacity of column LG-15M-120 was 15.4% and 46% greater, respectively, than that of column LS-15M-120 (Table 6.1). As shown in Figure 6.14(a), the lateral load capacity of column LS-15M-120 decreased after the peak load, while the lateral load capacity of column LG-15M-120 constantly increased until the crushing of the longitudinal bars occurred. Similar behavior was observed in other test specimens.

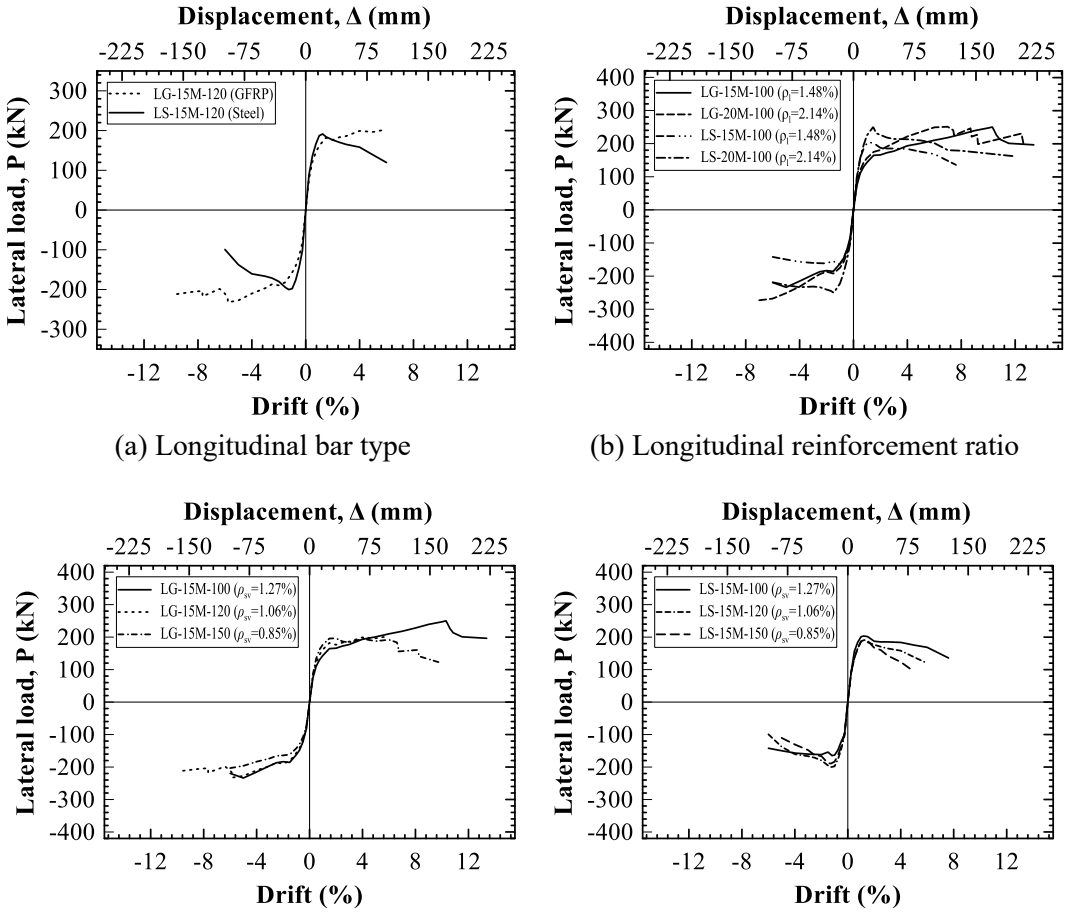

(a) Longitudinal bar type

(b) Longitudinal reinforcement ratio

(c) Lateral reinforcement spacing, GFRP-reinforced column

(d) Lateral reinforcement spacing, Hybrid reinforced column

Figure 6.14- Effect of studied parameters on lateral load–drift envelope curve

The longitudinal steel bars dissipated more energy per drift cycle after yielding due to plastic strain and the Bauschinger effect, which results in better behavior with regards to ductility (Fig. 6.11). Thus, column LS-15M-120 had a higher ductility index than column LG-15M-120. Similar behavior was observed in other test specimens except for columns LG-15M-150 and LS-15M-150, where the former had the higher ductility index. The hysteresis response (Fig. 6.8) of column LG-15M-150 revealed that the lateral load remained almost constant after the cover spalled, which could explain the higher displacement.

The strain in most stressed strain gauges attached to the GFRP spirals and cross ties in columns LG-15M-120 and LS-15M-120 were compared, as shown in Figure 6.15. The strain in the GFRP spiral and cross ties in column LS-15M-120 was higher at every drift ratio than that in column LG-15M-120 throughout the entire test. Using the failure of the first longitudinal bar as the base point, the strain in the GFRP spiral and cross ties in column LS-15M-120 was 26% and 22% higher than that in column LG-15M-120, respectively. The fact that the longitudinal steel bars experienced buckling, unlike the GFRP longitudinal bars, could account for the relatively higher strain that developed in the GFRP transverse reinforcement in the columns reinforced with longitudinal steel rebars. Other researchers have reported similar behavior (Kharal and Sheikh 2020).

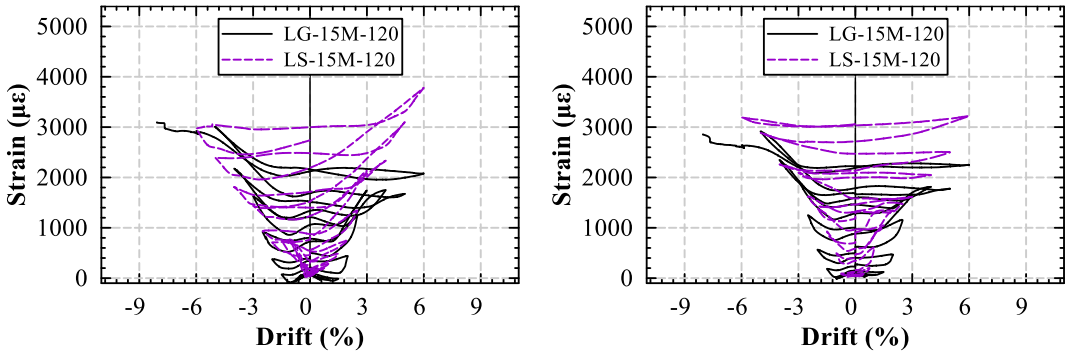

(a) Rectilinear spiral (b) Cross tie

Figure 6.15- Maximum strain developed in GFRP in specimens LG-15M-120 and LS-15M-120

Two longitudinal reinforcement ratios were used in our study: 1.48% for columns LG-15M-100 and LS-15M-100 and 2.14% for columns LG-20M-100 and LS-20M-100. The lateral resistance for the specimens LG-20M-100 and LS-20M-100 was higher at every drift ratio than that in columns LG-15M-100 and LS-15M-100, as shown in Figure 6.14(b), respectively. The achieved drift level dropped from 10.10% and 6.16% for columns LG-15M-100 and LS-15M-100, respectively, to 7.39% and 6.07% for columns LG-20M-100 and LS-20M-100. Therefore, improving the longitudinal reinforcement ratio by increasing bar size enhanced the lateral load capacity while lowering drift capacity. Figure 6.9 clearly shows that the longitudinal bar in columns LG-15M-100 and LS-15M-100 experienced greater strain at each drift ratio than columns LG-20M-100 and LS-20M-100, respectively. This explains the improved drift capacity in the columns with lower longitudinal reinforcement ratios. Furthermore, at the 4% drift ratio, column LG-15M-100 developed 62% more strain in the longitudinal bars, measured 150 mm below the column–stub interface, than column LG-20M-100.

6.5.6 Effect of lateral reinforcement spacing

To study the confinement level, both the hybrid reinforced, and the GFRP-reinforced columns had transverse reinforcement at three different ratios spaced at 100-, 120-, and 150-mm. Figure 6.14(c) shows that column LG-15M-100 had greater deformability than columns LG-15M-120 and LG-15M-150 without any reduction in the lateral load capacity. This demonstrates that increasing the lateral reinforcement ratio by decreasing the reinforcement spacing improved both the strength and deformability of the GFRP-reinforced columns. Other researchers have reported similar behavior (Ali and El-salakawy 2015; Elshamandy et al. 2018; Tavassoli et al. 2015).

Figure 6.14(d) shows the influence of transverse reinforcement ratio on the hybrid reinforced columns. The skeleton curve clearly shows that the lateral capacity of columns LS-15M-120 and LS-15M-150 decreased more rapidly after the peak load than that of column LS-15M-100. Thus, column LS-15M-100 was able to achieve 1.6 and 2.5 times the displacement ductility of columns LS-15M-120 and LS-15M-150 when the ultimate

displacement was restricted to $0.8P_{max}$. Decreasing the spacing improved the drift capacity, although the enhancement in the lateral load capacity was not significant.

Figure 6.9 shows the strain developed in the longitudinal bar along column height. The specimens with closer spacing of transverse reinforcement spacing had lower applied lateral stress on the longitudinal bars at the lower drift level due to the lateral expansion of the core concrete. Thus, the confinement provided by the closely spaced GFRP spiral and cross ties to the core concrete improved the lateral load capacity with lower strain in the GFRP longitudinal bars in the GFRP-reinforced concrete columns.

6.6 EVALUATION OF LATERAL LOAD CAPACITY PREDICTION

Table 6.3 compares the experimental lateral load capacity to theoretical load capacity for the GFRP-reinforced columns. Plane-section analysis using equivalent rectangular concrete stress distribution was performed with an assumption based on ACI 440.1R (2015), CSA S806 (2012), AASHTO (2018), and CSA S6 (2019). ACI 440.1R (2015) and AASHTO (2018) assumed the maximum concrete strain in the compression fiber to be 0.003, CSA S806 (2012) and CSA S6 (2019) assumed it to be 0.0035. ACI 440.1R (2015), AASHTO (2018), and CSA S806 (2012) ignore the contribution of longitudinal FRP bars in compression, whereas the latest edition of CSA S6 (2019) limits the compressive strength of FRP to a stress equivalent to a strain of 0.002. The concrete compressive strength $f_c^{'}$ = 34 MPa was used for all the columns. The provisions in ACI 318R (2019) and CSA A23.3 (2014) were adopted for the hybrid reinforced columns.

Both ACI 318R (2019) and CSA A23.3 (2014) neglect the effect of the strain hardening of steel in their nominal strength calculations. Therefore, the theoretical lateral resistance for the hybrid reinforced columns was computed according to ACI 318R (2019) and CSA A23.3 (2014). These values were quite close and equal to 175 kN and 207 kN for columns with longitudinal steel reinforcement ratios of ρ_l = 1.48% and ρ_l = 2.14%, respectively. The

P_e/P_{th} (where, P_e is the experimental maximum lateral load and P_{th} is the theoretical lateral load) had a maximum value of 1.21 and minimum value of 1.10 for columns LS-20M-100 and LS-15M-150, respectively (Table 6.1). The strength enhancement was higher in the well-confined column and critical for the lightly confined column.

Table 6.3- Comparison of lateral load using design codes

Specimen ID	f_c' (MPa)	P_e (kN)	P_{ACI} (kN)	$P_{CSA,S806}$ (kN)	$P_{CSA,S6}$ (kN)	$\frac{P_e}{P_{ACI}}$	$\frac{P_e}{P_{CSA,S806}}$	$\frac{P_e}{P_{CSA,S6}}$
LG-15M-100	31.57	250	138	141	150	1.81	1.77	1.67
LG-15M-120	34.23	232	138	141	150	1.68	1.65	1.55
LG-15M-150	33.48	196	138	141	150	1.42	1.39	1.31
LG-20M-100	34.42	251	147	151	164	1.71	1.66	1.53

Note: f_c' is the concrete compressive strength; P_e is the experimental lateral load in kN; P_{ACI} is the theoretical lateral load according to ACI 440. 1R (2015) and AASHTO (2018) provisions; $P_{CSA,S806}$ and $P_{CSA,S6}$ are the theoretical lateral load according to CSA S806 (2012) and CSA S6 (2019) provisions, respectively.

Table 6.3 gives the lateral load capacity of the GFRP-reinforced columns based on the different criteria in design codes. The provisions in ACI 440.1R (2015) and AASHTO (2018) gave lower computed lateral loads than the Canadian design codes (CSA S6 2019 and CSA S806 2012) due to the former having lower assumed values of maximum concrete strain. In contrast, the P_e/P_{ACI} found to be higher than $P_e/P_{CSA,S806}$ and $P_e/P_{CSA,S6}$, which indicates that the P_e/P_{ACI} was on conservative side when following ACI 440.1R (2015) and AASHTO (2018) provisions. The assumed increased in the maximum concrete strain from 0.003 in ACI 440.1R (2015) and AASHTO (2018) to 0.0035 in CSA S806 (2012) increased the lateral load for LG-15M-100 from 138 kN to 141 kN. $P_e/P_{CSA,S6}$ was consistently lower than the P_e/P_{ACI} and $P_e/P_{CSA,S806}$ for all the columns. This is due to the compressive strength of GFRP reinforcement being neglected in the calculation according to the provisions in ACI 440.1R (2015), AASHTO (2018), and CSA S806 (2012). In contrast, CSA S6 (2019)

limits GFRP compressive strength to 0.002 strain. Nevertheless, the computed lateral loads were higher for the hybrid reinforced column than the GFRP-reinforced column because of the lower elastic modulus of the GFRP longitudinal bars.

6.7 CONCLUSIONS

The behavior of the reinforced concrete bridge columns reinforced with the longitudinal GFRP and steel rebars and confined with GFRP spirals and cross ties were assessed. The comparison was made in terms of crack development and failure under reversed cyclic loading, hysteresis response (stiffness degradation, ductility, and energy dissipation), and the strain developed in the longitudinal and transverse reinforcement. The effect of longitudinal and transverse reinforcement ratios was also evaluated. The following conclusions can be drawn from the study:

1. The failure of the GFRP-reinforced columns was more gradual than that of the hybrid reinforced columns. The GFRP longitudinal strain developed at twice the rate in subsequent drift cycles, whereas steel rebar strain increased significantly at the column yielding drift cycle.

2. The GFRP-reinforced columns achieved higher lateral load and lateral drift than the hybrid reinforced columns. The compressive behavior of GFRP bars does not provide the significant plasticity required by columns for seismic response. In addition, it makes it more likely to fail in a brittle mode under high loads. In contrast, steel rebars give resilience to columns in the compression part. Thus, the hybrid reinforced columns behaved better under reversed cyclic loading and provided sufficient ductility.

3. The well-confined hybrid reinforced columns achieved a drift ratio greater than 4.0%, which is recommended in CSA S806 (2012) for ductile-based design and exhibited greater ductility than the equivalent GFRP-reinforced columns. Thus, the hybrid reinforced columns were found suitable for seismic-based design, although

the drift ratio and ductility were significantly affected by the spacing of the transverse reinforcement. Higher stiffness of the longitudinal reinforcement improved the column's lateral strength but reduced its drift capacity, which affects column ductility.

4. Using longitudinal GFRP reinforcement instead of steel improved the columns' lateral load capacity and achieved a higher drift ratio. Due to material linearity, however, the inelastic behavior due to cover spalling occurred at a later drift cycle than in the hybrid reinforced columns, thereby reducing the deformability of the GFRP-reinforced columns.

5. The stiffness of the hybrid reinforced columns at the column yielding point was lower than that of the GFRP-reinforced column and continued to drop until column failure. There was no sudden decay observed in the stiffness of GFRP-reinforced column.

6. The GFRP spirals and cross ties were found to be more efficient in confining the hybrid reinforced column than the GFRP-reinforced column. The strain in the GFRP spiral and cross ties in columns LG-15M-120 and LS-15M-120 were well below the 6000 με requirement in CSA S806 (2012). ACI 440.1R (2015), AASHTO (2018), CSA S806 (2012), and CSA S6 (2019) underestimated the lateral load capacity of the GFRP-reinforced columns, even with the GFRP compressive strength at 0.002 strain, as per CSA S6 (2019).

The information reported in this paper is expected to provide a better understanding of the seismic performance of concrete columns longitudinally reinforced with GFRP and Steel bar and confined with GFRP transverse reinforcement. However, further investigation including analytical models is required to implement adequate recommendations for bridge columns.

Chapter 7
CONCLUSIONS AND RECOMMENDATION

7.1 SUMMARY

The research program aimed at experimentally assessing the confinement behavior of glass-fiber reinforced polymer (GFRP) spiral and cross ties on reinforced concrete columns subjected quasi-static reversed cyclic load. Consequently, eight concrete columns reinforced entirely with GFRP and four other columns reinforced with hybrid longitudinal steel and transverse GFRP reinforcement were constructed and tested under simulated seismic loading. The fabricated and tested columns had a cross section of 400 × 400 mm and overall height of 1850 mm. The columns were casted with normal-weight concrete with a target compressive strength of 30 MPa. The test parameters can be summarized as longitudinal reinforcement type (GFRP and steel), longitudinal reinforcement ratio (1.48 and 2.14%), size of transverse GFRP reinforcement (#3, #4, and #5), and spacing of transverse reinforcement (100, 120, and 250 mm).

7.2 CONCLUSIONS

The following conclusions were drawn from the present research program based on the analysis of test results:

GFRP-reinforced concrete columns

- The well-confined GFRP-reinforced concrete columns showed stable hysteretic response with no strength degradation up to failure.

- There was no significant difference in the energy dissipation of the tested GFRP-reinforced concrete columns, regardless of longitudinal or transverse reinforcement ratio.
- The transition between the elastic and inelastic zone of the GFRP-reinforced columns was referred to as elastic deformations (Δ_e) and defined at a concrete compressive strain, 0.003. The ultimate deformation (Δ_u) was defined as corresponding to the displacement upon the crushing of the first longitudinal GFRP bar in compression.
- The well-confined GFRP-reinforced concrete columns with lower longitudinal reinforcement ratio showed increased strength and drift capacity compared to the specimens with less transverse reinforcement. This did not hold true for the columns with more longitudinal reinforcement where the spacing of the lateral reinforcement did not significantly affect drift capacity.
- Increasing the longitudinal bar size decreased the drift capacity of the well-confined column but improved both strength and drift capacity of the GFRP-reinforced columns with less confinement. The well-confined column G#5-#4-100 reinforced with longitudinal reinforcement ratio of 1.48% developed more strain in the longitudinal bar than column G#6-#4-100 with longitudinal reinforcement ratio of 2.14%, which supports the increased deformability in specimen G#5-#4-100.
- GFRP spirals and cross ties restrained the lateral expansion of concrete core in the case of the columns with lower spacing, which effectively improved the horizontal load resistance with lower maximum strain in the longitudinal bars.
- The GFRP-reinforced column reinforced with more lateral spirals and cross ties developed more strain, which helped enhance the strength and deformability of the specimen compared to columns with fewer lateral spiral and cross ties.

- The maximum strain developed in the spiral and cross ties at a 4% drift ratio in all the specimens was less than 0.006, which is the maximum strain allowed in CSA S806 (2012). The spirals and cross ties effectively limited the expansion of the concrete core after the cover spalled. The maximum strain developed in the lateral reinforcement at failure was, however, significantly lower than its rupture strain.

Hybrid reinforced (steel/GFRP) concrete columns

- All the test specimens showed flexure behavior with concrete crushing and buckling of longitudinal steel bar. The column with adequate confinement provided by GFRP spiral and cross ties exhibited stable behavior, achieving drift more than 4.0% before the occurrence 20% strength degradation. Thus, the concrete columns with hybrid reinforcement could be reviewed as being acceptable material for use in new construction for high earthquake hazard zones.

- At peak load, all the columns had a displacement ductility in excess of 1.50. The displacement ductility for the well-confined columns S#5-#4-100, S#5-#4-120, and S#6-#4-100 were 8.4, 5.3, and 6.2, respectively, with equivalent elastic-plastic bilinear curve at post-peak strength loss of 20%. This indicates that high ductility can be achieved with transverse GFRP reinforcement. In addition, the achieved drift exceeded the requirement of CSA S806 (2012).

- More energy dissipation was observed in the first cycle than in the second cycle for the same displacement amplitude. Narrower spacing of transverse GFRP reinforcement and higher longitudinal reinforcement ratio of steel is needed to improve the cumulative dissipated energy of hybrid-reinforced concrete columns.

- The development of strain in the longitudinal steel bars of the concrete columns with hybrid reinforcement behaved similarly to the concrete columns totally reinforced with steel ties. The strain developed in transverse GFRP reinforcement indicates effective confinement provided by GFRP spiral and cross ties after the

longitudinal reinforcement yielded. The GFRP cross ties provided an effective confinement up to and after yielding of longitudinal steel bars. As the core concrete expanded, the rectilinear GFRP spiral became more effective in confining the hybrid-reinforced concrete columns.

- The drift capacity of the columns decreases as the pitch of the transverse GFRP reinforcement increased, without significantly affecting the lateral load capacity. The larger steel bar improved the lateral strength but did not increase column drift capacity

- Probable flexural strength with $1.25f_y$ was 8% to 10% lower than the measured ultimate flexural strength of the well-confined columns. Thus, estimating the probable flexural strength estimated with a factor more than 1.25 could be justified, especially in the case of well-confined hybrid-reinforced columns.

- The experimental effective stiffnesses at first yielding of longitudinal steel bar in the hybrid-reinforced columns was close to the prescribed effective stiffness in American codes (ACI 318-19; ASCE/SEI 41-17) for steel-reinforced concrete columns. The Canadian code (CSA A23.3-19), however, overestimate it by more than 1.5. Thus, effective stiffness recommended by American codes (ACI 318-19; ASCE/SEI 41-17) can be used in defining the elastic point of load-deflection curve required in modelling ductile reinforced concrete structural element confined with GFRP spiral and cross ties.

- This preliminary study on the hybrid-reinforced (steel/GFRP) concrete columns returned results similar to the requirements in North American building design code requirements for steel-reinforced concrete columns. Moreover, the transverse GFRP reinforcement was found to be very effective in confining the concrete core, reaching strains greater than the yield strain of steel ($2000\mu\varepsilon$).

Difference between GFRP- and hybrid-reinforced columns

- The failure of the GFRP-reinforced columns was more gradual than that of the hybrid reinforced columns. The GFRP longitudinal strain developed at twice the rate in subsequent drift cycles, whereas steel rebar strain increased significantly at the column yielding drift cycle.

- The well-confined hybrid reinforced columns achieved a drift ratio greater than 4.0%, which is recommended in CSA S806 (2012) for ductile-based design and exhibited greater ductility than the equivalent GFRP-reinforced columns. Thus, the hybrid reinforced columns were found suitable for seismic-based design, although the drift ratio and ductility were significantly affected by the spacing of the transverse reinforcement. Higher stiffness of the longitudinal reinforcement improved the column's lateral strength but reduced its drift capacity, which affects column ductility.

- Using longitudinal GFRP reinforcement instead of steel improved the columns' lateral load capacity and achieved a higher drift ratio. Due to material linearity, however, the inelastic behavior due to cover spalling occurred at a later drift cycle than in the hybrid reinforced columns, thereby reducing the deformability of the GFRP-reinforced columns.

- The stiffness of the hybrid reinforced columns at the column yielding point was lower than that of the GFRP-reinforced column and continued to drop until column failure. There was no sudden decay observed in the stiffness of GFRP-reinforced column.

- The GFRP spirals and cross ties were found to be more efficient in confining the hybrid reinforced column than the GFRP-reinforced column. ACI 440.1R (2015), AASHTO (2018), CSA S806 (2012), and CSA S6 (2019) underestimated the lateral

load capacity of the GFRP-reinforced columns, even with the GFRP compressive strength at 0.002 strain, as per CSA S6 (2019).

- The GFRP-reinforced columns achieved higher lateral load and lateral drift than the hybrid reinforced columns. However, the compressive behavior of GFRP bars does not provide the significant plasticity required by columns for seismic response. In addition, it makes it more likely to fail in a brittle mode under high loads. In contrast, steel rebars give resilience to columns in the compression part. Thus, the hybrid reinforced columns behaved better under reversed cyclic loading and provided sufficient ductility.

7.3 RECOMMENDATIONS FOR FUTURE WORK

The present study is expected to improve understanding of how concrete columns reinforced entirely with GFRP reinforcement and reinforced with hybrid reinforcement (longitudinal steel bars and transverse GFRP spiral and cross ties) behaves under simulated seismic load. However, additional research investigations should be carried out, including the following:

- Experimental work on different concrete dimensions is required to study the effect of aspect ratios and shear span length.
- Impact of different concrete types such as fiber-reinforced concrete (FRC) and high-strength concrete (HSC) with FRP- and hybrid-reinforced concrete columns subjected to seismic load should be investigated.
- The present study focused on the feasibility of the GFRP lateral reinforcement as an alternative for conventional steel ties. However, the influence of different types of FRP such as carbon and basalt FRP may be examined.
- Investigation on concrete columns reinforced with hybrid longitudinal bars (FRP/steel) and confined with FRP reinforcement could be promising.

- Studying the effect of lap-splicing of longitudinal bars on the behavior of hybrid reinforced columns consisting of longitudinal steel bars and transverse FRP reinforcement under simulated seismic load is recommended.

The French version of this chapter is presented below.

7.4 SOMMAIRE

Le programme de recherche visait à évaluer expérimentalement le comportement de colonnes en béton armé d'armature longitudinale et transversale en matériaux composites de polymère renforcé de fibres de verre (PRFV) soumises à une charge cyclique inversée quasi-statique. Par conséquent, huit colonnes en béton entièrement renforcées avec du PRFV et quatre autres colonnes renforcées avec d'armature hybride constituée de barres d'acier longitudinales et des armatures transversales en PRFV ont été construites et testées sous une charge sismique simulée. Les colonnes fabriquées et testées avaient une section transversale de 400 x 400 mm et une hauteur totale de 1850 mm. Les colonnes ont été coulées avec du béton de poids normal avec une résistance à la compression cible de 30 MPa. Les paramètres d'essai peuvent être résumés comme suit : le type de ferraillage longitudinal (PRFV et acier), le taux de ferraillage longitudinal (1,48% et 2,14%), la taille du ferraillage transversal en PRFV (#3, #4 et #5) et l'espacement du ferraillage transversal (100, 120 et 250 mm).

7.5 CONCLUSIONS

Les conclusions suivantes ont été tirées du présent programme de recherche sur la base de l'analyse des résultats des essais:

Colonnes en béton armé de PRFV

- Les colonnes en béton armé de PRFV bien confinées ont montré une réponse hystérétique stable sans dégradation de la résistance jusqu'à la rupture.
- Il n'y avait pas de différence significative dans la dissipation d'énergie des poteaux en béton armé de PRFV testés, quel que soit le taux d'armature longitudinale ou transversale.
- La transition entre la zone élastique et inélastique des colonnes renforcées de PRFV a été appelée déformation élastique (Δ_e) et définie à une déformation de compression du béton égale à 0,003. La déformation ultime (Δ_u) a été définie comme correspondant au déplacement lors de l'écrasement de la première barre longitudinale en PRFV en compression.
- Les colonnes en béton armé de PRFV bien confinées avec un taux d'armature longitudinale bas ont montré une résistance et une capacité de dérive accrues par rapport aux spécimens avec moins de renforcement transversal. Cela ne s'appliquait pas pour les poteaux avec plus d'armatures longitudinales où l'espacement des armatures transversales n'affectait pas de manière significative la capacité de dérive.
- L'augmentation de la taille de la barre longitudinale a diminué la capacité de dérive de la colonne bien confinée, mais a amélioré à la fois la résistance et la capacité de dérive des colonnes renforcées en PRFV avec moins de confinement par l'armature transversale. La colonne bien confinée G#5-#4-100 renforcée avec un taux de renforcement longitudinal de 1,48% a développé plus de déformation dans la barre longitudinale que la colonne G#6-#4-100 avec un taux de renforcement longitudinal de 2,14%, ce qui a amélioré la déformabilité de la colonne G#5-#4-100.

- Les spirales et les épingles en PRFV ont restreint l'expansion latérale du noyau en béton dans le cas des colonnes avec armature transversale ayant un espacement réduit, ce qui a grandement amélioré la résistance à la charge horizontale avec une déformation maximale plus faible dans les barres longitudinales.

- La colonne renforcée de PRFV ayant plus de spirales latérales et d'épingles a développé plus de déformation, ce qui a contribué à augmenter la résistance et la déformabilité de la colonne par rapport aux colonnes avec moins de spirales latérales et d'épingles.

- La déformation maximale développée dans la spirale et les épingles en PRFV à un taux de dérive de 4% dans tous toutes colonnes était inférieure à 0,006, ce qui est la déformation maximale autorisée dans la norme CSA S806 (2012). Les spirales et les épingles ont effectivement limité l'expansion du noyau de béton après l'éclatement du l'enrobage de béton. La déformation maximale développée dans l'armature transversale à la rupture était cependant nettement inférieure à la déformation à la rupture.

Colonnes en béton armé d'armature hybride (acier / PRFV)

- Toutes les colonnes testées avec armature hybride constituée d'armature longitudinale d'acier et d'armature transversale en PRFV ont montré un comportement à la flexion avec écrasement du béton et flambage des d'acier longitudinale. La colonne avec une spirale et des épingles en PRFV a montré un comportement stable avec un taux de déplacement latéral de plus de 4,0% avant la perte de résistance post-pic de 20%. Ainsi, les colonnes en béton avec armature hybride constituée d'acier longitudinal et d'armature transversale en PRFV constitue une très bonne alternative dans une nouvelle construction pour une zone sismique élevée.

- À la charge maximale, la ductilité en déplacement latéral était supérieure à 1,50 pour toutes les colonnes testées. La ductilité pour les colonnes bien confinées S#5-#4-100, S#5-#4-120 et S#6-#4-100 était respectivement de 8,4, 5,3 et 6,2 avec une courbe bilinéaire élastique-plastique équivalente à 20% de perte de résistance post-pic. Cela indique qu'une ductilité élevée peut être obtenue avec un renforcement transversal en PRFV. De plus, le taux de déplacement latéral obtenu était plus élevé que l'exigence de la norme CSA S806 (2012).

- Plus de dissipation d'énergie a été observée dans le premier cycle que dans le deuxième cycle pour la même amplitude de déplacement. Un espacement plus petit des armatures transversales en PRFV et un taux d'armature en acier longitudinal plus élevé sont nécessaires pour améliorer l'énergie dissipée cumulative des colonnes en béton.

- L'évolution de la déformation dans les barres d'acier longitudinales des colonnes en béton avec armature hybride (acier longitudinal et PRFV transversal) a montré une tendance similaire avec des poteaux en béton totalement renforcés avec des armatures en acier. La déformation dans l'armature transversale en PRFV a montré un confinement efficace assuré par les spirales et les épingles en PRFV après la plastification de l'armature longitudinale. Les épingles en PRFV étaient plus efficaces dans le confinement du béton des colonnes jusqu'à la déformation des barres d'acier longitudinales. Il a été montré qu'avec l'expansion du noyau du béton central, la spirale rectiligne en PRFV devient plus efficace pour confiner les colonnes en béton armé avec armature hybride (acier / PRFV).

- Le taux de déplacement latéral des colonnes en béton armé d'armature hybride diminue avec l'augmentation de l'espacement des armatures transversales en PRFV et ce sans affecter significativement la capacité de charge latérale. Une grosseur de barre d'acier longitudinale plus élevée améliore la résistance latérale mais n'améliore pas la capacité de déplacement latéral de la colonne.

- La résistance à la flexion probable en utilisant $1,25f_y$ était de 8 à 10% inférieure à la résistance à la flexion ultime mesurée pour les colonnes bien confinées. Ainsi, la résistance à la flexion probable estimée à l'aide d'un facteur supérieur à 1,25 pourrait être justifiée, en particulier pour les colonnes en béton armé d'armature hybride.

- La rigidité effective expérimentale à la première plastification de la barre d'acier longitudinale des colonnes avec armature hybride était proche de la rigidité effective prescrite des codes américains (ACI 318-19; ASCE / SEI 41-17) pour les colonnes en béton armé d'acier tandis que le code canadien (CSA A23.3-19) surestime la valeur de plus de 1,5 fois. Ainsi, la rigidité effective recommandée par les codes américains (ACI 318-19; ASCE / SEI 41-17) peut être utilisée pour définir le point élastique de la courbe charge-déflexion nécessaire à la modélisation d'élément structurel ductile en béton armé confiné à une spirale et des épingles en PRFV.

- Cette étude préliminaire sur les poteaux en béton armé d'armature hybride (acier / PRFV) a montré une réponse similaire par rapport aux exigences aux code de conception du bâtiment nord-américains (ACI et CSA) pour les poteaux en béton armé d'acier. De plus, le renforcement transversal en PRFV s'est avéré plus efficace pour confiner le noyau de béton atteignant la déformation plus que la déformation élastique de l'acier ($2000\mu\varepsilon$).

Différence entre les colonnes en béton armé d'armatures en PRFV et armé d'armatures hybrides (acier-PRFV)

- La rupture des colonnes en béton armé d'armatures en PRFV a été plus progressive que celle des colonnes en béton armé d'armature hybride. La déformation longitudinale de l'armature en PRFV s'est développée deux fois plus vite dans les cycles de chargement, tandis que la déformation des barres d'armature en acier a

augmenté de manière significative lors du cycle de chargement correspondant à la plastification des barres d'acier.

- Les colonnes en béton armé ave armature hybride bien confinées ont atteint un taux de déplacement latéral supérieur à 4,0%, une valeur qui est recommandée dans la norme CSA S806 (2012) pour la conception ductile. Par ailleurs, Les colonnes en béton armé ave armature hybride bien confinées ont montré une plus grande ductilité que les colonnes équivalentes en béton armé seulement en PRFV. Ainsi, les colonnes en béton avec armature hybride se sont révélées adaptées à la conception sismique, bien que le taux de déplacement latéral et la ductilité aient été significativement affectés par l'espacement des armatures transversales. Une rigidité plus élevée de l'armature longitudinale d'acier a amélioré la résistance latérale du poteau mais réduit sa capacité de déplacement latéral, ce qui affecte la ductilité du poteau.

- L'utilisation d'un renforcement longitudinal en PRFV au lieu de l'acier a amélioré la capacité de charge latérale des colonnes et a permis l'obtention d'un taux de déplacement latéral élevé. Cependant, en raison du comportement linéaire du PRFV, le comportement inélastique dû à l'écaillage du recouvrement de béton s'est produit à un cycle de déplacement latéral plus tardif que dans les colonnes en béton armé d'armature hybride, réduisant ainsi la déformabilité des colonnes en béton armé en PRFV.

- La rigidité des colonnes en béton armé d'armature hybride au point d'écoulement plastique de la colonne était inférieure à celle de la colonne renforcée en PRFV et a continué à baisser jusqu'à la rupture de la colonne. Il n'y a pas eu de dégradation soudaine de la rigidité de la colonne renforcée en PRFV.

- Les spirales et les épingles en PRFV se sont révélées plus efficaces pour confiner les colonnes en béton armé d'armature hybride que les colonnes renforcées en PRFV. Les codes et guides de calcul ACI 440.1R (2015), AASHTO (2018), CSA S806 (2012) et CSA S6 (2019) ont sous-estimé la capacité de charge latérale des

colonnes renforcées en PRFV, même en tenant compte de la résistance à la compression du PRFV correspondant à une déformation égale 0,002 selon le CSA S6 (2019).

- Les colonnes renforcées en PRFV ont obtenu une charge latérale et taux de déplacement latéral plus élevés que les colonnes renforcées d'armatures hybrides (acier-PRFV). Cependant, le comportement en compression des barres en PRFV ne fournit pas la plasticité requise par les colonnes pour la réponse sismique. De plus, ces colonnes se rupturent en mode fragile à très hautes charges. Par contre, les barres d'armature en acier donnent de la résilience aux colonnes dans la zone de compression. Ainsi, les colonnes renforcées d'armatures hybrides se sont mieux comportées sous un chargement cyclique inversé et ont fourni une ductilité suffisante.

7.6 RECOMMANDATIONS POUR DES TRAVAUX FUTURS

La présente étude devrait améliorer la compréhension du comportement des colonnes en béton entièrement renforcées avec des armatures en PRFV et renforcées avec des armatures hybrides (barres d'acier longitudinales et armature transversale en PRFV) sous une charge sismique simulée. Cependant, des recherches supplémentaires devraient être menées, notamment celles décrites ci-dessous:

- Des travaux expérimentaux sur des colonnes de différentes dimensions sont nécessaires pour étudier l'effet des rapports d'aspect.

- L'impact de différents types de béton tels que le béton fibré (BAF) et le béton à haute résistance (BHR) avec des colonnes renforcées en PRF et hybrides soumis à une charge sismique doit être étudié.

- La présente étude s'est concentrée sur la faisabilité du renforcement latéral en PRFV comme alternative à celles en acier conventionnelles. Cependant, l'influence de

différents types de PRF tels que des armatures en fibres de carbone (PRFC) et de basalte (PRFB) peut être examinée.

- Une étude sur des colonnes en béton renforcées avec des barres longitudinales hybrides (PRF / acier) et confinées avec des armatures PRF pourrait être prometteuse.
- Il est recommandé d'étudier l'effet de la longueur de recouvrement des barres longitudinales sur le comportement des poteaux en béton armé d'armatures hybrides constituées de barres d'acier longitudinales et d'armatures transversales en PRF sous une charge sismique simulée.

REFERENCES

AASHTO. (2011). *AASHTO Guide Specifications for LRFD Seismic Bridge Design*. *American Association of State Highway and Transportation Officials, Washington, DC.*, American Association of State Highway and Transportation Officials, Washington, DC.

AASHTO. (2014). *LRFD bridge design specifications*. American Association of State Highway and Transportation Officials, Washington, DC.

AASHTO. (2018). *AASHTO LRFD Bridge Design Guide Specifications for GFRP-Reinforced Concrete*. American Association of State Highway and Transportation Officials, Washington, DC.

ACI Committee 318. (1995). *Building Code Requirements for Structural Concrete (ACI 318-95) and commentary (ACI 318R-95)*. American Concrete Institute, Farmington Hills, Michigan (USA).

ACI Committee 318. (2002). *Building code requirements for structural concrete (ACI 318-02) and commentary (ACI 318R-02)*. American Concrete Institute, Farmington Hills, Michigan (USA).

ACI Committee 318. (2008). *Building Code Requirements for Structural Concrete (ACI 318-08)*. American Concrete Institute, Farmington Hills, Michigan (USA).

ACI Committee 318. (2014). *Building Code Requirements for Structural Concrete (ACI 318-14)*. American Concrete Institute, Farmington Hills, Michigan (USA).

ACI Committee 318. (2019). *Building Code Requirements for Structural Concrete (ACI 318R-19)*. American Concrete Institute, Farmington Hills, Michigan (USA).

ACI Committee 374. (2013). *Guide for Testing Reinforced Concrete Structural Elements*

under Slowly Applied Simulated Seismic Loads (ACI 374.2R-13). American Concrete Institute, Farmington Hills, Michigan (USA).

ACI Committee 440. (2015). *Guide for the Design and Construction of Structural Concrete Reinforced with FRP Bars (ACI 440.1R-15)*. *American Concrete Institute*, Farmington Hills, Michigan (USA).

Afifi, M. Z., Mohamed, H. M., and Benmokrane, B. (2014). "Axial capacity of circular concrete columns reinforced with GFRP bars and spirals." *Journal of Composites for Construction*, 18(1), 1–11.

Al-Dulaijan, S. U., Nanni, A., Al-Zahrani, M. M., Bakis, C. E., and Boothby, T. E. (1996). "Bond evaluation of environmentally conditioned GFRP/concrete systems." *2nd International Conference on Advanced Composite Materials in Bridges and Structures*, Canadian Society for Civil Engineering, Montreal, 845–852.

Ali, M. A., and El-salakawy, E. (2015). "Seismic Performance of GFRP-Reinforced Concrete Rectangular Columns." *Journal of Composites for Construction*, 20(3), 1–12.

Alsayed, S. H., Almusallam, T. H., Amjad, M. A., and Al-Salloum, Y. A. (1999). "Concrete Columns Reinforced by Glass Fiber Reinforced Polymer Rods." *ACI Special Publication*, 188, 103–112.

Applied Technology Council (ATC). (2009). *Quantification of Building Seismic Performance Factors FEMA P695*. Applied Technology Council, Redwood City, California.

ASCE/SEI 41. (2017). *Seismic Evaluation and Retrofit of Existing Buildings*. American Society of Civil Engineers, Reston, Virginia, USA.

ASCE/SEI 7. (2016). *Minimum Design Loads and Associated Criteria for Buildings and Other Structures*. American Society of Civil Engineers, Reston, Virginia, USA.

ASTM. (2011). *Standard Test Methods for Tensile Properties of Fiber-Reinforced Polymer*

Matrix Composite Bars. ASTM D7205-11, American Society for Testing and Materials, Conshohocken, USA.

ASTM. (2014). *Standard Test Method for Strength of Fiber Reinforced Polymer (FRP) Bent Bars in Bend Locations*. ASTM D7914-14, American Society for Testing and Materials, Conshohocken, USA.

ASTM. (2016). *Standard Test Method for Tensile Properties of Fiber Reinforced Polymer Matrix Composite Bars*. ASTM D7205/D7205M-16, American Society for Testing and Materials, Conshohocken, USA.

Bae, S., and Bayrak, O. (2008). "Plastic hinge length of reinforced concrete columns." *ACI Structural Journal*, 105(3), 290–300.

Bakis, C. E., Freimanis, A. J., Gremal, D., and Nanni, A. (1998). "Effect of Resin Material on Bond and Tensile Properties of Unconditioned and Conditioned FRP Reinforcement rods." *First International Conference on Durability of Composites for COnstruction*, B. Benmokrane and H. Rahman, eds., Sherbrooke, QC, Canada, 525–535.

Bank, L. C. (1993). "Properties of FRP Reinforcements for Concrete." *Fiber-Reinforced-Plastic (FRP) Reinforcement for Concrete Structures*, Elsevier, 59–86.

Bank, L. C., Puterman, M., and Katz, A. (1998). "The effect of material degradation on bond properties of fiber reinforced plastic reinforcing bars in concrete." *ACI Materials Journal*, 95(3), 232–243.

Bayrak, O., and Sheikh, S. A. (1998). "Confinement Reinforcement Design Considerations for Ductile HSC Columns." *Journal of Structural Engineering*, 124(9), 999–1010.

Benmokrane, B. (1997). "Bond Strength of FRP Rebar Splices." *Third International Symposium on Non-Metallic (FRP) Reinforcement for Concrete Structures (FRPRCS-3)*, Japan Concrete Institute, Tokyo, Japan, 405–412.

Caballero-Morrison, K. E., Bonet, J. L., Navarro-Gregori, J., and Martí-Vargas, J. R.

(2012). “Behaviour of steel-fibre-reinforced normal-strength concrete slender columns under cyclic loading.” *Engineering Structures*, Elsevier Ltd, 39, 162–175.

Calvi, G. M., Priestley, N. M. J., and Kowalsky, M. J. (2008). “Displacement-Based Seismic Design of Structures.” *3rd Panhellenic Conference of Earthquake Engineering and Engineering Seismology*, Athens, Greece.

Choo, C. C. (2005). “Investigation of rectangular concrete columns reinforced or prestressed with fiber reinforced polymer bars or tendons.” *University of Kentucky Doctoral dissertation*, 20–24.

Choo, C. C., Harik, I. E., and Gesund, H. (2006). “Strength of rectangular concrete columns reinforced with fiber-reinforced polymer bars.” *ACI Structural Journal*, 103(3), 452–459.

“Corrosion of Embedded Materials.” (n.d.). <https://www.cement.org/learn/concrete-technology/durability/corrosion-of-embedded-materials> (Mar. 12, 2019).

CSA A23.3. (2014). *Design of Concrete Structures*. CSA A23.3-14, Canadian Standards Association, Ontario, Canada.

CSA A23.3. (2019). *Design of Concrete Structures*. CSA A23.3-14, Canadian Standards Association, Ontario, Canada.

CSA S6. (2014). *Canadian Highway Bridge Design code*. Canadian Standards Association, Mississaunga, Ontario, Canada.

CSA S6. (2019). *Canadian Highway Bridge Design Code*. CSA S6-19, Canadian Standards Association, Mississaunga, Ontario, Canada.

CSA S806. (2002). *Design and Construction of Building Components with Fibre-Reinforced Polymers (CAN/CSA S806-02)*. *Canadian Standards Association, Ontario, Canada*.

CSA S806. (2012). *Design and Construction of Building Structures with Fiber Reinforced Polymers (CAN/CSA S806-12).* Canadian Standards Association, Ontario, Canada.

CSA S807. (2010). *Specification for fibre-reinforced polymers*. CSA S807-10, Canadian Standards Association, Ontario, Canada.

De Luca, A., Matta, F., and Nanni, A. (2010). "Behavior of full-scale glass fiber-reinforced polymer reinforced concrete columns under axial load." *ACI Structural Journal*, 107(5), 589–596.

Deitz, D. H., Harik, I. E., and Gesund, H. (2003). "Physical Properties of Glass Fiber Reinforced Polymer Rebars in Compression." *Journal of Composites for Construction,* 7(4), 363–366.

Ehsani, M. R. (1993). "Glass-Fiber Reinforcing Bars." *Alternative Materials for the Reinforcement and Pressing of Concrete*, Blackie Academic & Professional, London, 34–54.

Ehsani, M. R., Saadatmanesh, H., and Tao, S. (1996). "Design Recommendations for Bond of." 122(March), 247–254.

El-Salakawy, E., Benmokrane, B., El-Ragaby, A., and Nadeau, D. (2005). "Field Investigation on the First Bridge Deck Slab Reinforced with Glass FRP Bars Constructed in Canada." *Journal of Composites for Construction*, 9(6), 470–479.

Elchalakani, M., Dong, M., Karrech, A., Mohamed Ali, M. S., and Huo, J.-S. (2020). "Circular Concrete Columns and Beams Reinforced with GFRP Bars and Spirals under Axial, Eccentric, and Flexural Loading." *Journal of Composites for Construction*, 24(3), 04020008.

Elshamandy, M., Farghaly, A. S., and Benmokrane, B. (2018). "Experimental Behaviour of GFRP-Reinforced Concrete Columns under Lateral Cyclic load." *ACI Structural Journal*, 115(2), 337–349.

Elwood, K. J., Matamoros, A. B., Wallace, J. W., Lehman, D. E., Heintz, J. A., Mitchell, A. D., Moore, M. A., Valley, M. T., Lowes, L. N., Comartin, C. D., and Moehle, J. P. (2007). "Update to ASCE/SEI 41 concrete provisions." *Earthquake Spectra*, 23(3),

493–523.

Faza, S. S., and GangaRao, H. V. S. (1991). “Bending and Bond Behavior of Concrete Beams Reinforced With Plastic Rebars.” *third Bridge Engineering Conference*, 185–193.

Freimanis, A. J., Bakis, C. E., Nanni, A., and Gremel, D. (1998). “A Comparison of Pull-out and Tensile Behaviors of FRP Reinforcement for Concrete.” *Second International Conference on Composites in Infrastructure (ICCI-98)*, Tucson, AZ, US, 52–65.

Grira, M. B. M. (1998). “Innovative Approaches to Column Confinement.” University of Ottawa.

Hadhood, A., Mohamed, H. M., Ghrib, F., and Benmokrane, B. (2017). “Efficiency of glass-fiber reinforced-polymer (GFRP) discrete hoops and bars in concrete columns under combined axial and flexural loads.” *Composites Part B: Engineering*, Elsevier Ltd, 114, 223–236.

Hadi, M. N. S., Karim, H., and Sheikh, M. N. (2016). “Experimental Investigations on Circular Concrete Columns Reinforced with GFRP Bars and Helices under Different Loading Conditions.” *Journal of Composites for Construction*, 20(4), 04016009.

Hassan, M., Ahmed, E., and Benmokrane, B. (2013). “Punching-Shear Strength of Normal and High-Strength Two-Way Concrete Slabs Reinforced with GFRP Bars.” *Journal of Composites for Construction*, 17(6), 04013003.

Hassanein, A., Mohamed, N., Farghaly, A. S., and Benmokrane, B. (2019). “Experimental investigation: New ductility-based force modification factor recommended for concrete shear walls reinforced with glass fiber-reinforced polymer bars.” *ACI Structural Journal*, 116(1), 213–224.

Ho, J. C. M. (2011). “Limited ductility design of reinforced concrete columns for tall buildings in low to moderate seismicity regions.” *The Structural Design of Tall and Special Buildings*, 20, 102–120.

Hwang, S. K., and Yun, H. Do. (2004). "Effects of transverse reinforcement on flexural behaviour of high-strength concrete columns." *Engineering Structures*, 26(1), 1–12.

ISIS Canada. (2007). *Reinforcing concrete structures with fibre reinforced polymers - Design manual No. 3. ISIS Canada Corporation.*

Karim, H., Sheikh, M. N., and Hadi, M. N. S. (2016). "Axial load-axial deformation behaviour of circular concrete columns reinforced with GFRP bars and helices." *Construction and Building Materials*, Elsevier Ltd, 112, 1147–1157.

Kassem, C., Farghaly, A. S., and Benmokrane, B. (2011). "Evaluation of flexural behavior and serviceability performance of concrete beams reinforced with FRP bars." *Journal of Composites for Construction*, 15(5), 682–695.

Kazem Sharbatdar, M., Saatcioglu, M., and Benmokrane, B. (2011). "Seismic flexural behavior of concrete connections reinforced with CFRP bars and grids." *Composite Structures*, Elsevier Ltd, 93(10), 2439–2449.

Kharal, Z., and Sheikh, S. A. (2018). "Seismic Performance of Square Concrete Columns Confined with Glass Fiber–Reinforced Polymer Ties." *Journal of Composites for Construction*, 22(6), 04018054.

Kharal, Z., and Sheikh, S. A. (2020). "Seismic Behavior of Square and Circular Concrete Columns with GFRP Reinforcement." *Journal of Composites for Construction*, 24(1), 04019059.

Koch, G. H., Brongers, M., Thompson, N. G., Virmani, Y. P., and Payer, J. H. (2002). *Corrosion Costs and Preventive Strategies in the United States [Summary]*. Federal Highway Administration, United States.

Lounis, Z., and Daigle, L. (2008). "Reliability-based decision support tool for life cycle design and management of highway bridge decks." *Annual Conference and Exhibition of the Transportation Association of Canada: Transportation - A Key to a Sustainable Future*, Toronto, Ontario, Canada, 1–19.

Mady, M., El-Ragaby, A., and El-Salakawy, E. (2011). "Seismic Behaviour of Beam-Column Joints Reinforced with GFRP Bars and Stirrups." *Journal of Composites for Construction*, 15(6), 875–886.

Mallick, P. K. (1988). *Fiber-Reinforced Composites: Materials, Manufacturing, and Design*. Marcell decker, Inc., New York.

Mohamed, H. M., Afifi, M. Z., and Benmokrane, B. (2014a). "Performance Evaluation of Concrete Columns Reinforced Longitudinally with FRP Bars and Confined with FRP Hoops and Spirals under Axial Load." *Journal of Bridge Engineering*, 19(7), 04014020.

Mohamed, N., Farghaly, A. S., Benmokrane, B., and Neale, K. W. (2014b). "Experimental Investigation of Concrete Shear Walls Reinforced with Glass Fiber-Reinforced Bars under Lateral Cyclic Loading." *Journal of Composites for Construction*, 18(3), 1–11.

Mohamed, N., Farghaly, A. S., Benmokrane, B., and Neale, K. W. (2014c). "Drift capacity design of shear walls reinforced with glass fiber-reinforced polymer bars." *ACI Structural Journal*, 111(6), 1397–1406.

Mosley, C. P. (2002). "Bond Performance of Fiber Reinforced Plastic (FRP) Reinforcement in Concrete." Purdue University, West Lafayette, IN.

Nanni, A., Nenninger, J. S., Ash, K. D., and Liu, J. (1997). "Experimental Bond Behavior of Hybrid Rods for Concrete Reinforcement." *Structural Engineering and Mechanics*, Techno-Press, 5(4), 339–353.

Naqvi, S., and El-Salakawy, E. (2016). "Lap Splice in GFRP-RC Rectangular Columns Subjected to Cyclic-Reversed Loads." *Journal of Composites for Construction, ASCE*, 21(4), 1–13.

National Research Council of Canada (NRC). (2015). *National Building Code of Canada (NBC)*. Canadian Commission on Building and Fire Codes, Ottawa, ON, Canada.

Pantelides, C. P., Gibbons, M. E., and Reaveley, L. D. (2013). "Axial Load Behavior of

Concrete Columns Confined with GFRP Spirals." *Journal of Composite for Construction*, 17(June), 305–313.

Paramanantham, N. S. (1993). "Investigation of the Behavior of Concrete Columns Reinforced with Fiber Reinforced Plastic Rebars." Lamar University, Beaumont, Texas.

Park, R. (1988). "Ductility Evaluation from Laboratory and Analytical Testing." *Ninth World Conference on Earthquake Engineering*, Tokyo-Kyoto, Japan, Vol. VIII, 605-616.

Park, R. (1989). "Evaluation of Ductility of Structures and Structural Assemblages from Laboratory Testing." *Bulletin of the New Zealand Society for Earthquake Engineering*, 22(3), 155–166.

Park, R., and Paulay, T. (1975). *Reinforced Concrete Structures*. John Wiley & Sons, Inc., New York, USA.

Park, R., and Sampson, R. A. (1972). "Ductility of Reinforced Concrete Column Sections in Seismic Design." *J Am Concr Inst*, 69(9), 543–551.

Paulay, T., and Priestley, M. J. N. (1992). *Seismic Design of Reinforced Concrete and Masonry Buildings*. John Wiley & Sons, Inc., New York, USA.

Phillips, L. N. (1989). *Design with advanced composite materials*. New York, NY (USA); Springer-Verlag New York Inc.

Priestley, M. J. ., Seible, F., and Calvi, G. M. (1996). *Seismic design and retrofit of bridges*. John Wiley & Sons, Inc.

Priestley, M. J. N. (2000). "Performance based seismic design." *Bulletin of the New Zealand Society for Earthquake Engineering*, 33(3), 325–346.

Renew Canada. (2014). "Silent but Deadly." <https://www.renewcanada.net/feature/silent-but-deadly/> (Dec. 29, 2020).

Saatcioglu, M., and Baingo, D. (1999). "Circular High-Strength Concrete Columns under Simulated Seimic Loading." *Journal of Structural Engineering*, 125(March), 272–280.

Sharbatdar, M. K. (2003). "Concrete Columns and Beams Reinforced with FRP Bars and Grids under Monotonic and Reversed Cyclic Loading." *Ph.D. Thesis*, University of Ottawa.

Sharbatdar, M. K., and Saatcioglu, M. (2009). "Seismic Design of FRP Reinforced Concrete Structures." *Asian Journal of Applied Sciences*, 2(3), 211–222.

Sheikh, S. A., and Khoury, S. S. (1993). "Confined concrete columns with Stubs." *ACI Structural Journal*, 90(4), 414–431.

Sheikh, S. A., and Yeh, C.-C. (1990). "Tied Concrete Columns under Axial Load and Flexure." *Journal of Structural Engineering*, 116(10), 2780–2800.

Shield, C. K., French, C. W., and Hanus, J. P. (1999). "Bond of Glass Fiber Reinforced Plastic Reinforcing Bar for Consideration in Bridge Decks." *Special Publication*, 188, 393–406.

Tavassoli, A., Liu, J., and Sheikh, S. A. (2015). "Glass Fiber-reinforced polymer-Reinforced circular columns under simulated seismic loads." *ACI Structural Journal*, 112(1), 103–114.

Tavassoli, A., and Sheikh, S. A. (2017). "Seismic Resistance of Circular Columns Reinforced with Steel and GFRP." *Journal of Composites for Construction*, 21(4), 1–13.

Tighiouart, B., Benmokrane, B., and Mukhopadhyaya, P. (1999). "Bond strength of glass FRP rebar splices in beams under static loading." *Construction and Building Materials*, 13(7), 383–392.

Tobbi, H., Farghaly, A. S., and Benmokrane, B. (2012). "Concrete columns reinforced longitudinally and transversally with glass fiber-reinforced polymer bars." *ACI*

Structural Journal, 109(4), 551–558.

Tobbi, H., Farghaly, A. S., and Benmokrane, B. (2014a). "Behavior of concentrically loaded fiber-reinforced polymer reinforced concrete columns with varying reinforcement types and ratios." *ACI Structural Journal*, 111(2), 375–385.

Tobbi, H., Farghaly, A. S., and Benmokrane, B. (2014b). "Strength model for concrete columns reinforced with fiber-reinforced polymer bars and ties." *ACI Structural Journal*, 111(4), 789–798.

Toutanji, H. A., and Saafi, M. (2000). "Flexural behavior of concrete beams reinforced with glass fiber-reinforced polymer (GFRP) bars." *ACI Structural Journal*, 97(5), 712–719.

Wambeke, B., and Shield, C. (2006). "Development Length of Glass Fiber Reinforced Polymers Bars in Concrete." *ACI Structural Journal*, 103(1), 11–17.

Wight, J. K. (1973). "Shear Strength Decay in Reinforced Concrete Columns Subjected to Large Deflection Reversals." *Research Project Report, University of Illinois.*, University of Illinois, Urbana, Illinois.

Wu, W. P. (1990). "Thermomechanical Properties of Fiber Reinforced Plastic (FRP) Bars." *PhD Dissertation*, West Virginia University, Morgantown, WV.

Yin, S. Y., Wu, T., Liu, T. C., Sheikh, S. A., and Wang, R. (2011). "Interlocking Spiral Confinement for Rectangular Columns." *Concrete International*, 38–45.

Zadeh, H. J., and Nanni, A. (2012). "Design of RC Columns Using Glass FRP Reinforcement." *Journal of Composites for Construction*, 17(3), 294–304.